INFORMATION TO USERS

This manuscript has been reproduced from the microfilm master. UMI films the text directly from the original or copy submitted. Thus, some thesis and dissertation copies are in typewriter face, while others may be from any type of computer printer.

The quality of this reproduction is dependent upon the quality of the copy submitted. Broken or indistinct print, colored or poor quality illustrations and photographs, print bleedthrough, substandard margins, and improper alignment can adversely affect reproduction.

In the unlikely event that the author did not send UMI a complete manuscript and there are missing pages, these will be noted. Also, if unauthorized copyright material had to be removed, a note will indicate the deletion.

Oversize materials (e.g., maps, drawings, charts) are reproduced by sectioning the original, beginning at the upper left-hand corner and continuing from left to right in equal sections with small overlaps. Each original is also photographed in one exposure and is included in reduced form at the back of the book.

Photographs included in the original manuscript have been reproduced xerographically in this copy. Higher quality 6" x 9" black and white photographic prints are available for any photographs or illustrations appearing in this copy for an additional charge. Contact UMI directly to order.

UMI

A Bell & Howell Information Company
300 North Zeeb Road, Ann Arbor MI 48106-1346 USA
313/761-4700 800/521-0600

The Optical Counterparts of the Luminous X-ray Binary Stars in Globular Clusters

by

Eric William Deutsch

A dissertation submitted in partial fulfillment
of the requirements for the degree of

Doctor of Philosophy

University of Washington

1998

Approved by Bruce H. Margon
(Chairperson of Supervisory Committee)

Program Authorized
to Offer Degree Department of Astronomy

Date 12/16/1998

In presenting this dissertation in partial fulfillment of the requirements for a Doctoral degree at the University of Washington, I agree that the Library shall make its copies freely available for inspection. I further agree that extensive copying of this dissertation is allowable only for scholarly purposes, consistent with "fair use" as prescribed in the U.S. Copyright Law. Requests for copying or reproduction of this dissertation may be referred to University Microfilms, 1490 Eisenhower Place, P.O. Box 975, Ann Arbor, MI 48106, to whom the author has granted "the right to reproduce and sell (a) copies of the manuscript in microform and/or (b) printed copies of the manuscript made from microform."

Signature Eric Dunstech

Date 12/16/1998

University of Washington

Abstract

The Optical Counterparts of the Luminous X-ray Binary Stars in Globular Clusters

by Eric William Deutsch

Chairperson of Supervisory Committee
Professor Bruce Margon
Astronomy Department

Ten percent of our Galaxy's luminous ($L_X \gtrsim 10^{36}$ erg s^{-1}) X-ray point sources are located in globular clusters (GCs), but globular clusters contribute a much smaller fraction of normal stars to the Galaxy. X-ray bursts have been observed from nearly all of them, indicating that these sources are low-mass X-ray binary (LMXB) systems containing a neutron star and a companion star from which matter is being transferred. The understanding of LMXB overabundance in globular clusters may well lead to important insights into the formation and evolution of these exotic binary systems as well as the dynamics of globular clusters themselves. The goals of this dissertation are to identify the optical counterparts to some GC LMXBs without previously identified counterparts, bring together and compare in the most homogeneous fashion all available *Hubble Space Telescope* (*HST*) optical observations of the current crop of GC LMXB counterparts, and discuss the implications for cluster dynamics and LMXB systems in general.

In this work, candidates for three additional optical counterparts to luminous X-ray binaries in globular clusters are presented, thereby doubling the number of optical

counterpart candidates. Two are very likely correct although require additional work to confirm the identifications, while the third remains somewhat tentative due to the positional discrepancy with the X-ray coordinates and the fact that the entire error circle is not surveyed. A homogeneous set of *HST* photometric measurements for all of the counterparts identified thus far is presented, and their optical properties are compared with those of field low-mass X-ray binaries. In addition, new and archival spectra and imaging data are analyzed to intercompare the UV/optical spectral energy distributions (SEDs) of GC LMXBs. A set of simple model SEDs is introduced and compared with the observations to infer accretion rates, disk diameters, and other properties of these systems. This work strengthens previous inferences that many if not most of the globular cluster LMXBs are ultra-compact systems with orbital periods less than 1 hr.

TABLE OF CONTENTS

LIST OF FIGURES

LIST OF TABLES

ACKNOWLEDGMENTS

My deepest thanks go to Bruce Margon who has most generously supported me over the years and involved me in a wide variety of exciting research projects, only a few of which are presented in this work. In addition, the facilities he has made available to me have made this research and my other work a pleasure. I would like to thank both Bruce and Scott Anderson for getting me interested in the group of objects I have studied here, preparing the groundwork for many of the observations used herein, and helping me to present all my work more clearly and effectively. Much appreciation also goes to Paul Hodge whose many useful comments improved the final draft of this dissertation. I am grateful to Ron Allen and especially Ralph Bohlin who guided me in research as an undergraduate, motivating me to pursue graduate work in astronomy.

A mountain of thanks and love goes to Kerry, my best friend in the whole world, for unwavering faith in all that I have done. To my parents, who have given me so many opportunities and have encouraged me to pursue anything I want — I could not have done all this without your support! I am grateful to Todd Creamer for pulling out his telescope on those frigid nights which kindled both our interests in the heavens. Thanks to all the other grad students for the good times hiking and skiing in the Cascades, playing volleyball, chatting in the halls and local eateries, and, of course, frequenting the pubs. Finally, I'd also like to thank Luis Mendoza, Ron Cook, and other friends in the Washington Yacht Club who have made sailing a favorite diversion in the last few years.

Chapter 1

INTRODUCTION

1.1 Overview

Not long after significant numbers of luminous ($L_X \gtrsim 10^{36}$ erg s^{-1}) X-ray sources were discovered, it was noticed that these sources appear to be overabundant in globular clusters (Katz 1975; Clark 1975). While globular clusters (GCs) contribute only a tiny fraction ($\sim 10^{-4}$) to the total number of stars and total mass in the Galaxy, a recent compilation by van Paradijs (1995) finds 10% of the known low-mass X-ray binaries (LMXBs) in globular clusters. The understanding of this circumstance may well lead to important insights into the formation and evolution of these systems as well as the dynamics of globular clusters themselves.

Early on it was proposed that the X-ray sources in globular clusters were central black holes of several hundred solar masses, accreting gas from the cluster core (Bahcall & Ostriker 1975; Silk & Arons 1975). The bright source in NGC 6624 was the first object observed to exhibit X-ray bursts. While these bursts were first interpreted as evidence of massive black holes (Grindlay & Gursky 1976), later work revealed that the X-ray bursts were the result of hydrogen fusion flashes on a neutron star surface (see, e.g., Lewin & Joss 1983 for a brief history of this advance). In addition better ($\sim 3''$ radius 90% confidence) *Einstein* X-ray positions for the globular cluster sources showed that they were not always precisely in the center of each cluster, but rather exhibited a radial distribution suggesting these systems contained only a few solar masses (Grindlay 1981, Grindlay et al. 1984).

As the first X-ray burst sources discovered were globular clusters sources and indeed the most famous example, the Rapid Burster, was discovered to lie within the previously unknown, highly extincted cluster Liller 1, it was initially believed by some that all bursters would prove to be located in globular clusters (Forman & Jones 1976). However, as more bursters were cataloged, it soon became clear that many field sources were also bursters (Lewin 1977). It has, however, turned out that nearly all GC LMXBs themselves are burst sources. With the recent discovery of bursts from the systems in NGC 6652 and NGC 6440 (in 't Zand et al. 1998a, 1998b), 11 of the 12 GC LMXBs have now exhibited bursts during observations capable of detecting such events. The remaining source in Terzan 6 has not yet received much scrutiny and may yet prove to be a burster.

Therefore nearly all of the luminous globular cluster X-ray sources are now recognized to be binary systems with neutron star primaries and low mass secondaries. A review of our current understanding of X-ray binaries is detailed in White, Nagase, & Parmar (1995) as well as in additional chapters in the same volume. Briefly, the geometry of LMXBs is such that the secondary just fills its Roche lobe and material spills over from the secondary through the L1 point toward the primary. The angular momentum of the infalling matter causes this material to enter a circular orbit about the primary but viscous forces subsequently cause material to slowly spiral inward and perhaps migrate outward as well, thereby creating an accretion disk around the primary. As the infalling matter reaches the neutron star surface copious X-rays are produced. The X-rays are observed directly or sometimes via scattering from the thin gas in an accretion disk corona. A large fraction of X-rays are also reprocessed into ultraviolet and optical light after being absorbed by the optically thick accretion disk and to some smaller degree the secondary star surface. The energy generated by the secondary star itself is usually insignificant compared with the other processes.

The location of globular cluster LMXBs make them of particular interest among all LMXBs for optical studies. LMXB optical counterparts are typically found in

crowded fields (see, e.g., Deutsch et al. 1996c), and those in globular clusters are in the most crowded regions of any, making optical studies very difficult, often only possible with *HST*. However this added difficulty is worth enduring since the distance and extinction to these sources, as members of a cluster, can be readily determined by careful studies of the clusters themselves. Once the distance and reddening are known, the optical luminosity and spectral shape can be accurately determined and model parameters for the system become considerably constrained. Finally, as several of the host clusters have very low extinction, these LMXB optical counterparts afford some of the best opportunities to study the far ultraviolet emission of such systems.

A recent review of the optical properties of LMXBs is presented by van Paradijs & McClintock (1995). Nearly all of the observed UV and optical light is due to reprocessed X-rays from the accretion disk which subtends a large solid angle as viewed from the origin of the X-rays. A typical spectrum of an LMXB shows numerous emission lines (principally He I, He II, and Balmer lines) superposed on a blue continuum. The continuum is often quite well described by a blackbody curve of ~ 30000 K although uncertainties in the reddening often do not permit precise determinations.

Over 30 LMXBs have known orbital periods, which range from $0.19 - 398$ hr, although most periods lie between 3 and 12 hr (White et al. 1995). The globular cluster source in NGC 6624 holds the distinction of having the shortest LMXB period and indeed the shortest orbital period of any known system[1] at 0.19 hr, observed both at X-ray and UV wavelengths. The LMXB with the next shortest period, determined with *HST* UV observations (Homer et al. 1996) at 0.36 hr, is also a GC system, that in NGC 6712. This circumstance is surely not a coincidence and suggests that globular cluster environments assist in the formation of ultra-compact binary systems. Two other GC LMXBs have known periods. A 5.7 hr periodicity in X-ray dips has been observed in the NGC 6441 source, and a high-amplitude 17.1 hr period has been

[1]A periodicity of 0.16 hr has recently been suggested as being orbital for the Polar RX J1914+24, which may prove to unseat X 1820-303 as the shortest-period system (Cropper et al. 1998).

seen in optical observations and also confirmed in subsequent reanalysis of X-ray data (Ilovaisky et al. 1993) for the source in M15. None of the other GC LMXBs have known periods, even though many have been searched to some degree for periodic X-ray variability.

The optical counterparts of LMXBs often display variability as a result of a variety of mechanisms. Many sources show periodic orbital modulations as well as random short- and long-timescale variability due to changes in the mass accretion rate. Transient sources can undergo many magnitudes of change as the accretion rate may change from near zero to an Eddington limited level. Periodic variations of weeks to months have been attributed to precession of the accretion disk in some sources. Optical analogs to X-ray bursts have also been observed in a few sources, usually delayed by a few seconds from the X-ray burst.

Some of these 12 GC sources are variously referred to as transients by some workers, although the criteria for applying this label are often vague. Several sources were indeed detected at high luminosity but have then gone undetected at detection limits many orders of magnitude fainter, clearly displaying separate bright and quiescent states. Others have only undergone changes in brightness by $\sim 10\times$ depending on spectral assumptions (often due to different instrumentation) and should probably not carry a "transient" tag. A recent review of X-ray transients, also referred to as X-ray novae or soft X-ray transients (SXTs), is given by Chen, Schrader, & Livio (1997). The *bona fide* GC transient sources may be different from the bulk of SXTs, however, as most of those are thought to be black hole systems. Thus far there is no evidence at all for any black hole systems in globular clusters, although they may be present, as yet undetected.

As some of the known sources are transients, it follows to ask how many LMXBs in quiescence may be lurking in other or these same globular clusters. This is difficult to answer since quiescent LMXBs may be nearly indistinguishable from single cluster stars if accretion stops or occurs at a very low rate. A serendipitous discovery of

type I X-ray bursts in a globular cluster not known to harbor an LMXB was made with *ASCA* by Gotthelf & Kulkarni (1997). In quiescence this source is many orders of magnitude fainter in X-rays than the other cluster LMXBs, and the burst itself is significantly sub-Eddington. Those authors suggest that this source is a highly magnetized neutron star accreting at a low rate and that there may be many such systems, accounting for the mysterious low-luminosity sources in globular clusters described below. Detection of more such events and understanding their implication will require extremely wide field monitoring instruments more sensitive than the *Rossi X-ray Timing Explorer (RXTE)* All-Sky Monitor instrument.

In addition to the twelve luminous sources discussed here, many if not most globular clusters appear to harbor several low luminosity ($L_X \lesssim 10^{35}$ erg s^{-1}) X-ray sources each. This fascinating topic may hold important implications for the population of GC LMXBs but will only be briefly discussed here. It seems likely that we have only seen the bright end of what must be a broad luminosity distribution down to at least $L_X \sim 10^{30}$ erg s^{-1}. The nature of these sources is not yet clear, but work so far suggests that the faint sources include several different species. Suggested explanations for the brightest objects include cataclysmic variables and quiescent LMXBs, as well as unrelated superpositions (Margon & Bolte 1987). Expected to be at lower luminosities than detected so far but present nonetheless are possibilities such as millisecond pulsars and RS CVn systems. The advent of AXAF will allow significantly deeper studies at higher resolution, which should initiate rapid progress in this field. We may soon find that we are observing only the small, currently active tail of the much larger distribution of GC LMXBs. See Johnston & Verbunt (1996) and references therein for an examination of the population of currently known low luminosity sources.

Not just another X-ray emitting denizen of globular clusters, the millisecond pulsar (MSP) is likely to be intimately related to the GC LMXB. MSPs, sometimes also called recycled pulsars, are currently understood to result from extreme spin-up of a

neutron star due to accretion angular momentum transfer in a LMXB system. Thus LMXBs may be the precursors to MSPs. There are still problems with this picture, not the least of which is the "birthrate problem," which recognizes that MSPs seem to vastly outnumber LMXBs in the globular clusters which have been carefully searched. Further understanding of both types of objects will resolve the current confusion. See Bhattacharya (1995) for a recent review of MSPs.

Binary systems have a great influence on globular cluster dynamical evolution and have been the subject of considerable work (see, e.g., Elson et al. 1987; Hut et al. 1992; McMillan et al. 1998). Although a decade ago it seemed that GCs possess extremely few binaries and perhaps no primordial ones, this view has now changed and it is generally thought that clusters begin their lives with of order 10% binaries, many of which still exist today. In addition to altering and destroying the primordial binaries, stellar interactions may also create additional binaries via three-body encounters and dissipative two-body collisions. The interactions will occur preferentially in the core of the cluster where the density is highest. Since mass segregation will cause the heaviest systems in the cluster to sink to the center, GC cores will create and harbor a host of exotic stellar systems which will affect the cluster's overall evolution. However our understanding of the number and nature of these systems remains vague and will require considerable progress before cluster evolution can be accurately modeled.

1.2 Individual Systems

In this section each of the twelve objects will be briefly discussed individually, indicating the current understanding of each system, both from X-ray observations as well as optical work. They will be discussed roughly in order of optical counterpart discovery or progress toward such identification.

X 2127+119 in M 15 was the first GC LMXB to be optically identified. Based on UV excess and variability Aurière et al. (1984, 1986) isolated the star AC 211 within

the *Einstein* error circle as the optical counterpart. As is was the first discovered and by far the brightest optical counterpart, numerous optical and UV studies of this object have been published. While an 8.5 hr period was initially suggested (e.g., Ilovaisky et al. 1987, Naylor et al. 1988), Ilovaisky et al. (1993) determined a more likely period of 17.112 hr using several years of ground-based data and confirmed this period in archival X-ray observations, although recent work by Homer & Charles (1998) indicates a significant period derivative as well. Ground-based and IUE spectra display both emission and absorption lines as well as a high systematic velocity difference from the cluster itself (Naylor et al. 1988, 1989, 1992). An *HST* FOS spectrum is similar to previously-published spectra but suffers from far less contamination (Downes et al. 1996). All the available *HST* observations will be reanalyzed together in chapter 4 of this work.

A variety of candidates for the optical counterpart to X1850–087 in NGC6712 were offered (e.g. Cudworth 1988; Nieto et al. 1990; Bailyn et al. 1991; Aurière & Koch-Miramond 1992) and the actual counterpart, the $B \sim 20$ Star S, was eventually unambiguously confirmed by Anderson et al. (1993) with *HST* images. WFPC2 time series photometry by Homer et al. (1996) yields a 4% modulation with a 20.6 min period which was interpreted as the orbital period of an ultra-compact double-degenerate system. Downes et al. (1996) present featureless, apparently composite *HST* FOS spectra which seem to confuse more than clarify. All the available *HST* observations for this source are also reanalyzed together in chapter 4 of this work.

The optical counterpart to X1820–303 in NGC6624 was dramatically detected by King et al. (1993) using far UV ($\sim$ 1400 Å) *HST* FOC images, in which this star was far brighter than all other cluster stars combined. This optical object will be henceforth referred to as Star K in this work. Anderson et al. (1997) detected 16% 11.5 min UV modulations corresponding to the long-known X-ray period (Stella et al. 1987) and thus confirming Star K as the optical counterpart. The amplitude is similar to that predicted by Arons & King (1993). The FOS spectrum presented by

Anderson et al. (1997) rises steeply in the far ultraviolet but appears featureless.

Discovery of a likely candidate for the optical counterpart to X 0512–401 in NGC 1851 using *HST* WFPC2 imaging will be described in chapter 2 of this work. These results have been previously published as Deutsch et al. (1996b). A single UV-excess object, Star A, is found in the X-ray error circle although a few other similarly UV-excess stars elsewhere in the cluster leave a small probability that this candidate is unrelated and has fallen in the error circle by chance. Recent X-ray observations of this system and a review of previous observations are described in Callanan, Penny, & Charles (1995).

The discovery of a strong candidate for the optical counterpart to X 1746–370 in NGC 6441 will be detailed in chapter 2 of this work. This analysis was published in Deutsch et al. (1998). While only a single UV-excess object, Star U1, is detected in the X-ray error circle, many other UV-excess objects also seen in this cluster contribute toward making this identification less secure. However, significant variability during the short series of exposures and over a one year timescale strengthen the association. This source exhibits a 5% modulation in X-ray dips with a 5.7 hr period (Parmar et al. 1989; Sansom et al. 1993). Such dipping behavior suggests that the system is viewed at a fairly high inclination and is likely to show easily detectable periodic optical variability as well.

The search for the optical counterpart to the X-ray source X 1832–330 in NGC 6652 will be discussed in chapter 2 of this work. These results have been previously published as Deutsch, Margon, & Anderson (1998a). A UV-excess star is discovered but its positional discrepancy with the X-ray coordinates leaves the association questionable. Type I X-ray bursts were also recently discovered by in 't Zand et al. (1998b) confirming that this system contains a neutron star primary. Not much further is known about this recently-discovered (Predehl et al. 1991) system but intensive work is underway.

The Rapid Burster (X 1730–335) in Liller 1 is one of the most famous X-ray

sources as the prototype of the type II burster class (of which there was just recently a second one found, GRO J1744–28; see Kommers et al. 1997 and references therein.) A detailed summary of our understanding of the Rapid Burster is given in Lewin et al. (1995) and additional extensive work using RXTE observations was presented by Guerriero et al. (1998). A 3″ radius 90% confidence X-ray position has long been known (Grindlay et al. 1984). Rutledge et al. (1998) have recently reported accurate coordinates for a radio source whose radio and X-ray intensities appear to be correlated, although the radio position lies well outside X-ray error circle. Previous attempts to detect bursts from an IR candidate using large-aperture single-channel photometers have produced some inconclusive detections as summarized by Lawrence et al. (1983) but no single candidate has thus far been suggested.

X 1745–203 in NGC 6440 has not received much recent attention but of the remaining cluster objects to be discussed here it suffers from the least amount of extinction and may therefore offer the best chance of discovery of an optical counterpart with the previous highly successful methods at near UV wavelengths. Detections and non-detections of this source with various X-ray satellites indicate that it is highly variable (by factors of 10^4) over long timescales; it is often called a transient source. *ROSAT* HRI coordinates and a summary of the existing X-ray observations are given by Johnston et al. (1995). Just recently in 't Zand et al. (1998a) detected type I X-ray bursts from this source, indicating that X 1745-203 is also a neutron-star LMXB. There has not yet been published a search for the optical counterpart to this source.

In the cluster Terzan 1, X 1732–304 was discovered as a transient burster by Makishima et al. (1981). Subsequent detections by *EXOSAT* (Parmar et al. 1989) and *ROSAT* HRI (Johnston et al. 1995) have steadily improved on the positional uncertainty of this source. Nonetheless no formal search for the optical/IR counterpart of the source has yet been presented.

X 1724-307, associated with Terzan 2, has been studied in X-rays by many satellites for many years. See Barret et al. (1998) for an extensive summary of X-ray work

and new *ASCA* observations. There is no published work about an optical or IR counterpart search.

X1745–248 in Terzan 5 was discovered as a transient burster by Makishima et al. (1981). It was detected by *EXOSAT* observations (Warwick et al. 1988). Subsequent detections by the *ROSAT* All-Sky Survey (Verbunt et al. 1995) and *ROSAT* HRI pointed observations (Johnston et al. 1995) have improved the positional uncertainty of this source to 5″. Nonetheless no formal search for the optical/IR counterpart of the source has yet been presented.

X1747–313 is the only luminous globular cluster source for which bursting has not yet been detected. This source in Terzan 6 was only recently discovered by Predehl et al. (1991) during the *ROSAT* All-Sky Survey (RASS). A more detailed analysis of the RASS data (Verbunt et al. 1995) improves the position and flux, and notes that the *ROSAT* HRI non-detection by Rappaport et al. (1994) suggests that the source faded by at least a factor of 150 between the two observations. Clearly many more X-ray observations will be necessary to achieve even a basic understanding of this source; its status as the only globular cluster source not known to burst is clearly not meaningful with only a single positive detection. The current 20″ 1σ radius positional uncertainty makes an optical/IR counterpart search impractical at this time.

1.3 Conclusion

The goals of this dissertation are to identify the optical counterparts to some GC LMXBs without previously identified counterparts, bring together and compare in the most homogeneous fashion all available *HST* data (new and archival) on the current crop of GC LMXB counterparts, and discuss the implications for cluster dynamics and LMXB systems in general. In the following chapter I will discuss the details of the discovery of three new optical counterpart candidates for the LMXBs in NGC 1851, NGC 6441, and NGC 6652. In chapter 3 I will discuss the ensemble optical properties

of the known optical counterparts. In chapter 4 the existing spectra and broadband spectral energy distributions of the individual sources will be presented. In the final chapter, I will discuss my conclusions and outline how future work will improve our understanding of this important group of objects.

Chapter 2

NEW OPTICAL COUNTERPART IDENTIFICATIONS

2.1 Introduction

Just five years ago, the situation regarding optical counterparts to GC LMXBs changed dramatically. With the advent of work by Anderson et al. (1993) and King et al. (1993), the number of very likely counterparts increased from a single one, known for a decade, to three. Since then progress has continued at a modest pace with the discovery of two additional likely candidates and another more tentative one. In this chapter I detail our work on the search for these three new optical counterparts.

2.2 An Optical Counterpart for X 0512–401 in NGC 1851

2.2.1 Introduction

What follows is a description of the search for and identification of the optical counterpart to X 0512–401 in NGC 1851. This work was previously discussed by Deutsch et al. (1996b).

X-ray observations of the strong source in NGC 1851 are virtually as old as satellite X-ray astronomy, dating back to the days of OSO–7 (Clark et al. 1975); Forman & Jones (1976) first observed the bursting nature of X0512–401 with *Uhuru*. Recent X-ray observations of the system have been made and reviewed by Callanan et al. (1995). This source would seem a particularly good candidate for an optical identification, as there is an accurate *Einstein* HRI X-ray position (Grindlay et al. 1984), and it lies over two core radii ($\sim$12″) north of the cluster center.

Ground-based imaging studies in NGC 1851 by Aurière et al. (1994; hereafter ABK) do not reveal any especially good optical candidate (e.g., no object with marked UV-excess) for the X-ray source X0512–401. However, these authors call attention to an object they denote as X1, as the best candidate they are able to resolve in a 3″ error circle. As its color (U−B∼0) is no more UV than many hot blue horizontal branch stars in the cluster, ABK speculate that X1 may be a new sort of low-mass X-ray binary (LMXB), in which there is very little X-ray heating of the accretion disk.

Previous studies of NGC 1851 using pre–servicing-mission *HST* images did not detect any better candidates (Margon et al. 1992; Deutsch et al. 1994). The WF/PC images used in those studies do not go nearly as deep as the WFPC2 data used in the present work. Deutsch et al. (1994) reported several objects which were bluer than X1 at the detection threshold of those images, but were unable to isolate any single object unusual enough to be considered a better candidate. These earlier studies would have easily revealed counterparts as luminous as AC 211 in M 15 or Star S in NGC 6712. Clearly, deeper exposures are required to look for fainter objects in NGC 1851.

2.2.2 Observations and Data Reduction

Planetary Camera Imagery

On 1996 April 10, we obtained *HST* WFPC2 images of NGC 1851. Two 900 s exposures through the F336W filter were taken, followed by four 300 s F439W exposures, and finally two more 900 s F336W exposures; the F336W and F439W filters are similar to Johnson U and B respectively. The frames have been processed through the standard data reduction pipeline at STScI. Further reduction was performed with software written in IDL by E.W.D. or available in the IDL *Astronomy User's Library* (Landsman 1993). Some photometry was performed with DoPHOT (Schechter et al.

1993).

Although the images were obtained with the fine-lock mode of *HST*, the PSFs clearly show elongation in the Y direction in the Planetary Camera (PC) images, with major to minor axis ratios of about 1.25. Furthermore, while the images show excellent registration in the X direction, Y offsets between exposures through the same filter are as high as 0.4 pixels.

For each filter, the set of four images is combined into one master image using software written by E.W.D. First, cosmic-ray hits are identified in each image and those pixels are set to zero in the data and "exposure mask" arrays. The identification algorithm is similar to the one decribed in Saha et al. (1996), and is carefully adjusted so that the undersampled cores of bright stars with sub-pixel shifts between images are not mistaken for cosmic-ray events. The four images and masks are aligned to $\sim$.01 pixel accuracy and summed. The summed frame is then divided by the mask to obtain the final image. In this way, cosmic-ray event pixels are excluded so that the information in neighboring pixels is not contaminated during interpolation.

Astrometry

In order to determine the position of the X-ray source coordinates on the *HST* PC image, we establish a coordinate system based on the *HST* Guide Star Catalog (GSC) reference frame. We begin with the astrometric solution from a digitized Quick V image used to generate the *HST* Guide Star Catalog (Lasker et al. 1990); this image, obtained directly from ST ScI, contains the astrometric solution in the image header. By centroiding 29 stars in the Quick V image and the corresponding objects in a short ground-based R-band CCD image, kindly provided by H. Ford, the astrometric reference frame is transferred to the CCD image with an error in the solution of $0\farcs1$. Next, the astrometric frame is transferred from the CCD image to the PC image using a set of 9 common isolated stars, with error in the solution of $0\farcs02$, negligible compared to the first step. The final result is that coordinates may be determined

on the PC image to within 0.″1 in the GSC reference frame. However, there may well be some systematic offset, $\sigma \sim 0.''5$, from frames based on other reference catalogs (Russell et al. 1990).

We calculate the weighted mean of the X-ray coordinates from reprocessed *Einstein* HRI data in the HRICFA database obtained through the High Energy Astrophysics Science Archive Research Center Online Service, provided by the NASA Goddard Space Flight Center. These coordinates are not significantly different from those in Grindlay et al. (1984), so we use the published coordinates in this work. The 90% confidence radius is reported by Grindlay et al. (1984) as 3″.

The optical position of the coordinates of the X-ray source chosen by ABK, which we estimate from Fig. 1 of that paper, is ∼1″ northeast of our location, which is not unreasonable given the different source of astrometric reference.

The left panel of Fig. 2.1 shows a 24″×24″ region of the cluster through the F336W filter. A 3″ radius error circle is overlaid, using our astrometric solution. The right panel of Fig. 2.1 shows a 8″×8″ region of the cluster through the F336W filter, centered on our optical position for the X-ray source, which we have marked with a cross.

Photometry

Photometry was performed on the combined F336W and F439W PC frames with the DoPHOT software (Schechter et al. 1993) and a PSF function-fitting procedure written by E.W.D. The results are similar, although DoPHOT was not able to converge accurately on some of the brighter objects; however, it performed better on the fainter objects. For this reason, we use the results derived from DoPHOT. The fitted magnitudes were calibrated with aperture photometry of several isolated objects. Aperture corrections are taken from Table 2(a) in Holtzman et al. (1995b). The photometric measurements have not been corrected for geometric distortions in the PC, but the simple correction for charge transfer efficiency losses detailed in Holtzman et al.

(1995b) has been applied. We use the photometric zero points for the STMAG system from Table 9 in Holtzman et al. (1995a). Systematic errors for all magnitudes due to uncertainties in detector performance, absolute calibration and filter transformations are ~5%.

The photometric results are displayed in Fig. 2.2 as a color-magnitude diagram of all ~5500 objects with reliable measurements in the PC frame. Objects which are mentioned in the discussion below are marked in the diagram.

2.2.3 Discussion

While ABK were only able to resolve 5 stars within a 3″ radius error circle, we are able to resolve and measure magnitudes for 194 objects with $15 \leq m_{439} \leq 23$.

Star X1, suggested by ABK as the best candidate, does have the brightest m_{336} magnitude within the error circle. However, its color and magnitude are unremarkable compared with other cluster horizontal branch stars. We resolve the star labeled as X2 by ABK into two main components, which we label X2a and X2b. Additional, fainter stars also contribute light to X2. Object X2a is nearly in the center of our error circle, but has normal colors. In the CM diagram, X2b is found to have a more UV color than star X1, but is also unremarkable compared with other stars in the cluster (Fig. 2.2).

In the color-magnitude diagram of the entire 34″×34″ PC field, there are two objects which stand out as having marked UV-excess, with colors similar to known LMXBs. One of these is 2.″15 away from our optical position for the X-ray coordinates; this is well within the 90% confidence error circle of the X-ray coordinates. We denote this object as star A and provide magnitude measurements in Table 2.1. Figure 2.3 shows a 3″×3″ region of our PC data centered on Star A. We also label Star B, which is probably unrelated to, but blended with, Star A, at a separation of only 0.″12. The photometry of these objects is slightly hampered by the fact that the elongation of PSFs, discussed in §2.1, is nearly in the same direction as the orientation of these two

stars. Future observations in the optical will be complicated by the proximity of the two objects.

We have also examined the data for possible time variability of star A. The first and last F336W exposures are separated by 3 hr, while the first and last F439W exposure are separated by only 70 min. Neither series shows any significant evidence for variability, although these data do not allow an adequate study. The 1σ photometric uncertainty from photon counting statistics is only 2% and 3% for star A for the F336W and F439W filter exposures, respectively. However, since Star A is blended with Star B, the measurements have a higher uncertainty. On the final F336W exposure, Star A was contaminated with a cosmic-ray event, increasing the error of the measurement for that exposure. We set a variability upper limit of 0.10 mag during the time of our observations. These data could not have detected any small-amplitude, short-term variability of the scale reported by Homer et al. (1996) for the globular cluster X-ray source counterpart Star S in NGC 6712. Archival WF/PC images of NGC 1851 have also been examined for variability. Star A is above the detection threshold only in F336W exposures taken on 21 August 1993. There is no obvious evidence that Star A has changed in brightness during this 2.6 yr interval, but the variability upper limit is not very stringent, $\sim$0.4 mag.

Since star A is not the only UV-excess object in its part of the CM diagram, there is some probability that it is not the X-ray counterpart, but rather an unrelated object similar to the other cluster UV objects. To estimate the probability, we measure magnitudes for all stars in the PC field as well as the three WF fields. Although this larger sample has 13$\times$ more area, it contains only 3$\times$ more stars than the PC field alone, as the latter is centered near the cluster core, and there is a sharp radial gradient of stellar density. Of the 16,000 stars for which we obtain good measurements, we find 4 objects with significant UV-excess of $(m_{336} - m_{439}) \leq -0.5$ in the range $15 \leq m_{439} \leq 22$. We also search each of the fields with an image-subtraction technique to further insure that no UV-excess objects are missed.

Therefore, approximately 1 in 4×10^3 stars with $m_{439} < 22$ in the cluster show a marked UV excess, and as we measure 194 stars within the error circle, we estimate a ~5% probability that one of these UV-excess objects unrelated to the X-ray source will be found in the error circle by chance. The hazards of these *a posteriori* probability estimates are well-known, so this result must surely be regarded as qualitative rather than quantitative. The nature of the faint UV-excess objects observed by *HST* in other globular cluster cores has been recently discussed by numerous authors.

In NGC 6712 the markedly UV-excess optical counterpart Star S is surprisingly optically subluminous as compared with LMXBs in the field. (Anderson et al. 1993). If the magnitude and color of Star S reported in Homer et al. (1996) are corrected for the difference in reddening and distance[1] between NGC 6712 and NGC 1851, one estimates that Star S, were it present in NGC 1851, would have $m_{439} = 19.4$, $(m_{336} - m_{439}) = -0.9$ in this CM diagram. Therefore, while the colors of Star S and the candidate presented here are similar, Star S is more luminous by 1 mag. If Star A is the correct identification of the NGC 1851 X-ray source, the luminosity discrepancy between the GC LMXBs and the field LMXBs is further exacerbated.

To quantify this issue, we use the STSDAS *synphot* package, and find that the blackbody spectrum which best fits the Star A color $(m_{336} - m_{439}) = -0.73$ has $T \sim 20,000$ K. Using a thermal spectrum of this temperature, we derive approximate relations to convert to Johnson U and B magnitudes: $(U - m_{336}) = 0.43$ and $(B - m_{439}) = 0.65$. Applying these zeropoint offsets, we estimate $U = 20.2$, $B = 21.1$, $(U - B) = -0.9$. A typical LMXB in the field has $M_V \sim 1.2$, $(B - V) \sim 0$, and $(U - B) \sim -0.9$ (van Paradijs 1983). Therefore, the NGC 1851 candidate has $(U - B)$ typical of LMXBs, but is underluminous by over 4 mag, with $M_B = 5.6$. One model for the system described by Callanan et al. (1995) invokes a subgiant secondary star;

---

[1]A distance of 12.2 kpc and E(B−V) = 0.02 for NGC 1851, and 6.8 kpc and E(B−V) = 0.46 for NGC 6712 were adopted from Peterson (1993). The reddening curve of Savage & Mathis (1979) was used.

our faint counterpart rules out this possibility if it is indeed the proper identification.

2.2.4 Conclusion

We recompute and confirm the previously-published optical position of the *Einstein* HRI 3″ radius error circle for the bright X-ray source in NGC 1851 using the *HST* GSC as a reference frame. With WFPC2 observations 194 stars are resolved and photometered within the error circle. Star X1, the best candidate previously offered in the literature, is resolved as a single star, but is not remarkable in a CM diagram of the region. Star X2 is resolved as two separate stars, the brighter of which is more UV-excess than X1, but still not remarkable.

However, we find two UV-excess objects in the PC frame, one of which is only 2.″15 from the X-ray source position. Therefore, we suggest this as a much more likely candidate for the optical counterpart of the X-ray source, and we denote it as Star A. We search for, and find no variability for this object in these and archival data. However, the time coverage is poor, and a proper variability study is desirable. We find a total of 4 markedly UV-excess objects in the ∼16,000 objects measured in all four WFPC2 fields, and therefore estimate that there is ∼5% probability that a UV-excess star has fallen in the *Einstein* HRI 3″ radius error circle by chance. Future studies of Star A will be complicated by the presence of an unremarkable but comparably bright companion 0.″12 distant.

Star S in NGC 6712 is known to be significantly underluminous in the optical compared to the typical LMXBs in the field. Star A in NGC 1851 is yet one magnitude fainter. It will be interesting to learn if we are merely sampling a broad underlying luminosity dispersion, or are instead discerning a consequence of a physical property of cluster LMXBs that is fundamentally different from those in the field.

Table 2.1: Photometry and coordinates for selected objects in NGC 1851

Object	$\alpha(2000)$ 5^h14^m (s)	$\delta(2000)$ $-40°02'$ (arcsec)	m_{336}	m_{439}	$(m_{336}-m_{439})$
Star A [a]	6.428	38.38	19.73	20.46	-0.73
Star B	6.425	38.26	20.43	19.92	0.51
Star X1 [b]	6.523	35.81	16.58	15.52	1.06
Star X2a [c]	6.556	36.81	17.51	16.40	1.11
Star X2b [c]	6.592	36.59	16.85	15.92	0.93

[a] Optical counterpart for X0512−401 suggested in this work

[b] Designation from Aurière et al. 1994

[c] X2, a designation from Aurière et al. 1994, is multiply resolved in the current work

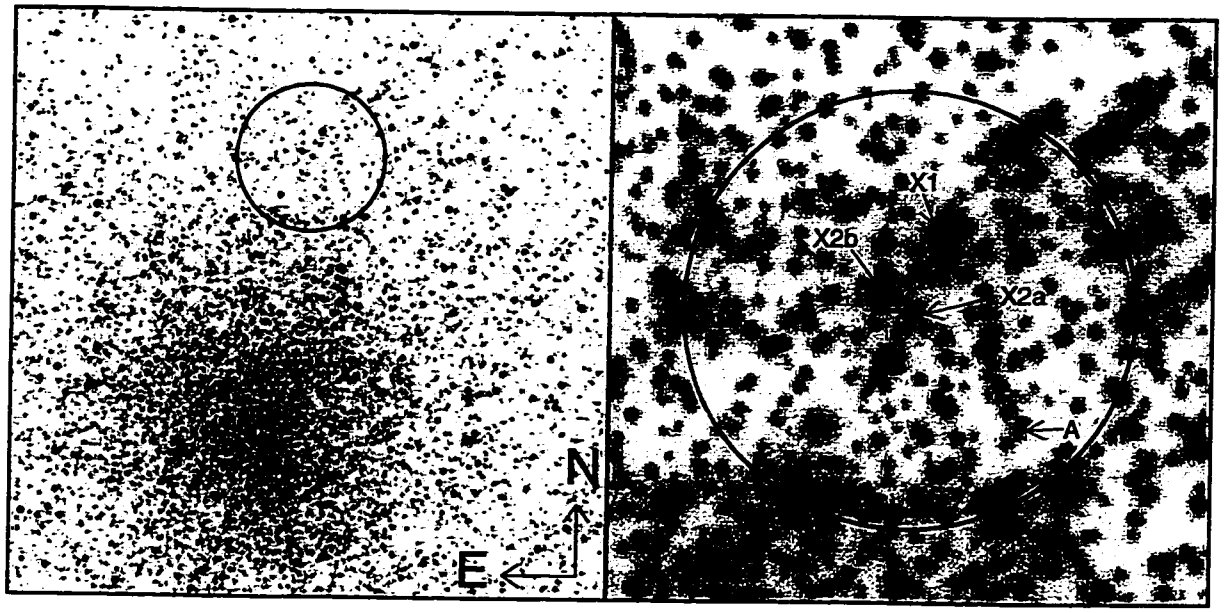

Figure 2.1: *Left Panel*: 24″×24″ section of the *HST* PC image of NGC 1851 with the F336W filter. The image has been reoriented so that North is up and East is left. A 3″ radius error circle is drawn about the position of the X-ray coordinates. *Right Panel*: 8″×8″ section of the same image centered at the X-ray coordinates. A cross denotes the optical position, derived in this work from the GSC source data, of the X-ray coordinates, and the 3″ radius error circle is overlaid. Several objects discussed in the text are labeled. Star A is selected as the optical counterpart due to a significant UV excess.

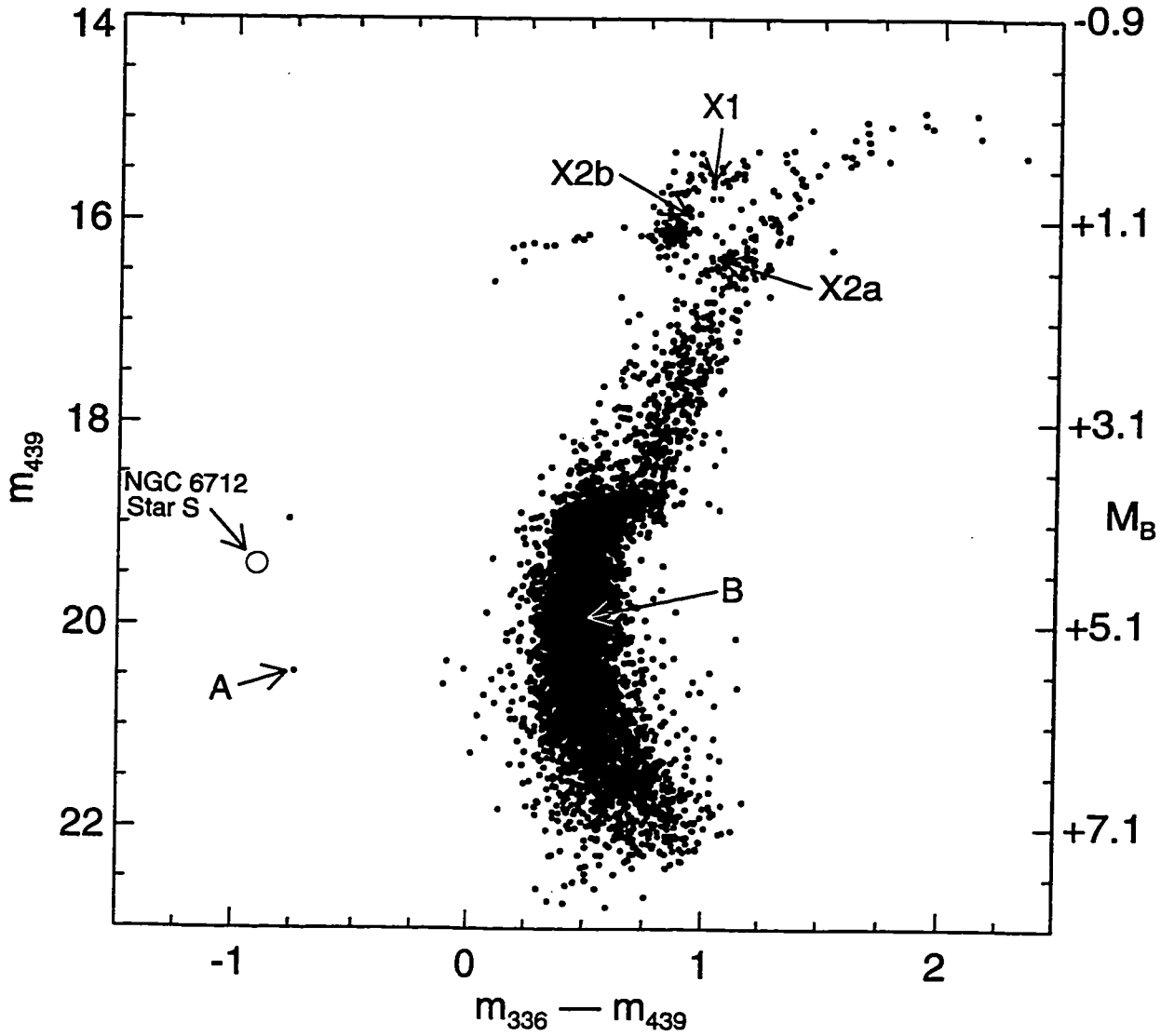

Figure 2.2: A color-magnitude diagram for ~5500 stars in the PC frame of NGC 1851. Magnitudes are in the STMAG system; see text for details. All objects which are discussed in the text are labeled here, including Star A which we select as the optical counterpart due to a significant UV excess. An approximate M_B scale is also provided, assuming (m−M)=15.43, E(B−V)=0.02, and $(B-m_{439}) = 0.65$. This latter correction changes slightly with stellar color; 0.65 is appropriate for F type through the hottest stars, while 0.4 is more appropriate for M0 stars. We also add the distance- and reddening-corrected magnitude and color of Star S in NGC 6712 for comparison.

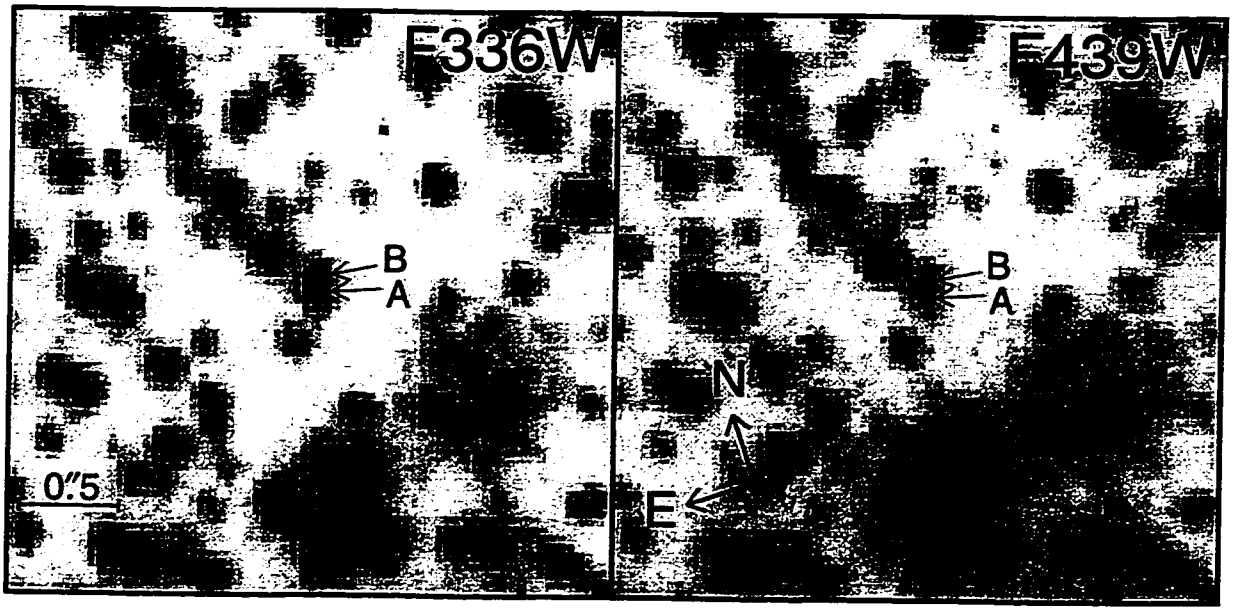

Figure 2.3: $3'' \times 3''$ sections of the F336W (U) and F439W (B) images centered on star A, which we select as the optical counterpart due to a significant UV excess. These images are still in the original orientation, so North and East are labeled. Star B, $0''.12$ distant, is apparently unremarkable, but may complicate future observations.

2.3 An Optical Counterpart for X 1746–370 in NGC 6441

2.3.1 Introduction

What follows is a description of the search for and identification of the optical counterpart to X 0512–401 in NGC 1851. This work was previously discussed by Deutsch et al. (1998).

The intense X-ray source in the core of NGC 6441, X 1746–370 (= 4U 1746–37), is a "classical", high X-ray luminosity ($L_X \sim 6 \times 10^{36}$ erg s^{-1}) burster observed for many years, by many satellites. However, it is distinguished by being one of the few cluster sources with a periodic X-ray modulation, exhibiting a 5.7 hr period of $\sim 5\%$ amplitude (Parmar et al. 1989, Sansom et al. 1993). The source is located just 6″ ($\sim 1\ r_c$) from the cluster center, and thus the optical field is very crowded. To our knowledge there has not even been a past suggestion of a candidate optical counterpart before this work, despite some effort (Bailyn et al. 1988). The small number of high luminosity cluster sources for which details are available already presents a confusing picture: despite similar X-ray luminosities, their optical luminosities and orbital periods differ by several orders of magnitude. The orbital period of this object is intermediate between the NGC 6624/6712 sources and M 15 AC 211.

We report here on the results from WFPC2 images in NGC 6441. This work extends the preliminary results and original counterpart identification suggested in Deutsch et al. (1996a).

2.3.2 Observations and Data Reduction

Planetary Camera Imagery

On 1994 August 8, we obtained *HST* WFPC2 images centered on NGC 6441 through the F336W (50 s, 2 × 500 s) and F439W (50 s, 500 s) filters. These frames are free of any artifacts or scattered light from the nearby bright star HR 6630 ($V \sim 3$)

which often hinders observations of this cluster. The images were processed through the standard data reduction pipeline at ST ScI. Further reduction is performed with software written in IDL by E.W.D. or available in the IDL Astronomy User's Library (Landsman 1993).

The sets of exposures are combined with a cosmic-ray rejection algorithm. We use DoPHOT (Schechter et al. 1993) to photometer stars in all four chips of the WFPC2. The PSF-fit magnitudes are calibrated using aperture photometry of isolated stars, where aperture corrections are taken from Table 2(a) in Holtzman et al. (1995b). The photometric measurements are not corrected for geometric distortions, nor is any correction for charge transfer efficiency losses (Holtzman et al. 1995b) applied, as there is sufficient charge on the chips to minimize this effect. We use the photometric zero points for the STMAG system from Table 9 (Z_{STMAG}) in Holtzman et al. (1995a). Systematic errors for all magnitudes due to uncertainties in detector performance and absolute calibration are $\sim$5%. As discussed later, severe crowding may lead to larger overall photometric uncertainties for some objects.

Astrometry

In order to determine the position of the X-ray source coordinates on the *HST* PC image, we establish a coordinate system based on the *HST* Guide Star Catalog (GSC) reference frame as done in §2.2.2. By centroiding 38 stars in the Quick V image and the corresponding objects in a ground-based CCD image, kindly provided by G. Jacoby, the astrometric reference frame is transferred to the CCD image with an error in the solution of $0\farcs03$.

There are only three stars which are sufficiently isolated to be well-resolved in the ground-based data within the PC field of view, so instead of transferring the solution from the CCD to the PC image, we correct the astrometric information originally provided in the PC header for the average observed offset in position for these three stars (coordinates measured in the PC frame are adjusted by $\Delta\alpha = +0\farcs2$

and $\Delta\delta = +0\farcs5$). The final result is that coordinates may be determined on the PC image to within $\sim 0\farcs1$ in the GSC reference frame. However, there may well be some systematic offset, $\sigma \sim 0\farcs5$, from frames based on other reference catalogs (Russell et al. 1990). It should be noted that NGC 6441 is near the edge of the Quick V plate, where systematic errors can be higher.

Figure 2.4 shows the entire $33'' \times 33''$ F336W PC frame, with our position for the $3''$ radius X-ray error circle overlaid, as well as the $8'' \times 8''$ region around the circle. The X-ray coordinates are derived from *Einstein* HRI observations by Grindlay et al. (1984), who report the 90% confidence error as $3''$.

2.3.3 Discussion

Color-Magnitude Diagram

From all four WFPC2 chips we select $\sim$17,000 stars for which we have obtained good photometry, and plot their colors and magnitudes in Fig. 2.5. The scatter in the diagram is largely due to the extreme crowding, even by *HST* standards, in this cluster. There is also doubtless some contamination from field stars for this low Galactic latitude cluster ($b \sim -5°$).

We label five objects on the diagram. Star U1 is the most UV-excess object within the X-ray error circle (but not in the cluster!). U7, a star of similar color and magnitude, but well outside the error circle, is discussed below. Stars B1 and B2 are bluer than the other 245 objects in the error circle (except U1), but seem to be part of a large population of stars which compose a formidable blue tail of the horizontal branch; they are not likely to be related to the X-ray source. We also indicate a rare object, the central star of the globular cluster planetary nebula JaFu 2 (Jacoby & Fullton 1994; Jacoby et al. 1996, 1997). These five objects are discussed further below.

An isochrone from Bertelli et al. (1994) is added to the diagram for compari-

son. We select a 14 Gyr isochrone with [Fe/H] = −0.40, the closest available to the published metallicity for NGC 6441, [Fe/H] = −0.53 (Djorgovski 1993), and apply distance modulus $(m - M)_0 = 15.15$ (Djorgovski 1993). The isochrone U and B magnitudes are converted to m_{336} and m_{439}, where the corrections depend on color; these corrections are estimated using the STSDAS *synphot* package. Finally, we apply reddening to the isochrone, although we find that $E(B - V) = 0.50$ yields a better fit to the giant branch than the published value $E(B - V) = 0.42$ (Djorgovski 1993). However, the uncertainties in the metallicity and filter conversion may easily account for this small shift. Qualitatively, the turnoff and giant branch are modeled well by the isochrone. The known planetary nebula central star lies near the predicted track. The M_{B_0} scale uses a filter correction $B - m_{439} = 0.65$. This correction changes slightly with stellar color; 0.65 is appropriate for F type through the hottest stars, while 0.4 is more appropriate for M0 stars.

Typically a metal-rich cluster such as NGC 6441 has a very red horizontal branch, and so it is surprising that our diagram exhibits a bimodal horizontal branch distribution with such an extensive blue tail. These peculiarities in NGC 6441 were recently discussed in results from a study of several metal-rich globular clusters with *HST* by Rich et al. (1997), where some possible explanations are explored.

NGC 6441 also appears to contain a sizable population of supra-horizontal branch stars, which can be seen in our diagram as well as in Rich et al. (1997). The bluest supra-horizontal branch stars and members of the blue tail may be the principal contributors to the significant but unresolved far-ultraviolet radiation detected with *IUE* by Rich et al. (1993). It is possible that some of these objects are not cluster members, but they do seem to follow the same radial distribution as other cluster stars.

Finally we point out a group of stars even bluer than the extreme blue horizontal branch stars. Two noteworthy members of this population are U1 and JaFu 2, our candidate for the optical counterpart to the X-ray source and a planetary nebula

central star, respectively. It remains to be seen if the nature of the other stars in this group is equally exotic.

Star U1

The UV-excess object which we denote U1 is the only unusual star in the X-ray error circle, and it is therefore an obvious optical counterpart candidate to the globular cluster bursting X-ray source X 1746–370. Figure 2.6 shows a $3''\times3''$ section of both the F336W (U) and F439 (B) images centered on this object. Its $M_{B_0} = 3.0 \pm 0.1$ and $(U-B)_0 = -1.0 \pm 0.1$ may be compared with the typical X-ray burster in the field which has $1 \lesssim M_B \lesssim 5$ and $(U-B) = -1.0$ (van Paradijs 1995). Therefore, not only is the color unusual for a globular cluster star, but the color and magnitude naturally associate the object with known X-ray burster optical counterparts. Based on our astrometric solution derived from the *HST* GSC, we find coordinates for Star U1 $\alpha(2000) = 17^{\rm h}50^{\rm m}12\overset{\rm s}{.}61$, $\delta(2000) = -37°03'06\overset{''}{.}5$. The measurement uncertainty here is negligible compared to the external uncertainties discussed in §2.2.

To explore possible variability of Star U1, we perform aperture photometry on this object and two other nearby objects of similar magnitude and color for all publicly-available *HST* WFPC2 and (pre-COSTAR) FOC observations of this field, and present the results in Table 2.2. Magnitudes are in the STMAG system for both instruments (therefore permitting intercomparison) and 1σ errors are provided. The considerable reddening correction has not been applied to these magnitudes.

We find clear evidence for ~30% variability between our two long F336W exposures, taken only 27 min apart. Another short F336W exposure and an FOC F342W image also indicate large variability, although the photometric errors are higher and filter/instrument differences could be responsible for at least part of the apparent discrepancy. Additional evidence for the variability of Star U1 comes from a ~60% change in m_{439} between our observations and similar observations in the archive taken 1.1 yr later for another program. During the same period, measurements for Stars U7

and B2 (UV and blue stars respectively of similar magnitude) are consistent with no variability within the uncertainties. Such large-amplitude variability for U1 clearly adds considerable confidence that it is indeed the optical counterpart to the low-mass X-ray binary (LMXB).

We note that the X-ray source in NGC 6441 shows variability on timescales of 0.25 hr at amplitudes of ~15% (Parmar et al. 1989). Assuming our suggested identification is correct, our data indicate $L_X/L_{opt} \sim 10^3$, implying that X-ray fluctuations may be promptly reprocessed into detectable optical variability. Thus the similarity of the observed X-ray and optical variability timescales may not be coincidental.

Despite the unusual color and variability, this identification is not completely secure, however, due to a large number of other UV-excess objects in the cluster, as can be seen in the color-magnitude diagram. In order to estimate the probability that one of these UV-excess stars has fallen in the X-ray error circle by chance, we note that there are 21 objects with $(m_{336} - m_{436}) < 0.0$ in our sample of ~17,000 stars. Therefore, approximately 10^{-3} of the stars with $m_{439} < 22$ in the cluster have marked UV excess, and as we measure 245 stars within the error circle, we estimate a ~30% probability that one of the UV-excess population objects would fall by chance in the error circle and might be mistaken for the optical counterpart to the X-ray source. The hazards of these *a posteriori* probability estimates are well-known, so this result must surely be regarded as qualitative rather than quantitative, but the conclusion can also be reached visually from the distribution of UV sources seen in Fig. 2.7. We find the fraction of ultraviolet-excess stars in the cluster intriguing; it exceeds by $\sim 5\times$ an analogous observation for NGC 1851 by Deutsch et al. (1996b) (and §2.2).

Previous workers have noted the marked dispersion in optical luminosities of globular cluster X-ray source counterparts. If U1 is indeed the correct counterpart of the NGC 6441 source, it falls at an optical luminosity similar to that of the NGC 6624 source and intermediate between the sources in NGC 6712 (Anderson et al. 1993) and NGC 1851 (§2.2 and Deutsch et al. 1996b), which are remarkably faint, and that of

M15 AC211.

We also attempted *HST* spectroscopic observations of U1 with the Faint Object Spectrograph on 1995 July 25, using G160L and G570H gratings, which cover the 1150−2500 Å and 4600−6800 Å regions, respectively. The resulting G570H spectrum exhibits only spectral features typical of a late G star. The absolute flux level in the spectrum is about 4× higher than m_{555} for Star U1 in Table 2.2, but is consistent with the total F555W light in a 0.″5 diameter circle (the size of the FOS aperture used) centered on this object as measured on a WFPC2 image. We conclude that most of the light in this spectrum is most probably contributed by nearby sources other than Star U1.

The count rate in the G160L spectrum is so low that flux coming from the source cannot be distinguished from an imperfect scattered light subtraction. We set upper limits of order 3×10^{-17} erg cm^{-2} s^{-1} Å^{-1} at 1600 Å and 1×10^{-17} erg cm^{-2} s^{-1} Å^{-1} at 2100 Å. These upper limits are $\sim 3\times$ lower than the measurements obtained from FOC and WFPC2 observations of this source. This may indicate very large amplitude variability, for which of course there is already direct imaging evidence. However, the FOS observations were executed by making a blind offset from a nearby bright star, and it cannot be guaranteed that Star U1 was actually in the aperture for either the G160L or G570H spectra.

2.3.4 Planetary Nebula JaFu 2

Planetary nebulae are rare in globular clusters; only 4 have been discovered despite considerable effort (Jacoby & Fullton 1994; Jacoby et al. 1997). We measure a magnitude and color for the central star of the planetary nebula JaFu 2 in NGC6441 (Jacoby & Fullton 1994; Jacoby et al. 1996) which are remarkably similar (Fig. 2.5) to that of Star U1, our proposed X-ray source optical counterpart. This similarity naturally leads to the possibility that Star U1 may be of comparable nature to JaFu 2, but we believe that the similarity must be coincidental. The planetary nebula

star lies quite close to predicted evolutionary tracks, and so its observed properties are consistent with photospheric radiation from a hot, single star. The X-ray source, on the other hand, must be a low-mass binary system containing a neutron star, as X-ray bursts are observed (Li & Clark 1977; Sztajno et al. 1987), and thus its integrated light contains contributions from the compact star, the accretion disk, and the companion. The observed magnitude and colors of Star U1 are consistent with those of bursters in the field. Therefore, despite the unusual nature of both objects, one could have predicted in advance that they could both occupy the same place in the cluster color-magnitude diagram and yet be physically dissimilar.

The natures of two of the UV-excess objects in this cluster have now probably been determined, but the other UV-excess sources remain unexplained. Since they are not luminous in X-rays, they are not similar to Star U1. They may well be planetary nebula central stars, where the surrounding nebula has long since dispersed. However, the cases of Star U1 and JaFu 2 have shown that a similarity in color and magnitude in this diagram does not allow us to infer similarity in nature.

2.3.5 Conclusion

We have examined WFPC2 images in NGC 6441 for the optical counterpart to X 1746–370. A color-magnitude diagram of ~17,000 stars in all 4 chips reveals a bimodal horizontal branch with a long blue tail. Nearly two dozen strongly UV-excess objects are also seen in the CM diagram. Our astrometry, based on the *HST* GSC, places the 3″ X-ray error circle accurately onto the PC frame. Only one of the UV-excess objects or otherwise unusual stars falls within this error circle. The magnitude ($M_{B_0} = 3.0$) and color ($U - B_0 = -1.0$) for Star U1 are typical of the average properties of bursting X-ray sources in the field. We detect a ~30% variability between our F336W images separated by 0.5 hr, and a ~60% variability between our F439W frames and F439W images taken 1.1 yr later. The color and variability combine to make U1 a very strong candidate for the optical counterpart.

We do note that there is a sizable population of UV-excess stars in the cluster and calculate a ~30% probability that a member of this population would have fallen in the X-ray error circle by chance. An FOS spectrum ostensibly of Star U1 detects no significant UV flux with an upper limit 3× lower than fluxes obtained from imaging, indicating either very high UV variability or target acquisition failure. We plan *HST* STIS time-resolved spectroscopy to attempt to confirm the candidate and lead to better understanding the nature of this object.

Table 2.2: Photometry for selected objects in current observations and archival *HST* data of NGC 6441

Filter (Camera)	Obs Date	Start Time	Exp. Time	Star U1		Star U7		Star B2	
			(s)	(mag)	(err)	(mag)	(err)	(mag)	(err)
F140W (FOC)	93/09/28	03:29	996	19.20	0.24	19.03	0.15	> 20.8	0.8
F210M (FOC)	93/09/28	04:51	996	20.22	0.36	19.56	0.18	20.01	0.25
F218W (WFPC2)	95/09/12	06:13	500	19.73	0.18	19.16	0.15	20.19	0.26
		06:24	1000	19.94	0.15	19.44	0.11	20.14	0.15
F336W (WFPC2)	94/08/08	13:37	50	19.12	0.07	18.61	0.05	19.09	0.07
		13:40	500	18.87	0.02	18.62	0.01	19.07	0.02
		14:07	500	19.19	0.03	18.65	0.02	19.08	0.02
F342W (FOC)	93/09/28	05:13	496	18.81	0.09	18.79	0.04	19.07	0.10
F439W (WFPC2)	94/08/08	13:52	50	19.19	0.10	18.91	0.05	18.67	0.05
		13:55	500	19.28	0.04	18.87	0.02	18.65	0.03
	95/09/12	06:01	50	18.77	0.06	18.91	0.06	18.57	0.06
		06:04	160	18.80	0.04	18.78	0.04	18.61	0.04
		06:08	160	18.75	0.04	18.80	0.04	18.63	0.04
F555W (WFPC2)	95/09/12	05:55	14	18.94	0.06	19.25	0.06	18.95	0.06
		05:57	50	18.95	0.04	19.26	0.06	18.94	0.07

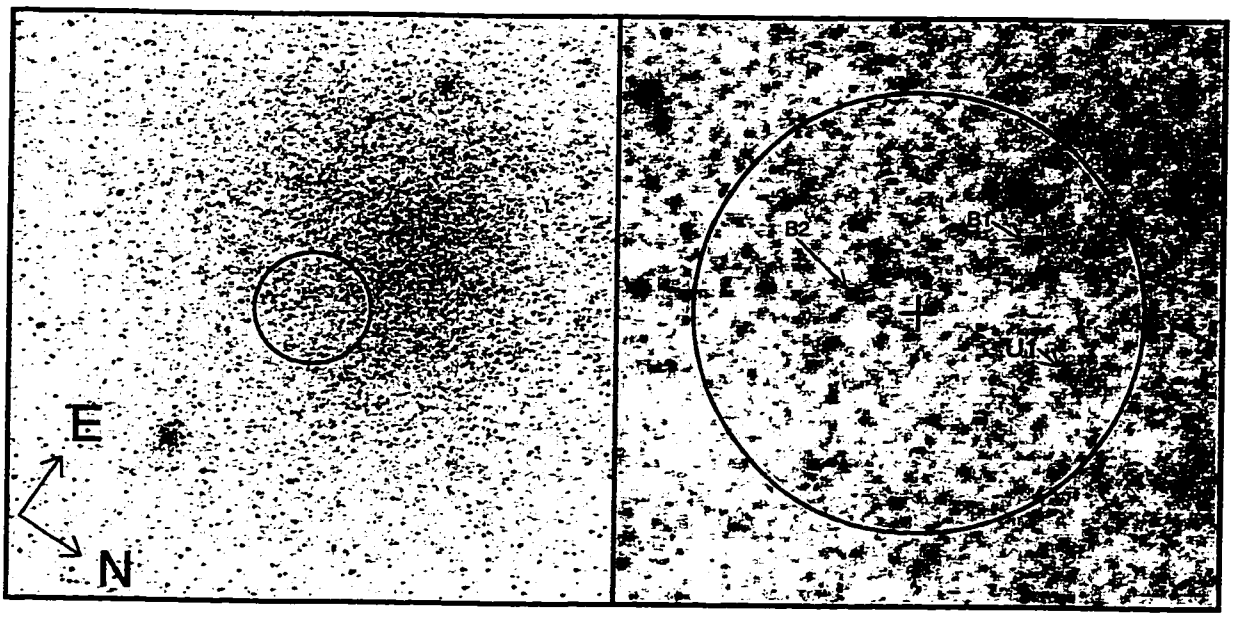

Figure 2.4: *Left panel*: 33″×33″ *HST* WFPC2 PC image of the core of NGC 6441 with the F336W (U) filter. A 3″ radius error circle has been drawn about the *Einstein* HRI coordinates for the luminous bursting X-ray source X1746–370. *Right panel*: 8″×8″ section of the same image, centered at our optical position for the X-ray coordinates (indicated with a cross). Ultraviolet-excess object U1, which we offer as a likely optical-counterpart candidate, is indicated along with two blue stars (labeled B1 and B2) which also fall within the error circle.

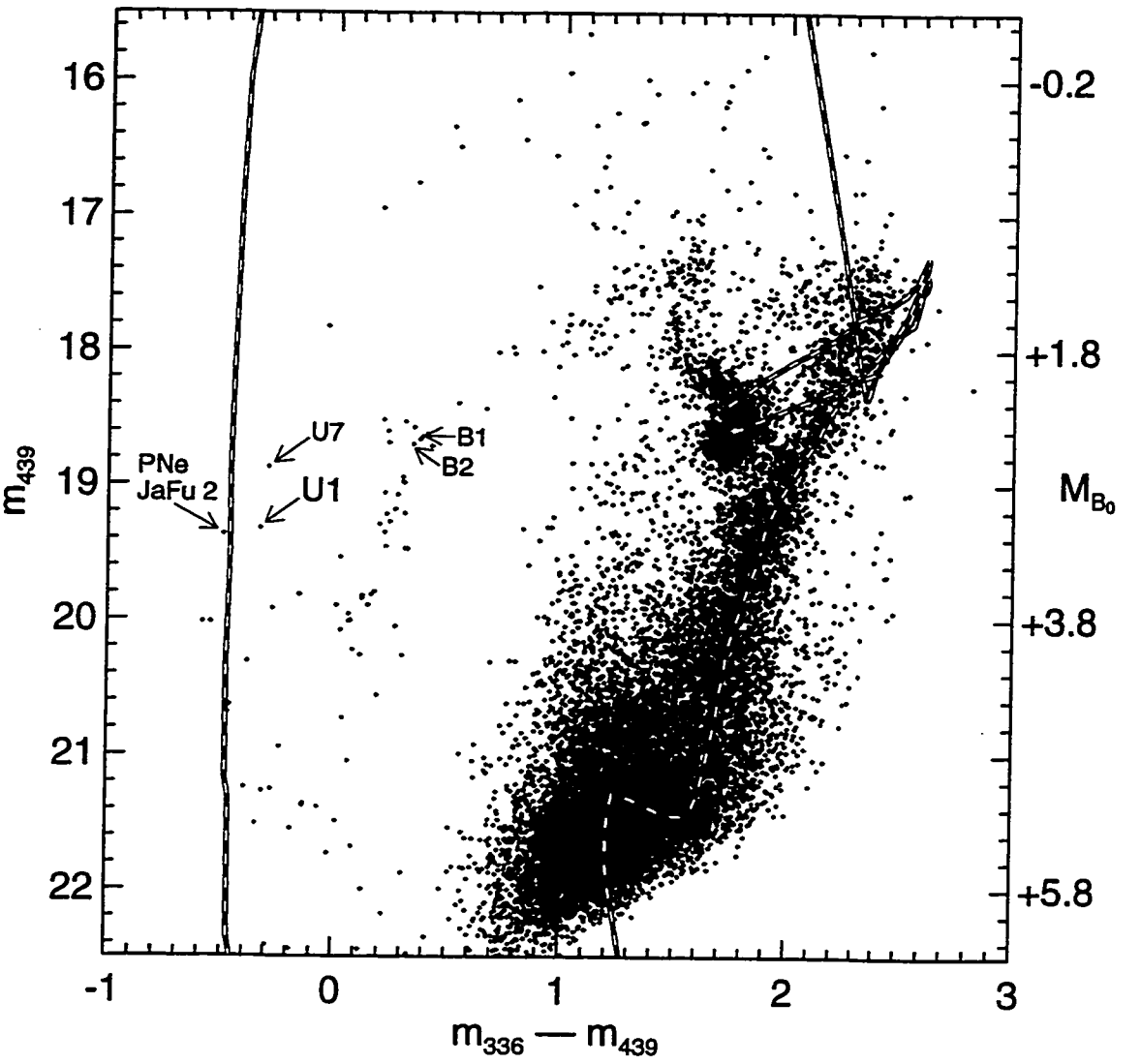

Figure 2.5: Color-magnitude diagram for ~17,000 stars in NGC 6441 on all 4 chips of the WFPC2 exposures. Magnitudes are in the STMAG system; see text for details. Objects which are discussed in the text are labeled: Star U1, which we select as a candidate optical counterpart due to significant UV excess and variability; the central star of cluster-member planetary nebula JaFu 2; blue Stars B1 and B2, which also fall within the X-ray error circle but are probably not related to the X-ray source; Star U7, one of several objects with similar color and magnitude to U1. Note the surprisingly well-populated branch of extreme blue horizontal branch stars typified by B1 and B2. An isochrone from Bertelli et al. (1994) is also overlaid; see text for more details.

Figure 2.6: $3'' \times 3''$ sections of the F336W (U) and F439W (B) images centered on Star U1, which we select as a candidate optical counterpart due to significant UV excess and variability. These images were obtained on 1994 August 8 (cf. Table 2.2).

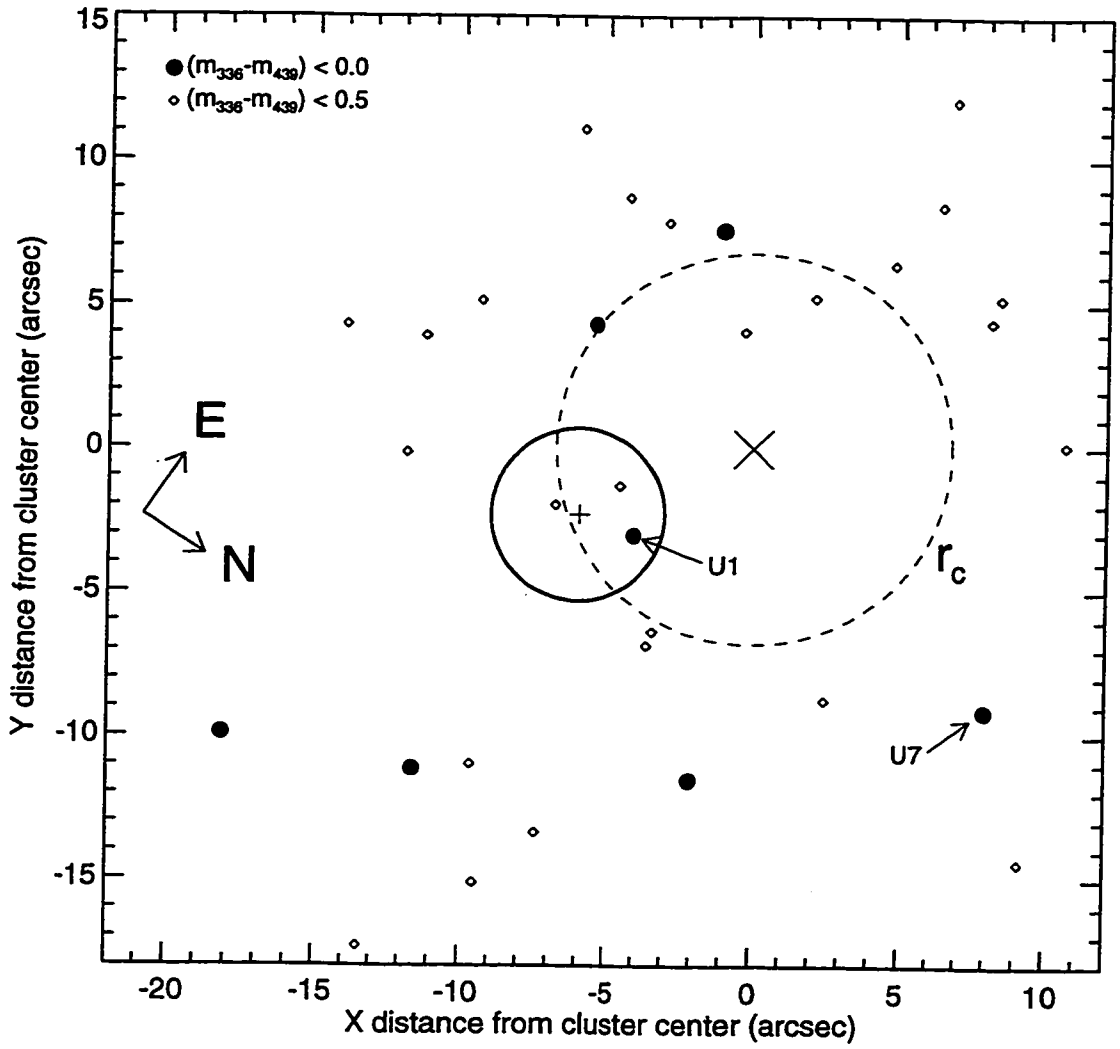

Figure 2.7: The locations of the UV stars $(m_{336} - m_{436}) < 0.0$ and blue stars $(m_{336} - m_{436}) < 0.5$ on the PC image (compare to Fig. 2.4). The *Einstein* X-ray error position (cross) and 3″ radius error circle are shown (solid line). The cluster center and core radius are shown with a × and dashed-line circle, respectively. Stars U1, B1, and B2 are within the error circle, but a considerable population of both UV and blue stars can be seen throughout the entire PC image. Note that the bluest objects do not appear to have a marked central concentration.

2.4 A Tentative Optical Counterpart for X 1832–330 in NGC 6652

2.4.1 Introduction

Here I present results on a search for the optical counterpart, for which there is as yet no candidate, to X1832–330, the luminous ($L_X \sim 10^{36}$ erg s^{-1}) X-ray burst source near the center of the globular cluster NGC 6652, previously discussed by Deutsch, Margon, & Anderson (1998a). This section extends the preliminary work presented by Deutsch, Margon, & Anderson (1997).

This X-ray source was probably first detected as H1825–331 in the HEAO-1 survey. However, as the 2.7 deg^2 90% confidence error box contained the cluster, but was very close to the Galactic Center, Hertz & Wood (1984) conservatively allowed that an association with NGC 6652 would be premature. With the significantly-better spatial resolution of the *ROSAT* All-Sky Survey (RASS), Predehl et al. (1991) reported a bright X-ray source which was indeed coincident with NGC 6652 to within 1′. Using reprocessed RASS data, Verbunt et al. (1995) estimate that the flux was as much as $\sim 10\times$ higher (depending on spectral assumptions) than during the HEAO-1 detection. Pointed observations with the *ROSAT* PSPC 1.5 yr after the RASS find the source somewhat brighter still, and show ∼20% variations on a time scale of a few hours (Johnston et al. 1996). X-ray luminosity estimates inferred from these various observations span the range $L_X = 10^{35} - 10^{36}$ erg s^{-1}, all normalized to the 0.5–2.5 keV band and distance adopted below. This luminosity variation prompted Verbunt et al. (1995) to label this source as a transient, although the variability observed thus far seems orders of magnitude less than that of sources indisputably called transients. Most luminous globular cluster X-ray sources are known to be bursters, indicating that the primaries are neutron stars. Just recently X1832–330 joined the ranks of known bursters when two Type I bursts were reported by in 't Zand et al. (1998).

Ortolani et al. (1994) present the first color-magnitude study of NGC 6652. They derive $(m - M)_0 = 14.85$ ($d = 9.3$ kpc), $E(B-V) = 0.10$, and estimate [Fe/H] ≈ -0.9.

These values are similar to previous determinations except for the distance, which is 30% closer. From the compilation of Trager et al. (1993), we adopt a core radius $r_c = 4\farcs3$. X1832–330 should be a relatively easy target for a search for an optical counterpart as NGC 6652 is neither heavily reddened nor extremely dense, whereas most of the clusters which harbor luminous X-ray sources do fall into one or both of these two categories. However, as the cluster is near the Galactic center ($l = 1\fdg5$, $b = -11\fdg4$) the contamination of the field by bulge stars is of some concern. A brief study of this issue is presented by Ortolani et al. (1994). Finally we note that in their color-magnitude diagram, Ortolani et al. (1994) indicate a sizable population of blue stragglers.

2.4.2 Observations and Data Reduction

X-ray Coordinates

While the initially-reported RASS coordinates had only 1′ accuracy, they were refined by Verbunt et al. (1995) to a 1σ uncertainty of 20″; even the latter would make a search for an optical counterpart difficult. However, a short pointed *ROSAT* HRI observation of NGC 6652 obtained on 1994 March 28 is available in the archive. From these observations, we measure coordinates $\alpha(2000) = 18^{\rm h}35^{\rm m}44\fs0$, $\delta(2000) = -32°59'29''$, which agree with the position given as preliminary by Grindlay (1995).

The uncertainty of these coordinates is almost entirely due to the uncertain telescope aspect, as the source is well detected. From a study by Voges (1998) of the correlation between *ROSAT* HRI source positions and stars in the Tycho Catalog (ESA, 1997), we infer based on ∼3500 matches that the 1σ, 90% confidence, and 2σ uncertainties are $5\farcs3$, $8\farcs3$, and $10\farcs2$, respectively. These values are consistent with the analysis of HRI uncertainties by David et al. (1992).

These X-ray coordinates are more uncertain than the *Einstein* HRI positions available for some sources in other clusters. Unfortunately no X-ray sources appear in the

ROSAT HRI exposure other than the cluster source, so correction of the X-ray aspect via association with other optical identifications, e.g. bright foreground stars, is not possible. However, the coordinates are centered 20.″5 (4.8 r_c) from the cluster center where the crowding is not severe by *HST* standards, so the search of a large error circle is still feasible.

Ground-Based Imagery

To find the precise optical position of the X-ray coordinates, we create an astrometric solution for a ground-based B-band CCD image (kindly provided by S. Wachter) by using 21 isolated stars in common between the CCD image and the Digitized Sky Survey, which is based on the *HST* Guide Star Catalog (GSC) reference frame. The uncertainty in this transfer is 0.″04. With this transferred coordinate system, we place a cross at our optical position for the X-ray coordinates in Fig. 2.8. The systematic uncertainty in the GSC frame with respect to other astrometric frames for a typical region is ∼0.″5 (Russell et al. 1990). Overlaid in Fig. 2.8 are 5.″3 (1σ) and 10.″2 (2σ) radius X-ray error circles. From this CCD image, obtained in 1.″3 seeing conditions, it is clear that the field is quite crowded from the ground. As only one color was obtained, these data are not directly suitable for searching for an optical counterpart.

On 10 June 1997 we obtained brief U (300 s) and B (100 s) exposures of NGC 6652 with the Taurus Tunable Filter (TTF) (Bland-Hawthorn & Jones 1998) in a broad-band imaging mode on the Anglo-Australian Telescope (AAT). Despite the 3.″5 seeing and cirrus conditions at the time of the exposures, these frames are deep enough to search part of the range of expected luminosities. We subtract the two frames in order to search for some excess UV flux in the error circles, but find none. If we assume that the counterpart has $(U-B)_0 \sim -1$, similar to the other known cluster counterparts, we are able to set a lower limit $M_{B_0} \gtrsim 3.5$ within the entire 2σ X-ray uncertainty radius, using artificial star tests. Three of the five currently-known optical counterparts have luminosities brighter than this (Deutsch et al. 1998), and therefore could have been

detected with these data, had they been in NGC 6652.

HST Imagery

The recent success in discovering optical counterparts to the globular cluster X-ray sources has largely been due to their considerable UV excess, $(U-B)_0 \sim -1.0$, observed in *HST* images. We therefore take this same approach here, and search for UV-excess objects in a color-magnitude diagram of the cluster. *HST* WF/PC and WFPC2 observations of this cluster, taken as part of unrelated programs, are available in the *HST* data archive, and we have extracted these images for this work. The *HST* fields of view are overlaid on the ground-based CCD frame in Fig. 2.8. The WF/PC observations were obtained at three different offsets and exposure times for each filter, while the WFPC2 observations were all at the same pointing. It can be seen from the figure that, simply by chance, the X-ray error circles extend somewhat beyond the boundaries of the *HST* frames. While these data are clearly not optimal, there is a reasonably good chance of success in isolating the optical counterpart to X1832–330.

To place the position of the X-ray coordinates on the *HST* images, we transfer the astrometric solution from the CTIO CCD image discussed in §2.2 to these images. The internal errors in the transfer are negligible compared to the systematic uncertainties in the GSC frame as discussed above.

For the WFPC2 images, measured magnitudes are calibrated to the STMAG system using the photometric zero points from Table 9 (Z_{STMAG}) in Holtzman et al. (1995a). Aperture corrections are taken from Table 2(a) in Holtzman et al. (1995b). There has not been any correction applied for geometric distortions or charge transfer efficiency losses (Holtzman et al. 1995b) as the small errors introduced by these effects are not of concern for our purposes here.

The WFPC2 observations used the F218W (500 s, 900 s), F439W (50 s, 2 × 160 s), and F555W (10 s, 50 s) filters; the latter two closely resemble Johnson B and V

filters, respectively. There are no objects detected within 15″ of the X-ray position in the F218W exposures (which do not image the entire error circle), with lower limit $m_{218} > 19.7$. If we assume that the optical counterpart has $(m_{218} - m_{439})_0 = -1.4$, similar to the optical counterpart in NGC 6441 (§2.3 and Deutsch et al. 1998), we infer a lower limit of $m_{439} > 20.5$ or $M_{B_0} > 5.2$ in the region of the error circles subtended by the WFPC2 exposures. This value may be compared with $M_{B_0} = 5.6$ for the least luminous globular cluster counterpart, Star A in NGC 1851 (Deutsch et al. 1998).

As the optical counterparts in other clusters have been strongly UV excess with unremarkable $(B - V)_0$ colors, the F439W and F555W images are not suitable for isolating a counterpart based on color alone. However, observed variability can be used to identify a counterpart, as optical/UV variability has been detected for all of the known counterparts for which a suitable study has been performed. Unfortunately, these short consecutive snapshots are unlikely to allow detection of anything but extremely-short timescale, high-amplitude variability. The images have been examined for objects of such variability, but none are found.

Although not as deep as the WFPC2 observations, the (pre–servicing-mission) WF/PC images have better areal coverage of the error circle and use two near-optimal filters, F336W (300 s, 900 s, 1200 s) and F439W (100 s, 300 s, 400 s), those also used to identify several other counterparts. We concentrate here on the regions of the WF/PC images which include the X-ray error circles. In Fig. 2.9 we show a corner section of one of the F439W exposures, with a cross placed at the X-ray coordinates. 5.″3 and 10.″2 error circles are displayed as in Fig. 2.9. All images have been cleaned of cosmic-ray hits by an algorithm written by E.W.D. The images were then carefully inspected and any shortcomings of this algorithm were repaired manually; stars which have been clearly hit by a cosmic-ray event were excluded from the color-magnitude diagram.

Initial photometric zero points were taken from the PHOTFLAM keywords in

the headers. However, another correction was applied to calibrate the WF/PC m_{439} magnitudes to the WFPC2 m_{439} magnitudes. This correction was calculated using a set of isolated stars in common between images from both cameras, and is primarily an aperture correction, which is difficult to determine for WF/PC images. This same correction was applied to the m_{336} magnitudes.

2.4.3 Discussion

Color-Magnitude Diagram

Figure 2.10 shows a color-magnitude diagram derived from aperture photometry of the WF/PC F336W and F439W observations. Included are the ~150 objects in PC6 which are detected in the F336W data. Stars within $r < 2\farcs5$ from the cluster center are excluded as the crowding there causes large errors in the photometry. All objects in this excluded region are $> 18''$ from the X-ray position, and thus this procedure does not affect the search for the optical counterpart. Magnitudes are in the STMAG system, and formal 1σ error bars are provided for each source. Non-negligible flat-fielding imperfections as well as the numerous low-level cosmic-ray hits will cause some sources to be in error by more than the estimated uncertainties.

We overlay an isochrone from Bertelli et al. (1994) for comparison. The 12 Gyr, [Fe/H] $= -0.7$ isochrone has been converted to the STMAG system (conversion factors derived using the STSDAS *synphot* package), corrected for $(\mathrm{m} - \mathrm{M})_0 = 14.85$, and reddened by $\mathrm{E}(B-V) = 0.10$. The isochrone does not fit in detail but indicates that the distance, reddening, and metallicity parameters yield an isochrone which follows the observed points reasonably well, particularly given the uncertainties in the filter transformations and absolute calibration. It can be clearly seen, however, that these data do not even reach the main-sequence turnoff adequately. The M_{B_0} scale incorporates the filter correction $(B - m_{439}) = 0.50$, although the true correction should vary slightly with stellar color; 0.65 is appropriate for stars hotter than type

F, and the correction decreases to 0.40 for M0 stars. We also plot open circles for the distance- and reddening-adjusted magnitudes of the five known optical counterparts of luminous globular cluster X-ray sources (Deutsch et al. 1998), if they were relocated to NGC 6652.

A population of stars is seen blueward of the red giant branch in the color-magnitude diagram of Fig. 2.10. Each of these stars was examined individually, and none are obviously due to cosmic-ray hits or other defects in the data. Most of these objects are, without question, stars bluer than the red giant branch, although their nature is not at first obvious. These stars do fall in the region where one expects blue straggler stars (BSS) based on the extension of the main sequence of the isochrone, and as Ortolani et al. (1994) found an abundance of BSS in this cluster, we checked to see if many of these stars might be BSS.

A detailed comparison between the blue stragglers discovered by Ortolani et al. (1994) (obtained in electronic form from CDS) and blue objects isolated here, shows that four of our blue objects correspond directly to four BSS (OBB 772, 857, 858, 865) discovered by Ortolani et al. The other 5 BSS candidates from Ortolani et al. which fall in the PC6 frame do not correspond to remarkable objects in our color-magnitude diagram, and most may be inaccurately photometered blends in the ground-based data. The remaining dozen blue objects in Fig. 2.10 are crowded by neighboring stars such that they would be very difficult to isolate in ground-based images. In addition, these objects are more numerous near the center of the cluster than in other parts of the frame and many, therefore, are likely to be cluster members.

As the contamination by nonmembers is not negligible, we briefly examine the expected contamination from such stars in the color-magnitude diagram. Although the *HST* fields are too close to the cluster to study the contamination with these data, we estimate from the contamination investigation in Fig. 5 of Ortolani et al. (1994) that $\sim$10 bulge stars with $m_{439} < 20$, and only a few bulge stars with $m_{439} < 18$ are expected to appear in PC6. We conclude that a few of the blue stars in our diagram

may be nonmembers, but most appear to be cluster members and are likely to be blue stragglers. In any event, none of these blue stars is within the X-ray error circles, and these objects are unlikely to be related to X1832–330.

Optical Counterpart Candidates

Within the partial coverage of the 5.″3 radius 1σ error circle of the *ROSAT* HRI coordinates, there are no obvious UV-excess candidates with $m_{439} < 20.6$ ($M_{B_0} < 5.9$), a limit slightly stronger than the least luminous known globular cluster optical counterpart, Star A in NGC 1851 (§2.2 and Deutsch et al. 1996b), when all counterparts are corrected for distance and reddening. However, it is important to stress that the region beyond 4″, while completely covered by our AAT data, is not completely imaged by these *HST* frames (Fig. 2.9); a faint optical counterpart mischievously located $> 4''$ due west of the nominal coordinates could not have been seen with existing *HST* observations.

In the $35'' \times 35''$ region examined here, only one object stands out as a candidate based on similar color to the other known counterparts. This faint UV-excess object, which we denote Star 49, is the only unusual star in this region, and we therefore offer it as a possible optical counterpart to the luminous globular cluster X-ray source X1832–330. From Fig. 2.10 it can be seen that Star 49 has color similar to the other known counterparts, and a luminosity nearly equal to Star A in NGC 1851 (Deutsch et al. 1998). For Star 49 we measure $m_{336} = 19.69 \pm 0.06$, $m_{439} = 20.2 \pm 0.2$, $(m_{336} - m_{439}) = -0.5 \pm 0.2$, and apply approximate filter corrections to estimate $B_0 = 20.4$, $(U - B)_0 = -0.9$, and $M_{B_0} = 5.5$.

However, for Star 49 we measure a position in the GSC frame of $\alpha(2000) = 18^{\rm h}35^{\rm m}44\overset{\rm s}{.}57$, $\delta(2000) = -32°59'38\overset{''}{.}3$, which is $11\overset{''}{.}7$ away from the X-ray coordinates, at a distance greater even than the estimated $10\overset{''}{.}2$ 2σ uncertainty. About 2% of *ROSAT* HRI aspect solutions seem to be in error by more than 12″, so this object should not be discounted, although it must be treated with caution.

Star 49 itself is near the detection threshold in both filters. The object does, however, appear to be weakly detected in four separate exposures, two F439W frames and two F336W frames (each filter pair at a different spatial offset). It is too faint to be expected to be detected in the other two shorter-exposure *HST* images, and indeed does not appear. In Fig. 2.11 we show coadded F336W and F439 frames of Star 49 and the surrounding $8''\times8''$ region. The existing WFPC2 observations are not helpful for further studying this object, as it falls just outside the WFPC2 field of view.

2.4.4 Conclusion

We have presented a search of the optical counterpart for X1832–330, the luminous globular cluster X-ray source in NGC 6652. Using the GSC reference frame, we determine the optical position of the *ROSAT* X-ray coordinates on a CCD image. U and B ground-based images from the AAT allow us to set a limit $M_{B_0}\gtrsim3.5$ for the counterpart at the time of those observations, provided the color is $(U-B)_0=-1$. Archival *HST* WFPC2 exposures which subtend most but not all of the error circle allow us to infer $M_{B_0}>5.2$ for the counterpart if in that region, again provided at the time of observation the source has a UV-excess $(m_{218}-m_{439})_0=-1.4$, like the counterpart in NGC 6441. Archival WF/PC observations allow a more sensitive search; within the approximately 90% of the $5\farcs3$ radius 1σ X-ray error circle contained in the WF/PC images, we detect no objects at $m_{439}<20.6$ ($M_{B_0}<5.9$) with colors compatible with the other known optical counterparts in globular clusters. The region outside a radius of $4''$ is not completely imaged by these data, and therefore a faint UV-excess counterpart could have been missed with these *HST* observations.

We do weakly detect a faint UV-excess object $11\farcs7$ from the *ROSAT* coordinates. This is only a 2.3σ deviation from the X-ray coordinates, and thus this object certainly should not be completely ruled out based on its position. If it is indeed the correct identification, this object provides another example of an extremely underluminous optical counterpart such as seen in NGC 1851. We measure for Star 49 $m_{439}=$

20.2 ± 0.2, $(m_{336} - m_{439}) = -0.5 \pm 0.2$, and estimate $B_0 = 20.4$, $(U-B)_0 = -0.9$, and $M_{B_0} = 5.5$.

Should the X-ray coordinates prove to be accurate to better than 4″, the likely conclusion is that the true optical counterpart, not yet identified, is the intrinsically faintest cluster source yet known, at least at the time of these observations, and Star 49 may be yet another example of a faint UV-excess cluster object of unknown nature (see, e.g., Deutsch et al. 1996b, 1998). Another possibility is that the optical light from the system was not dominated by the hot accretion disk at the time of these observations, but rather by the secondary, thereby rendering the object's color unremarkable in our color-magnitude diagram; however, such behavior has not been observed for the other identified cluster sources. Clearly, deep F336W, F439W WFPC2 observations placing the X-ray coordinates in the center of the PC chip are desirable to search this field more thoroughly, and a more accurate X-ray position would reduce the number of objects which must be considered as possible candidates.

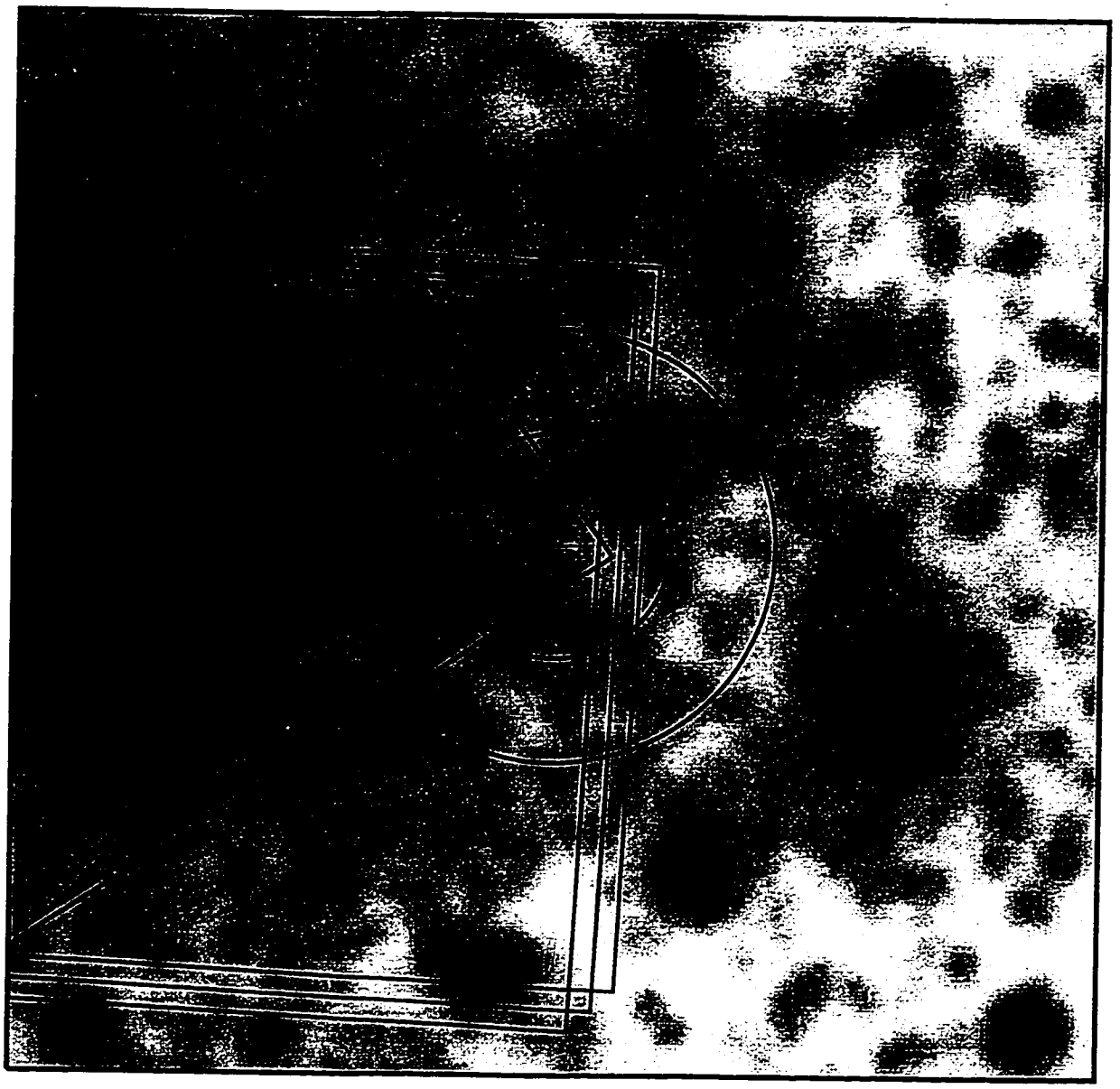

Figure 2.8: 50″×50″ ground-based B-band CCD image centered (cross) on the *ROSAT* HRI coordinates for the luminous globular cluster X-ray source X1832–330. North is up and East is left. Overlaid are 5.″3 1σ and 10.″2 2σ radius X-ray error circles. The image was obtained in 1.″3 seeing conditions, and shows that the field is quite crowded from the ground. Also overlaid are the multiple archival *HST* exposure fields of view. The WF/PC observations were obtained at three different offsets and exposure times for each filter, while the WFPC2 observations were all at the same pointing. Unfortunately, the X-ray error circles extend beyond the boundaries of the *HST* frames.

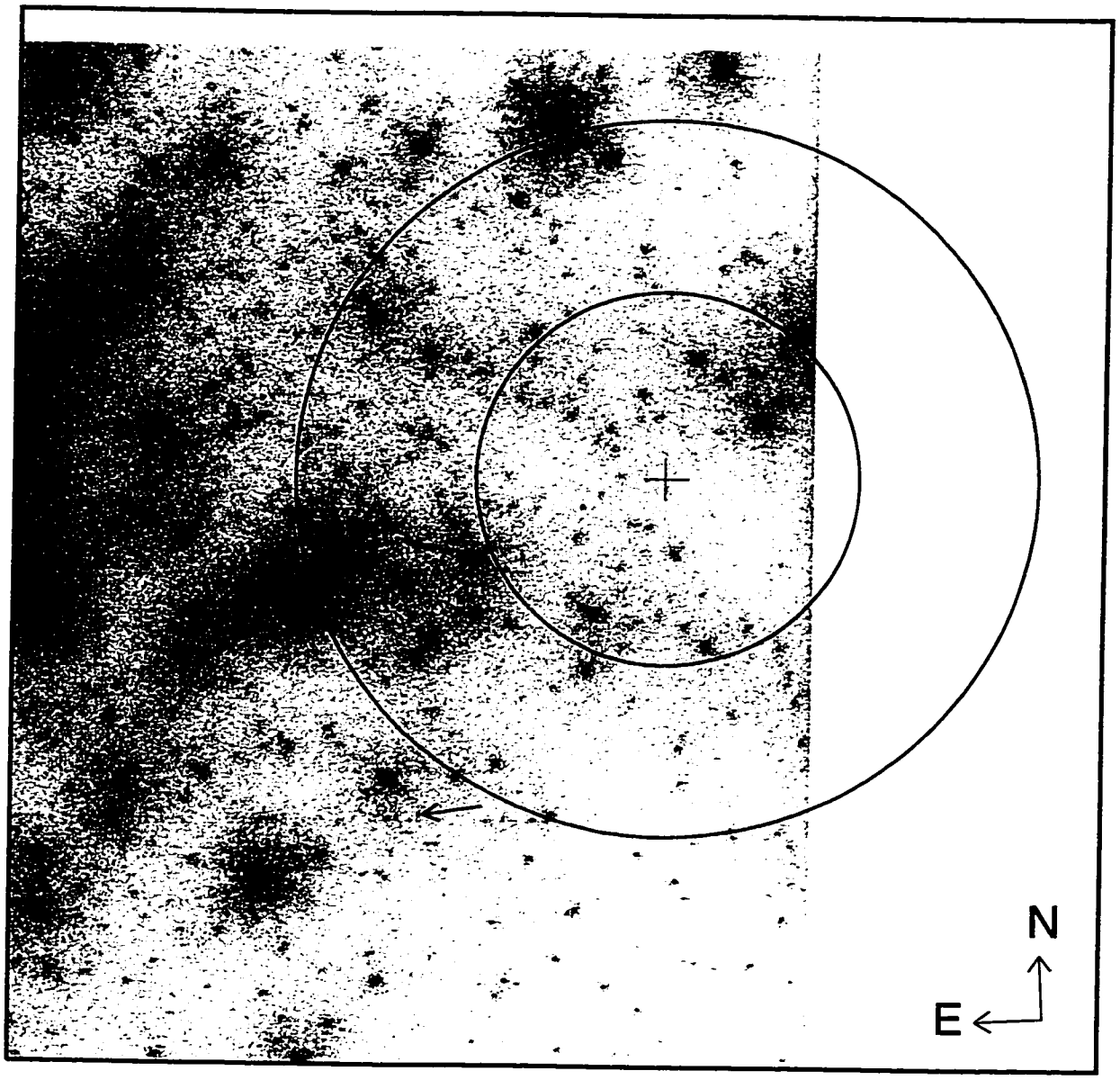

Figure 2.9: 22″×29″ corner section of the 300 s F439W (B) WF/PC image of NGC 6652, which has been cleaned of cosmic-ray hits. Our optical position for the X-ray coordinates is marked with a cross. 5.″3 1σ and 10.″2 2σ error circles are displayed as in Fig. 2.8. The field is not severely crowded by *HST* standards, although there are still ∼40 objects within the 1σ error circle. A faint object, discussed in the text as a possible counterpart, is marked with an arrow.

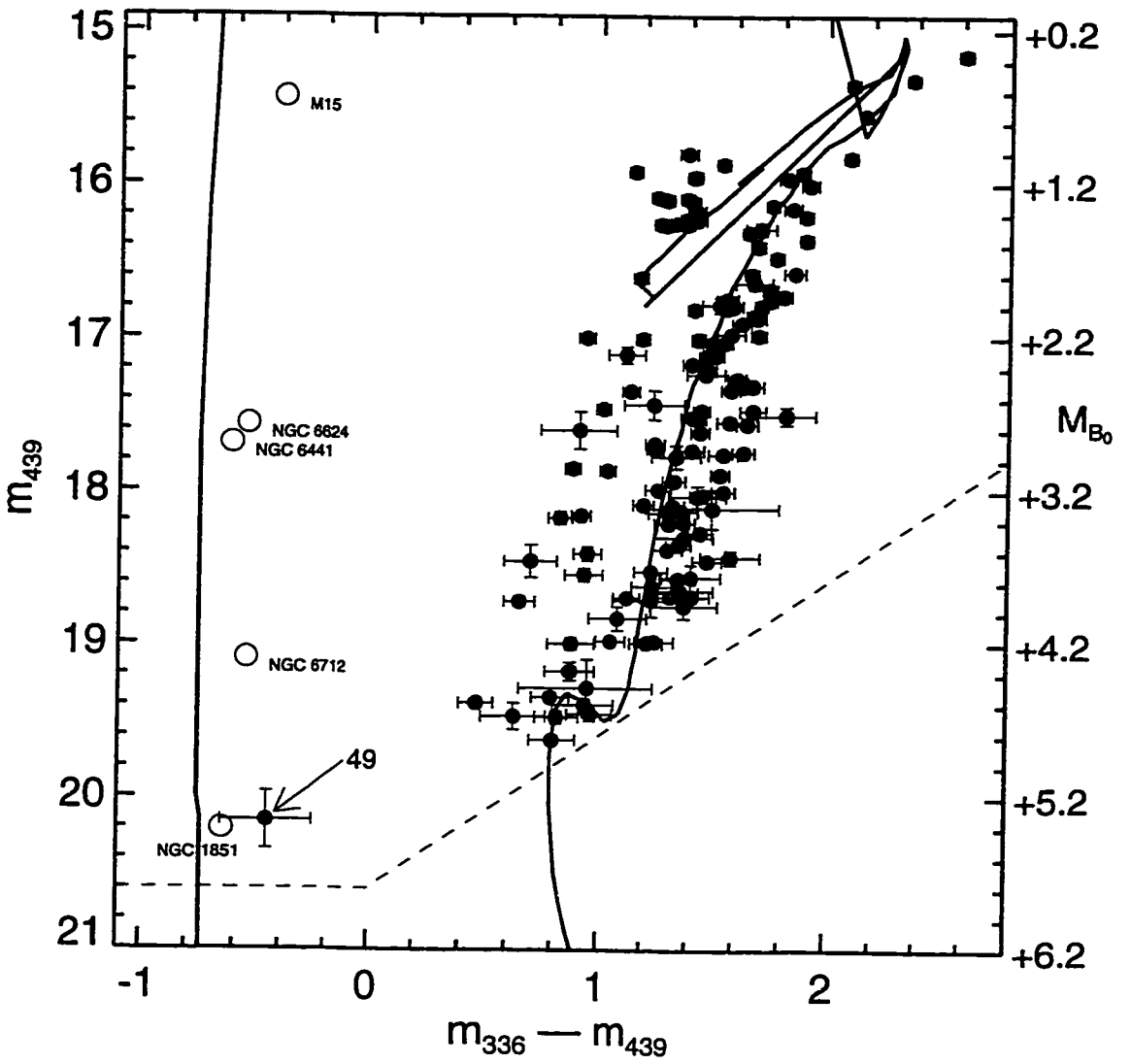

Figure 2.10: Color-magnitude diagram of NGC 6652 derived from the WF/PC F336W and F439W observations for the ~150 objects in PC6 which are detected in both passbands. Magnitudes are in the STMAG system, and formal 1σ error bars are provided for each object, although a few objects will have greater error due to low-level cosmic-ray hits which could not be identified and flagged. Solid line: a 12 Gyr, [Fe/H] = −0.7 isochrone from Bertelli et al. (1994), added for comparison. Dashed line: approximate detection threshold for these data. The distance- and reddening-adjusted locations for the five known optical counterparts of luminous globular cluster X-ray sources (Deutsch et al. 1998) are plotted as open circles. Only one object near the X-ray source, which we denote Star 49, has color and magnitude similar to other known optical counterparts.

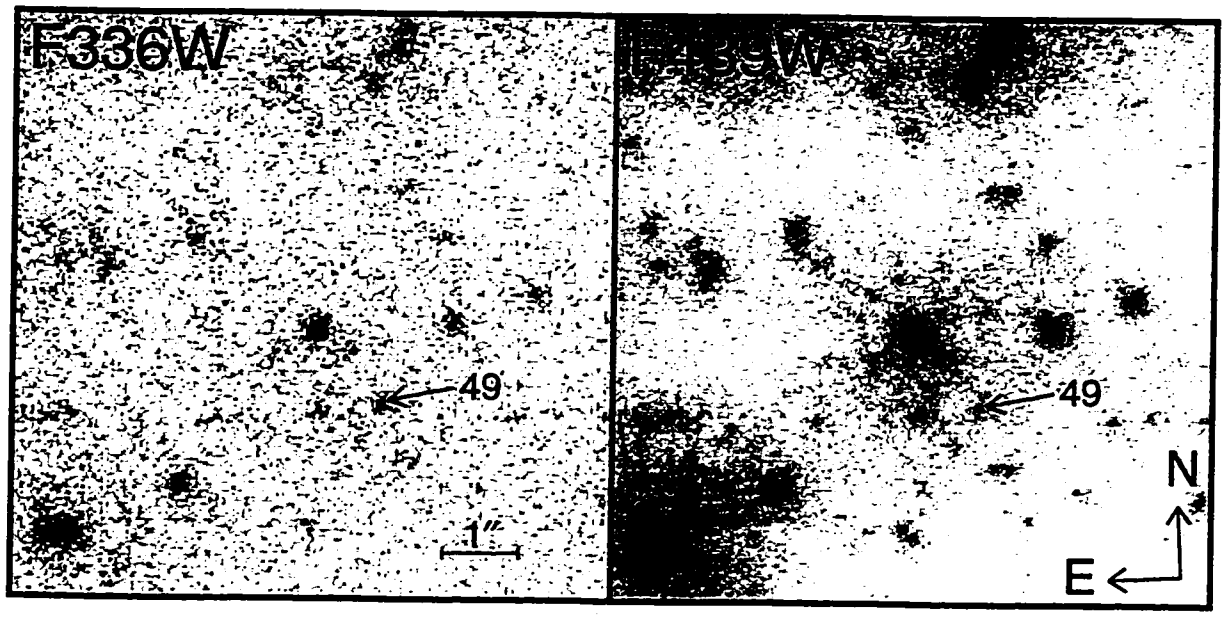

Figure 2.11: 8″×8″ sections of the F336W (U) and F439W (B) images of the region near Star 49, which we select as a possible optical counterpart due to significant UV excess, similar to other known cluster optical counterparts. These *HST* WF/PC data were obtained on 1992 October 10. Each frame is the sum of the two longest images for each filter.

Chapter 3

ENSEMBLE OPTICAL PROPERTIES OF THE KNOWN COUNTERPARTS

3.1 Introduction

In this chapter I will discuss the ensemble optical properties of the known optical counterparts to GC LMXBs and some related advances. Some points in this chapter have been previously discussed by Deutsch, Margon, & Anderson (1998a, 1998b), Deutsch et al. (1998), and Deutsch (1998).

3.2 Luminosities and Colors

Of the 12 luminous LMXBs associated with globular clusters listed in van Paradijs (1995), five now have confirmed or likely optical counterparts (the NGC 6652 source remains tentative and will be left out of this discussion). In order to make a comparison between this sample of globular cluster sources and sources in the field, we have extracted images of each cluster from the *HST* data archive and measured m_{336} and m_{439} for each globular cluster (GC) LMXB optical counterpart; these values are presented in Table 3.1.

Photometric errors are typically dominated by the $\sim$5% systematic calibration uncertainties. The uncertainty for Star A in NGC 1851 is higher, 0.1 mag, due to a presumably unrelated companion 0.″12 distant (Deutsch et al. 1996b). Observations of the source in NGC 6624 are complicated by an even closer blend (separation 0.″08, King et al. 1993), completely unresolvable with WFPC2, although easily resolved in an F430W FOC image. We estimate m_{439} for both stars in WFPC2 observations

by measuring the total light in the blend and using the flux ratio of the two stars in the F430W FOC image. We then estimate m_{336} for the X-ray source counterpart by subtracting the amount of light expected from the companion, assuming that the latter has the same color as other stars with its m_{439}. The uncertainty in the measurements for this optical counterpart is $\sim$0.2 mag, comparable to the observed amplitude of variability (Anderson et al. 1997). Indeed, it should be noted that we have obtained only instantaneous magnitudes for all these objects, and the sources are known to be variable in optical or ultraviolet light, except in the case of NGC 1851 (for which there has not yet been an adequate light curve study). Nonetheless, the results are entirely sufficient for our purpose here.

With this homogeneous set of photometric measurements from WFPC2 observations, $\mathrm{E}(B-V)$ and $(\mathrm{m}-\mathrm{M})_0$ values from Table 3.2, and approximate color-dependent conversion relations between STMAG system magnitudes and Johnson U,B (derived using the STSDAS *synphot* package), we calculate B_0, $(U-B)_0$, and M_{B_0}, and list them in columns 4-6 of Table 3.1.

We summarize a variety of parameters for all of the GC LMXB sources in Table 3.2. Columns 1 and 2 list the X-ray source designation and cluster name, respectively. The reddening, distance modulus, and metallicity of the clusters are listed in columns 3-5. We list the absolute B magnitude of each of the known optical counterparts in column 6 (although full precision is given of a particular measurement, it should be reiterated that the sources are variable). In column 7 we list $\xi = B_0 + 2.5 \log \mathrm{F_X}(\mu\mathrm{Jy})$, the parameter used by van Paradijs & McClintock (1995; hereafter vPM) to characterize the ratio of X-ray to optical flux. We use $\mathrm{F_X}$ values from column 9, which we derive by taking a simple mean of the *RXTE* ASM flux measurements since 1996, and applying a simple correction to convert approximately to μJy. In column 10, we apply the distance correction and give an approximate X-ray luminosity in 10^{36} erg s^{-1} for the 2-10 keV ASM band. The absolute calibration should probably be treated with caution, but the relative values should be reliable. We have also listed the orbital

period in hours where available in column 8.

By virtue of their cluster membership, the distances to and foreground reddenings of these GC LMXBs can be determined easily, unlike for those in the field. This allows a comparison of $(U-B)_0$, M_{B_0}, and ξ for GC sources with those of field LMXBs for which these quantities are known. vPM find for the field sources an average $(U-B)_0 = -0.97 \pm 0.17$ (1σ). All five GC LMXBs measured in Table 3.1 fall within 1σ of this average.

vPM find an average $(B-V)_0 = -0.09 \pm 0.14$ for the field LMXB, so we assume $M_B = M_V$ in the comparison of absolute magnitudes, as we do not have V data available for several objects. This is likely to be a good assumption, since the $(U-B)_0$ colors show a small dispersion and for Star U1, $(B-V)_0 = 0.0$ (based on the 1995 September 12 data in Table 2.2). In addition, $(B-V)_0 \sim 0.15$ for AC 211 (Ilovaisky et al. 1993), the reddest object in our table.

M_V for bursting sources in the field ranges considerably in vPM, from 1 to 5 with a slight overabundance near $M_V = 1$. Our distribution in M_B for the 5 GC LMXBs, which are all bursting sources, is similar: a range from 1 to 6, but with no overabundance near $M_V = 1$. In fact, there is evidence that the globular clusters sources are on average less luminous: while 70% of field bursters have $M_V < 2.5$, only one of the globular cluster bursters has $M_B < 2.5$. Fig. 3.1 shows a comparison of M_B between the globular cluster sources and the sample of field bursting sources for which comparison is possible. With only seven and five sources in each group, respectively, the difference may not be significant, although we note that the NGC 6652 source, if correctly identified, furthers this trend.

vPM noted that the bursters they considered (mainly in the field) as a group appear to have systematically lower optical luminosity counterparts than other LMXBs. The data on additional counterparts to the globular cluster bursters discussed here add further evidence for such a difference.

Finally we examine how field and globular cluster LMXBs compare in ξ. The

source in M 15 has long been known to be optically overluminous and is already singled out at the bright end of vPM's histogram. The other four GC sources span the entire main distribution of field LMXBs; they do not seem to show a peak near $\xi = 22$ as do the field sources, although of course the sample is small.

In summary, the sample of GC LMXB optical counterparts obtained thus far appears to be identical in $(U-B)_0$ and similar in M_B to the sample of field bursting sources for which comparison is possible. The uniformity in $(U-B)_0$ might well be expected, as the light at these wavelengths may be dominated by a hot accretion disk, whose spectral slope is rather insensitive to temperature in this regime. However, the GC sources show a very broad distribution in ξ rather than the peak of $\xi = 21.8 \pm 1.0$ (1σ) seen by vPM; in fact, ξ for only one of the five cluster sources falls within 1σ of the average for the field LMXBs.

Gnedin & Ostriker (1997) have recently reevaluated destruction rates of globular clusters, and concluded that these timescales are more rapid than previously inferred. A substantial fraction of all initial globular clusters may have been destroyed in a Hubble time, and thus a large fraction of the current stellar population of the bulge may come from clusters. LMXBs are the most luminous stars in globular clusters, and might be useful as a tracer of this hypothesis (see also Grindlay 1985). Indeed, Ostriker (1997) points out that luminous (near-Eddington limited) LMXBs are overabundant in the bulge relative to other galactic locations, just as they are over-represented in globular clusters. The similarity that we infer here between the optical properties of LMXBs in clusters and those in the bulge is compatible with this interesting concept for the origin of the bulge sources, although clearly the sample size is small. As the bulge LMXBs obviously cannot have been radiating at their current X-ray luminosities for a Hubble time, there are also missing evolutionary parts of this picture.

3.3 Optical Luminosity, X-ray Luminosity, Period Relation

That the optical luminosity should depend upon the X-ray luminosity and the size of the accretion disk has been quantified by van Paradijs & McClintock (1994; hereafter vPM94). They define the parameter $\Sigma = (L_X/L_{\rm Edd})^{1/2}(P/1\,{\rm hr})^{2/3}$ and find a strong correlation, such that $M_V = 1.57(\pm0.24) - 2.27(\pm0.32)\log\Sigma$. In Fig. 3.2 we show a similar figure as in vPM94, but we use M_B instead of M_V, which is likely to be reasonable as vPM94 find an average $(B-V)_0 = -0.09 \pm 0.14$ for field LMXBs. The "+" symbols denote field LMXBs from vPM94. The data for globular cluster LMXBs are derived from this work. These sources are plotted with diamonds. When two or more symbols are connected with a line, the entire known range of optical or X-ray luminosity is indicated. The dotted line indicates the 1σ parameter space implied by the best fit by vPM94. The solid lines denote the apparent full range of possible values (using vPM94's best fit slope). For NGC 1851, no orbital period is known, but the optical and X-ray luminosities are known. We therefore draw a line which is likely to encompass the likely range of orbital periods, $0.2 - 0.85$ hr, where the lower bound is taken to be the shortest orbital period known and the upper bound is the maximum period implied by our solid line bounds. We predict that the orbital period of X 0512–401 will prove to be less than 1 hr.

3.4 Prospects for Finding More Counterparts

Identification of optical counterparts in the remaining clusters with luminous X-ray sources will be difficult using current techniques, as is seen in Fig. 3.3. Here we have plotted the m_{336} apparent magnitudes, either observed or predicted, of the optical counterparts of luminous X-ray sources in the cores of globular clusters. The objects are ordered by right ascension, so the units on the abscissa are of no significance. Clusters with boxed names are those with optical counterparts already identified (or tentatively suggested as for Star 49 in NGC 6652); all but one required *HST* observa-

tions. The dashed vertical lines denote the 5 mag range of the luminosity dispersion implied by the current complement of identifications, adjusted for the distance and reddening of each cluster (cluster parameters principally from the compilation of Djorgovski 1993). The filled squares are the observed m_{336} magnitudes derived from our *HST* photometry (Deutsch et al. 1998); the positions of the squares within the dashed lines indicate the luminosities compared with the luminosity range of all the known sources (e.g., the object in NGC 1851 appears at the bottom of the dashed line as it is the least luminous one). For the six sources with no current identification, the six open diamonds indicate where each of the known identifications would fall if relocated to the target cluster, again with appropriate distance modulus and reddening. The horizontal line at $m_{336} = 23$ denotes the approximate flux reached by a typical short WFPC2 program, i.e., 10% photometric precision in a two-orbit multicolor exposure series in a moderately crowded field.

Of the "easy" clusters, i.e. those for which the optical counterpart can be expected to be detected in one or two *HST* orbits, NGC 6652 is the last for which a candidate has been put forth. Due to the considerable foreground extinction, the remaining unidentified luminous cluster X-ray sources will be difficult to identify with current techniques at the UV and blue wavelengths where these sources have in the past been studied. A possible exception is NGC 6440, which could be adequately studied in a few orbits. For the remaining clusters, the amount of time required to detect a low-luminosity counterpart in an F336W frame with the WFPC2 becomes prohibitive, although detection of counterparts at the high end of the luminosity range is feasible. Variability searches in the infrared may afford a way to identify and study the remaining, heavily-reddened sources. Future searches will also be facilitated when arcsecond-accuracy X-ray coordinates become available via AXAF observations, thereby drastically reducing the number of optical objects which must be considered.

Table 3.1: F439W and F336W photometry for globular cluster LMXB optical counterparts from *HST* WFPC2 data

Optical Counterpart	m_{439}^{a}	$(m_{336} - m_{439})^{a}$	B_0	$(U-B)_0$	M_{B_0}
NGC 1851 Star A	20.46	-0.73	21.03	-0.98	5.60
NGC 6441 Star U1	19.30	-0.30	18.18	-1.06	3.03
NGC 6624 King Star	17.99	-0.37	17.46	-0.98	2.92
NGC 6712 Star S	19.88	-0.19	18.58	-1.02	4.42
M15 AC 211	15.49	-0.45	15.91	-0.81	0.80

[a] Photometric uncertainties are discussed in the text; note that most of these objects are known to be variable and the rest are likely to be as well.

Table 3.2: X-ray source and corresponding globular cluster data

Source	Cluster	E(B–V)	DM[a]	[Fe/H]	M_B	ξ[b]	$P_{\rm orb}$[c]	F_X[d]	L_X[e]
X0512-401	NGC 1851	0.02	15.43	-1.29	5.60	22.92		5.7	2.0
X1724-307	Terzan 2	1.42	14.37	-0.25				35.1	4.5
X1730-335	Liller 1	3.00	14.68	0.20				13.8	2.4
X1732-304	Terzan 1	1.64	13.85	-0.71				7.1	0.6
X1745-203	NGC 6440	1.00	14.64	-0.34				5.4	0.9
X1745-248	Terzan 5	1.87	14.50	-0.28					
X1746-370	NGC 6441	0.45	15.15	-0.53	2.43	21.10	5.70	25.7	6.8
X1747-313	Terzan 6	2.04	14.16	-0.61					
X1820-303	NGC 6624	0.27	14.54	-0.37	2.99	23.62	0.19	272.9	41.2
X1832-330	NGC 6652	0.10	14.85	-0.99	5.59	23.07		11.3	2.3
X1850-087	NGC 6712	0.46	14.16	-1.01	4.48	20.86	0.33	7.7	0.8
X2127+119	NGC 7078	0.09	15.11	-2.17	0.66	18.66	17.10	14.3	3.6

[a] Distance modulus $(m - M)_0$

[b] $\xi = B_0 + 2.5 \log \mathrm{F_X}(\mu\mathrm{Jy})$

[c] System orbital period in hours

[d] Average *RXTE* ASM X-ray flux $(2 - 10$ keV) since 1996, approximately calibrated to units of μJy

[e] Average X-ray luminosity from ASM, approximately calibrated to units of 10^{36} erg s^{-1} $(2 - 10$ keV)

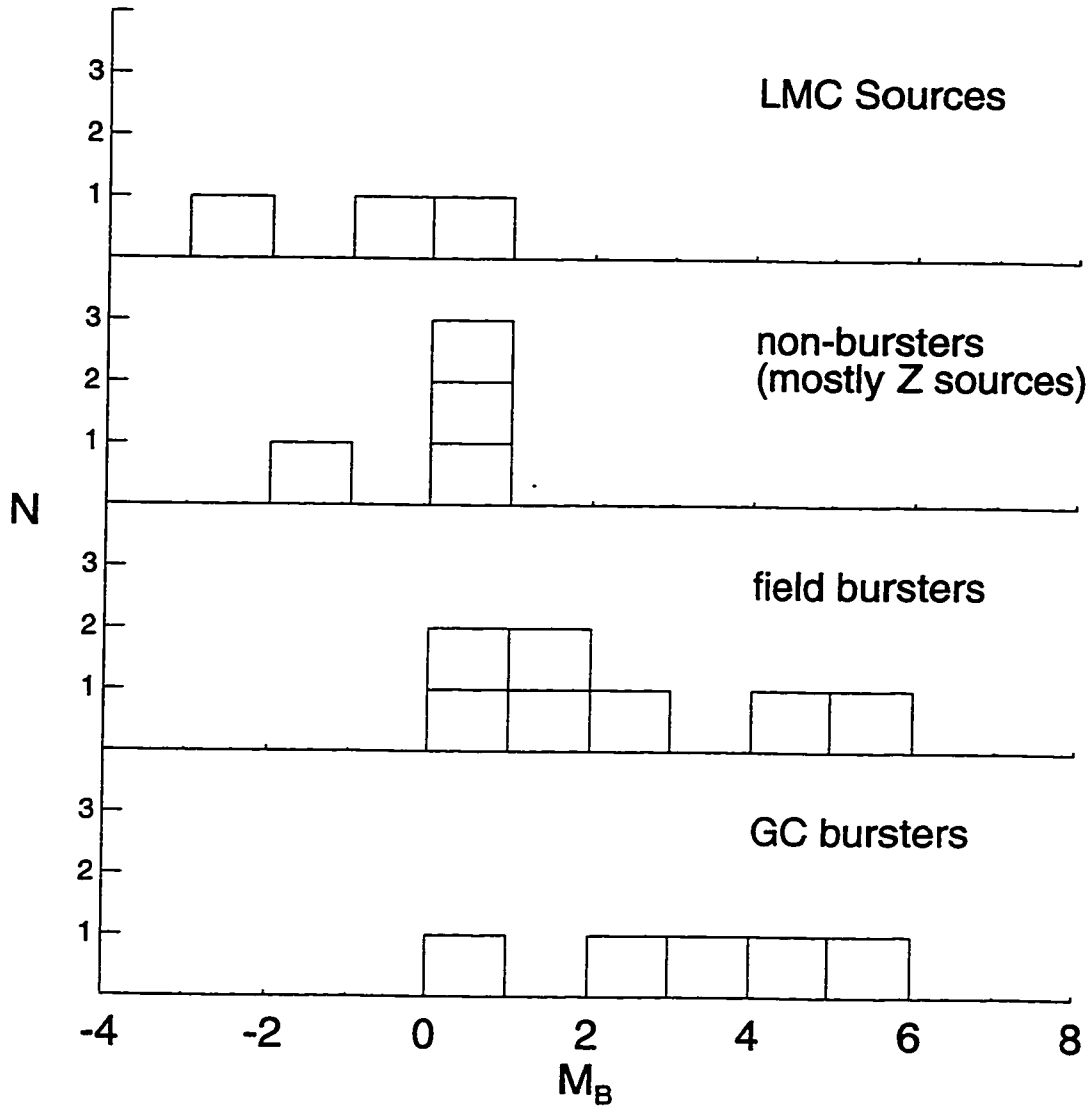

Figure 3.1: $M_B \approx M_V$ values for four different classes of LMXBs. Luminosities for globular cluster (GC) bursters are from Table 3.1. Luminosities for other classes are taken from van Paradijs & McClintock (1995).

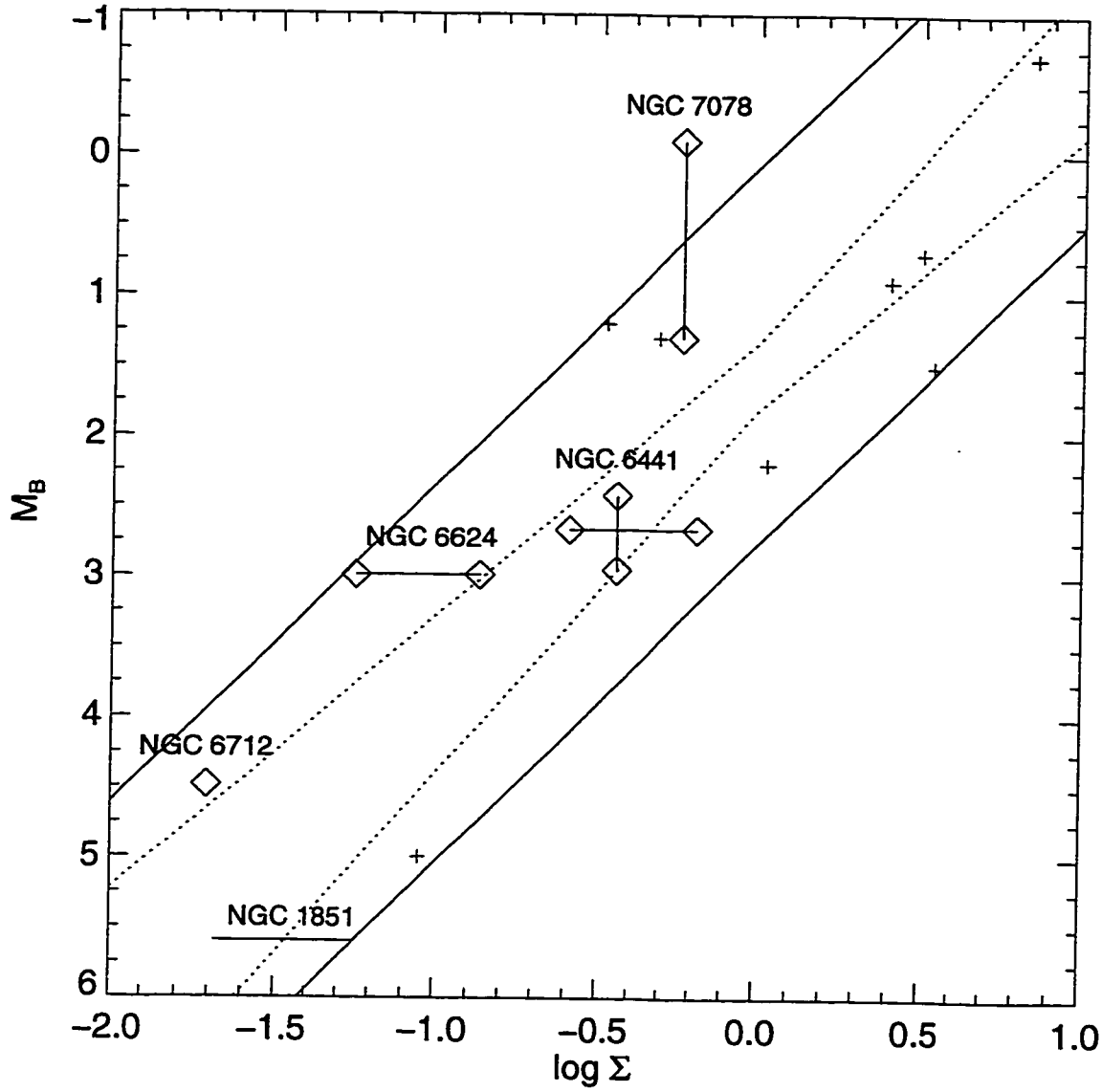

Figure 3.2: Absolute magnitude of LMXBs versus $\Sigma = (L_X/L_{\rm Edd})^{1/2}(P/1\ {\rm hr})^{2/3}$. Field LMXBs from van Paradijs & McClintock (1994) are denoted with "+" symbols. Globular cluster LMXBs are displayed with diamonds and connecting lines to indicate known variability in X-ray or optical luminosity. Dotted lines indicate the 1σ parameter space of a fit by Paradijs & McClintock; the solid lines indicate a range which seems to include nearly all sources. Based on these solid line boundaries, we predict a orbital period for the source in NGC 1851 of less than 0.85 hr.

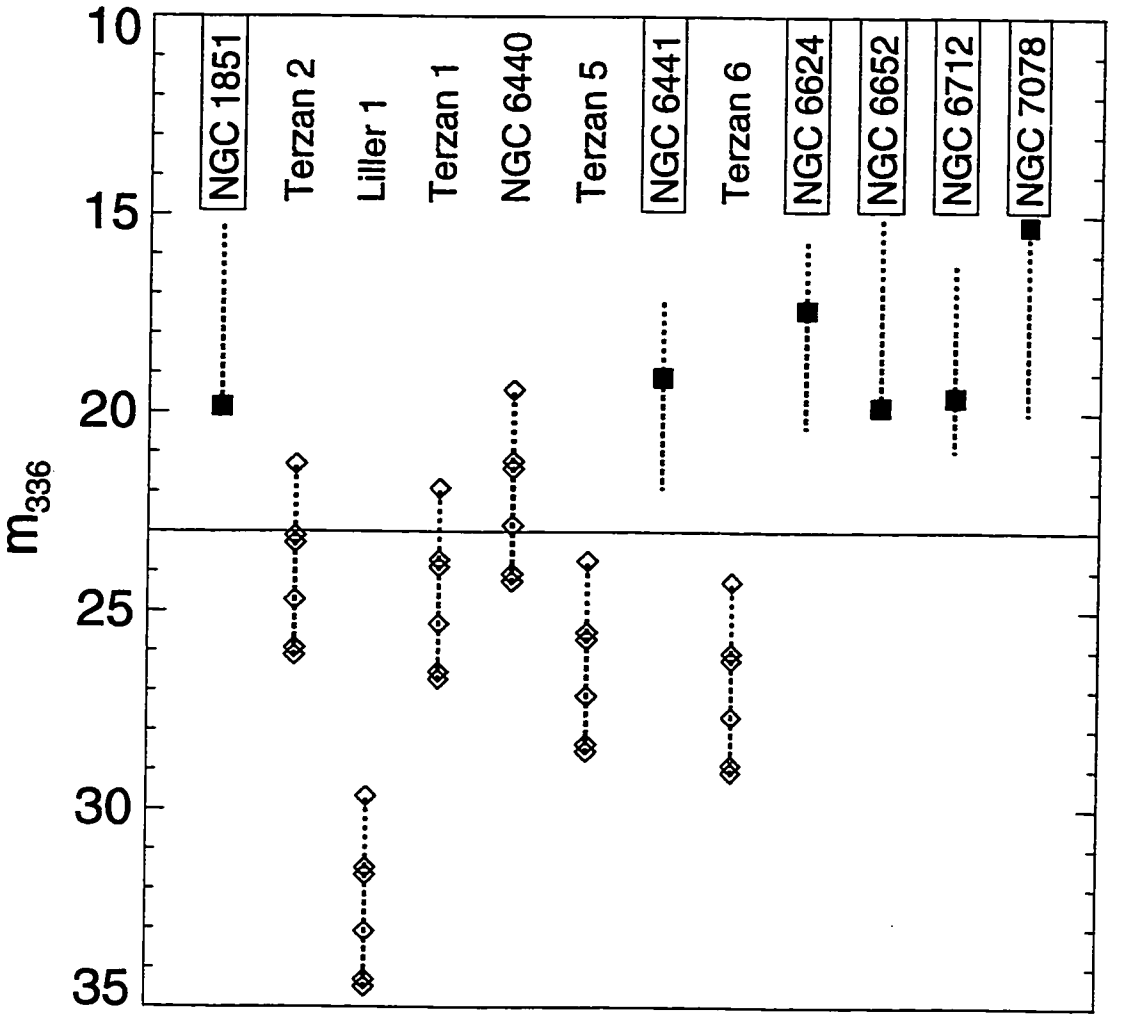

Figure 3.3: Apparent m_{336} magnitudes for the six confirmed or suggested optical counterparts to luminous globular cluster X-ray sources (filled squares), full range of optical luminosities of the ensemble of the current candidates (dashed vertical lines), and predicted magnitudes for each of the known identifications if relocated to other target clusters with appropriate distance modulus and reddening (open diamonds). The horizontal line at $m_{336} = 23$ denotes an estimate of the S/N=10 limit in a sequence of 4 × 700 s WFPC2 F336W exposures in moderate crowding conditions, i.e. part of a typical short WFPC2 program. Of the "easy" clusters, i.e. those for which the luminosity range is entirely above the short *HST* program detection limit, NGC 6652 is the last for which a candidate has been suggested.

Chapter 4

ULTRAVIOLET/OPTICAL SPECTRAL ENERGY DISTRIBUTIONS

4.1 Introduction

In this section I reanalyze all the available *HST* observations for the known counterparts and examine what the resulting spectra and spectral energy distributions can tell us about cluster LMXBs and LMXBs as a class. This work extends some preliminary work presented in Deutsch, Margon, & Anderson (1998b).

These *HST* observations give unprecedented observational constraints on the accretion disk models and the resulting broad UV/optical spectral energy distributions of LMXBs. The reasons for this are threefold: the *HST* instruments are very well calibrated to a standard absolute system; the distance and reddening to these sources is well known from studies of the host clusters; and finally, the reddening to these sources is among the lowest of all LMXBs thereby making UV observations feasible. A summary of accretion disk theory in close binaries is given by King (1995) and references therein. A recent look at the current status of observations of accretion disks in X-ray binaries is discussed by Verbunt (1998). Reasonably successful applications of accretion disk models to multiwavelength observations of Cyg X–2 (Vrtilek et al. 1990) and Sco X–1 (Vrtilek 1991) reveal disk sizes, mass accretion rates, and many other insights into these systems. Arons & King (1993) applied a very similar model as presented herein to the discovery FOC images of Star K in NGC 6624, predicting the UV modulation amplitude later observed by Anderson et al. (1997)

4.2 *HST* Observations

First we present the new and archival *HST* observations used here to study the overall spectral energy distributions of these sources. The spectra were obtained at various epochs with the Faint Object Spectrograph (FOS) and will be discussed individually below. Except in the case of the NGC 6624 data, which was acquired in a special mode, we have reprocessed the raw data with the latest CALFOS reduction algorithm (Lindler & Bohlin 1994) and calibration files. When compared to the imaging photometry, the FOS spectra are converted to the STMAG system with the usual relation $m(\lambda) = -2.5 \log f_\lambda(\lambda) - 21.1$.

Imaging observations with the WFPC2 have been acquired from the *HST* Data Archive in order to compare broadband photometry measurements with the spectra. The WFPC2 frames used were processed through the standard data reduction pipeline at STScI. Both DoPHOT (Schechter et al. 1993) profile-fitting software and standard aperture photometry are used as appropriate. Aperture corrections are taken from Table 2(a) in Holtzman et al. (1995b). The photometric measurements have not been corrected for geometric distortions, nor is any correction for charge transfer efficiency losses (Holtzman et al. 1995b) applied; for most of the images, these effects should contribute errors of only a few percent. We use the photometric zero points for the STMAG system from Table 9 (Z_{STMAG}) in Holtzman et al. (1995a). Systematic errors for all magnitudes due to uncertainties in detector performance and absolute calibration are $\sim$5%. When plotting WFPC2 magnitudes we use the effective central wavelength of each filter for a 20000 K blackbody calculated using the STSDAS *synphot* package.

Unless otherwise noted, all data reduction was performed with software written in IDL by E.W.D. or available in the IDL Astronomy User's Library (Landsman 1993). All magnitude measurements presented here are written m_λ where λ is the filter designation, approximately denoting the central wavelength of the filter in nanometers.

In the STMAG system, zero points are set such that a flat spectrum ($f_\lambda = \text{constant}$) source will have identical magnitudes at all wavelengths. FOS spectra and WFPC2 imaging magnitudes are therefore on the same scale and directly comparable. We now discuss the available observations for each of four of the five objects individually. Star U1 in NGC 6441 is not discussed in this section as there are no new data to present. All existing *HST* data were analyzed in Deutsch et al. (1998).

4.2.1 Star A in NGC 1851

On UT 1997 January 10 we obtained *HST* FOS UV spectra of Star A in NGC 1851, a 2510 s and 1300 s exposure through the G160L grating in two consecutive orbits. The 0.″5 square aperture was used for both exposures. In Fig. 4.1 we present the coadded flux-calibrated spectrum (*top panel*) and a calibrated counts spectrum (*bottom panel*). These spectra are binned 3× to increase the signal to noise per bin for this weak spectrum. In each panel, the upper spectrum indicates the detected signal, and the lower spectrum indicates the 1σ uncertainty in each 5.2 Å bin. There is clearly continuum flux detected, increasing toward the UV. Ly α is clearly detected, but is likely to be geocoronal. The location of He II λ1640, which would normally be expected to be the most prominent emission line in the spectrum of such an object, is marked, but clearly any detection is at the 2σ level at best.

The spectrum does seem to contain three features at 2324, 2433, and 2470 Å. The feature at 2433 Å is far too broad to be real and indeed is merely the Ly α feature in the second order. The other two features, which seem to correspond to [O III] $\lambda\lambda$2321, 2331 and [O II] λ2470, are mystifying. These lines can be found in planetary nebulae, but not typically in LMXBs. In addition, He II λ1640 is typically far stronger than these forbidden oxygen lines. Thus we conclude that they are more likely to be instrumental artifacts than real emission lines, but a spectrum taken by another instrument should be obtained to verify this conclusion.

In Table 4.1 we list the broadband magnitudes derived from the available WFPC2

images. The columns are the object name, archive dataset name, UT date and start time of the observation, exposure time, filter or grating name, measured magnitude and 1σ uncertainty, and finally the orbital phase if an ephemeris is available. Measurements from the discovery images (Deutsch et al. 1996b) as well as data acquired during unrelated programs are listed. An ephemeris for Star A is not yet available. The long time scale variability seems to be small from the data available thus far, but two consecutive m_{218} measurements disagree significantly and may indicate some short timescale variability. Star A is crowded by a presumably-unrelated companion only $0\farcs12$ distant (§2.2 and Deutsch et al. 1996b), which makes accurate photometry difficult in the m_{439} and m_{555} measurements.

4.2.2 Star K in NGC 6624

On UT 1996 May 1 we obtained *HST* FOS G160L UV spectra of Star K in NGC 6624, and these exposures have previously been presented by Anderson et al. (1997). The 11 min orbital period is clearly detected as 16% peak-to-peak oscillations in these time-resolved observations.

For completeness, we show in Fig. 4.2 the coadded flux-calibrated spectrum (*top panel*) and a calibrated counts spectrum (*bottom panel*). These spectra are binned $2\times$ to increase the signal to noise per bin. In each panel, the upper spectrum indicates the detected signal, and the lower spectrum indicates the 1σ uncertainty in each 3.5 Å bin. A hot UV continuum is clearly detected, as is the 2200 Å interstellar absorption feature. Ly α emission is also present, but is likely to be geocoronal. There does appear to be strong, broad Ly α absorption, seemingly far too wide to be geocoronal or interstellar. The location of He II λ1640, which would normally be expected to be the most prominent emission line in the spectrum of such an object, is marked, but clearly no emission is present. In fact, there is marginal evidence for a very faint detection of He II absorption. Second order Ly α at 2433 Å is also quite visible in this spectrum.

In Table 4.2 we list the available broadband WFPC2 magnitudes for this object. Due to blending with a presumably unrelated star only 0.″08 distant, photometry of Star K is very difficult redward of m_{336}. The pair are resolved in *HST* FOC images, but they are unresolved in the undersampled PC images. See §3.2 for details on how these magnitudes are estimated.

4.2.3 Star S in NGC 6712

Ultraviolet and optical FOS spectra obtained for Star S in NGC 6712 were first discussed by Downes et al. (1996). Here we reprocess and reexamine the same spectra, but draw several different conclusions with the aid of new broadband WFPC2 measurements out to the near infrared.

In Fig. 4.3 we show the coadded UV flux-calibrated spectrum (*top panel*) and corresponding calibrated counts spectrum (*bottom panel*). These very weak spectra are binned 4× to increase the signal to noise per bin. For this UV spectrum, the corresponding uncertainty spectrum, even after reprocessing, is clearly incorrect, and is therefore not shown. A hot UV continuum is detected, as is the broad 2200 Å interstellar absorption feature. Very strong Ly α emission is also present, but is likely to be geocoronal. The location of He II λ1640, which would normally be expected to be the most prominent emission line in the spectrum of such an object, is marked, but clearly no feature is present. The 2433 Å artifact, discussed in the previous section, is also quite prominent in this spectrum. No other emission or absorption features are evident.

In Fig. 4.4 we show the coadded optical flux-calibrated spectrum (*top panel*) and corresponding raw counts spectrum (*bottom panel*). These spectra have been binned 2× to 12 Å per bin. In each panel, the upper spectrum indicates the detected signal, and the lower spectrum indicates the 1σ uncertainty in each bin. The locations of He II λ4686 and Hα, which would normally be expected to be the most prominent emission line in the spectrum of such an object, are marked, but clearly no features

are present. We also mark possible identifications of He I λ4889 and the G band in absorption. If these are real features, the spectrum is clearly composite. We note that unlike the other spectra discussed in this chapter, this spectrum was obtained before the first *HST* servicing mission, and some contamination from nearby stars is likely. This issue will be examined in further detail below when the spectra are compared with the WFPC2 photometry.

In Table 4.3 we list broadband WFPC2 magnitudes for this object. All measurements were acquired at the same epoch. Although the orbital period for this object is only 21 min, the observed ultraviolet modulation amplitude at this epoch is only 4% (Homer et al. 1996), and thus these magnitudes are virtually free of uncertainties due to intrinsic variability of the object. Further, as Star S is in a sparse field (by *HST* standards), we are able to obtain precise photometric measurements out to 8100 Å. Photometry based on some of these data has been presented in Homer et al. (1996), although the magnitudes given there were converted to the Johnson system.

4.2.4 Star AC211 in M 15

Ultraviolet and optical FOS spectra obtained for AC 211 in M 15 were first discussed by Downes et al. (1996). Here we reprocess and reexamine the same spectra, and try to understand them with the aid of new broadband WFPC2 measurements.

In Fig. 4.5 we show the coadded UV flux-calibrated spectrum (*top panel*) and corresponding calibrated counts spectrum (*bottom panel*). The spectra are binned 2× to increase the signal to noise per bin. In each panel, the upper spectrum indicates the detected signal, and the lower spectrum indicates the 1σ uncertainty in each 3.5 Å bin. A hot UV continuum is clearly detected, and a slight depression about the 2200 Å interstellar absorption feature is seen. A weak Ly α emission feature is also present, but is likely to be geocoronal. However, an extremely broad Ly α absorption component may be present and will be discussed later. He II λ1640 is strong, but is the only apparent emission line in this UV spectrum. We mark the location of most

of typical interstellar absorption features of Si II, Si III, Si IV, O I, C II, C IV, and Fe II, nearly all of which are detected in this spectrum. A notable absence are the C IV $\lambda\lambda 1548, 1551$ lines; we postulate that some emission in these lines (often seen in conjunction with He II $\lambda 1640$) may cancel the interstellar absorption. As noted by Downes et al. (1996), an unusual strong feature appears to coincide with Al III $\lambda 1854$. Its appearance remains puzzling. Second order Ly α at 2433 Å is not evident here.

In Fig. 4.6 we show the coadded optical flux-calibrated spectrum (*top panel*) and corresponding raw counts spectrum (*bottom panel*). These spectra have not been binned. In each panel, the upper spectrum indicates the detected signal, and the lower spectrum indicates the 1σ uncertainty in each 6.1 Å bin. He II $\lambda\lambda 4542, 4686$, He I $\lambda 6678$, and Hα are clearly detected in emission. As discussed in Downes et al. (1996) and Naylor et al. (1988), the Hα and Hβ lines show an emission component and a blueshifted absorption component. Higher in the Balmer series, only absorption is seen at this resolution. We have marked all Balmer lines through Hθ (with unlabeled vertical lines), all of which are detected. We also detect in absorption He I $\lambda\lambda 3889, 4471, 4388, 5876$. The structure in the spectrum between 4000 and 4200 Å is curious, but unexplained at present. The count rate is falling off very quickly below 3800 Å and the continuum level may not be very accurate in this region.

In Table 4.4 we list broadband WFPC2 magnitudes for this object. The measurements were acquired at various epochs; the data and time for each measurement is tabulated as well as the binary phase at the start of each exposure, using the ephemeris of Ilovaisky et al. (1993). This object is isolated and bright enough to obtain WFPC2 measurements out to the near infrared, but at present only F336W, F439W, and F555W WFPC2 images are available in the Hubble Data Archive. This object is known to be highly variable, and its variability is obvious from the photometry in Table 4.4; this complicates the analysis of data taken at so many different epochs.

4.3 UV/Optical Spectral Energy Distributions

Having assembled the spectra and broadband photometry, we now assess how well various models describe the overall ultraviolet and optical spectral energy distributions of these objects. First, a simple single-temperature blackbody and a metal-poor Kurucz stellar atmosphere (Kurucz 1992) are considered. These model curves are arbitrarily scaled to best match the observations. In some cases, these models fit rather well, but in most cases, a multitemperature accretion disk model describes the SED best and the input parameters which are used to generate the models lead to further insights into the nature of each system.

We consider two accretion disk models. The first describes a geometrically thin, optically thick disk heated only by viscous interactions during mass accretion and we use the standard disk temperature distribution

$$T_{\rm acc}(r) = \left\{ \frac{3GM\dot{M}}{8\pi\sigma r^3} \left[1 - \left(\frac{R_\star}{r} \right)^{1/2} \right] \right\}^{1/4}$$

from Shakura & Sunyaev (1973). Each model uses $R_\star = 10$ km and $M = 1.4 M_\odot$ for the radius and mass of the neutron star, respectively. We will refer to a spectrum derived from this temperature distribution as model 1.

The second disk model considers a disk of the same geometry heated by both accretion and reprocessing of X-rays from the central region, as detailed in Vrtilek et al. (1990). For the accretion component we use the relation for $T_{\rm acc}(r)$ above. For the reprocessing component we use

$$T_{\rm rep}(r) = \left[\frac{f_2 L_X \omega \sqrt{f_1 k/\mu m_H}}{14\pi\sigma GM} \right]^{2/7}$$

where f_1 is a factor of order unity which depends on the vertical structure of the disk, f_2 is the fraction of incident X-rays absorbed by the disk, μ is the molecular weight of the disk material, and $\omega = \sqrt{GM/r^3}$ is the Keplerian rotation frequency. In all

models we set $f_1 = 1$, $f_2 = 0.5$, and $\mu = 0.5$. L_X and $\dot{M}$ are related by

$$L_X = f_3 \frac{GM\dot{M}}{R_*}$$

where f_3 is factor taking into account possible anisotropy of radiation and is set to 0.5 here for all models. We combine the two components to arrive at the final temperature distribution of the disk with

$$T_{\rm disk}(r) = \left[T_{\rm acc}(r)^4 + T_{\rm rep}(r)^4\right]^{1/4}$$

which will be referred to as model 2.

The spectrum as observed from a distance D at inclination i is then generated by integrating a blackbody curve as a function of $T(r)$ times the area of each ring within the disk

$$f_\lambda = \frac{4\pi hc^2 \cos i}{\lambda^5 D^2} \int_{R_*}^{R_D} \frac{r\ {\rm d}r}{e^{hc/\lambda k T_{\rm disk}(r)} - 1}.$$

We use the distance to each cluster as a fixed parameter, and therefore the only free parameters in these disk models are the mass accretion rate $\dot{M}$, the outer radius of the disk R_D, and the system inclination angle i. The slope of the flux shortward of 3000 Å is more sensitive to $\dot{M}$ and the flux at longer wavelengths is more sensitive to R_D; the overall flux is increased by increasing either parameter. $\cos i$ is merely a scaling factor which does not alter the SED slope. It is usually just set to something reasonable based on what is known about the system thus far or simply set to a median value of 45°.

We constrain the outer radius of the disk R_D to be greater than or equal to the circularization radius $R_{\rm circ} = a\ (1+q)\ (0.500 - 0.227 \log q)^4$, where a is the orbital separation of the two stars, and q is the mass ratio M_2/M. The expected angular momentum of material transferred from the secondary via Roche lobe overflow is such that this material will initially settle to a circular orbit at the circularization radius; subsequent disk evolution will cause some of this material to migrate inwards, and possibly some outwards. The outer radius of an accretion disk is probably also

confined to not exceed the Roche lobe radius $R_L = a\ (0.38 - 0.20\ \log q)$ as material outside R_L is not bound only to the primary. Therefore of the three free parameters, two do have fairly tight constraints; only $\dot{M}$ is allowed to take on any value.

In each of the following sections, we discuss the overall spectral energy distributions and the models for each of the five objects individually. All spectra and broadband magnitudes are in the STMAG system, and have been dereddened with the curve of Savage & Mathis (1979). Reddening and other fixed parameters used are listed in Table 3.2. A summary of the best values for the free parameters is listed in Table 4.5.

4.3.1 Star A in NGC 1851

The FOS G160L spectrum and WFPC2 magnitudes are plotted in Fig. 4.7. The top panel shows a $T_{\rm eff} = 17000$ K Kurucz model ([Fe/H] $= -1.0$, $\log g = 5.0$) as well as a $T_{\rm BB} = 27000$ K blackbody curve overplotted. The stellar atmosphere model fits the dereddened UV spectrum very well, but the Balmer decrement is far too large to be compatible with the WFPC2 measurements. The single-temperature blackbody curve fits the WFPC2 magnitudes quite well, but agrees only crudely with the shape of the UV spectrum.

In the lower panel, we show the same observations, but with the best fit for the disk model 2 overplotted. The orbital period of this system is still not known, although its low optical luminosity implies a short period. Thus for both the disk models we begin with the assumption that the orbital separation is $a = 0.30\,R_\odot$ since the similarity in SED shape to Star S and Star K imply an ultracompact system. As no orbital modulation has yet been identified, there is is no information on the orbital inclination, so we arbitrarily assign a median value of $i = 45°$. For model 1, the parameters $R_D = R_L = 0.18\,R_\odot$, $\dot{M} = 0.55 \times 10^{-9} M_\odot$ yr^{-1}, and inclination $i = 45°$ yield an excellent fit. For model 2 we find a smaller disk is required: $R_D = 0.7\,R_L = 0.13\,R_\odot$, $\dot{M} = 0.25 \times 10^{-9} M_\odot$ yr^{-1}, and inclination $i = 45°$ yields a nearly identical fit; this

latter curve is overplotted in the lower panel of Fig. 4.7. Model 2 cannot produce a good fit at $R_D = R_L$ for this system size. Only if the orbital separation is lowered to $a = 0.20\,R_\odot$ (essentially equal to the Star K system size, the smallest known) can a good fit be obtained with $R_D = R_L$. If the system size is larger, the disk must be smaller with respect to the Roche lobe radius and the inclination must be high. A good fit can be obtained with parameters $a = 0.60\,R_\odot$, $R_D = R_C = 0.58\,R_L = 0.12\,R_\odot$, $\dot{M} = 1.20 \times 10^{-9} M_\odot$ yr^{-1}, and inclination $i = 80°$. However, an inclination angle as high or higher than this would surely have produced detectable X-ray periodic modulation in existing observations. We conclude from the SED that the system size must be less than $0.60\,R_\odot$, and therefore orbital period for this system must be shorter than 1 hr for reasonable mass assumptions.

A determination of the orbital period for this system will clearly constrain the model further, although the order-of-magnitude geometry of this system seems clear: similar to the LMXBs in NGC 6624 and NGC 6712, this is an extremely compact system.

4.3.2 Star U1 in NGC 6441

HST STIS spectra for this object are scheduled for observation sometime during the next year, but for the moment only broadband magnitudes are available. All photometry discussed here is tabulated in Deutsch et al. (1998) and is therefore not listed in this chapter. NGC 6441 has been imaged by *HST* on three separate occasions, twice by WFPC2 and once by FOC. In Fig. 4.8 we plot all these broadband magnitudes, dereddened with $E(B-V) = 0.42$. Three different symbols are used, each representing a different epoch. The filled circles denote the most useful epoch (1995 September 12); here two or three consistent measurements were obtained in each of the F218W, F439W, and F555W filters within a span of 0.5 hr. Other measurements suggest considerable variability on short and long timescales, and thus until the variability of this source is better understood, only contemporaneous magnitudes

are likely to be useful in determining the SED of this source (as is the case with AC 211). The 1994 August 8 observations (open diamonds) clearly indicate variability in m_{336} during the sequence, and thus do not improve the constraints on the SED. Finally, the FOC measurements (asterisks) have fairly large uncertainties and do not add additional constraints, except in the broadest sense where they seem compatible with these crude models.

Both a $T_{\rm eff} = 15000$ K Kurucz model and a $T_{\rm BB} = 14000$ K blackbody spectrum match the available contemporaneous magnitudes acceptably. In the lower panel of the Fig. 4.8, we show the same observations, but with an accretion disk model 2 overplotted. We set $i = 60$ as the observed X-ray dips suggest a fairly high inclination. By choosing $R_D = R_L$ model 1 does not reproduce the SED well, although a larger R_D may do so. By choosing $R_D = R_L$ model 2 can reproduce the filled-circle data points very well at $\dot{M} = 2.27 \times 10^{-9} M_\odot$ yr^{-1} (shown in figure). In this scenario the X-ray reprocessing dominates the energy source in this large disk, thereby generating a flatter SED. Such a flat SED is required if all of the solid circles in Fig. 4.8 are to be fit. If the m_{228} measurements are allowed to be ~ 0.5 mag brighter, a number of higher $\dot{M}$, hotter disk models become viable. A UV spectrum of this source would be extremely valuable in constraining the SED of this system. In any case, the high optical luminosity and shallow SED of this source has clear implications: this system contains a much larger accretion disk, allowing the cooler regions to contribute significant light to the SED. This is not surprising as this source seems to have a 5.7 hr orbital period from X-ray observations (Sansom et al. 1993).

4.3.3 Star K in NGC 6624

The dereddened FOS G160L spectrum and WFPC2 magnitudes are plotted in Fig. 4.9. As with all these objects, the broadband photometry was obtained at different epochs and the object is known to be variable. The spectrum is averaged over many system orbits, but the WFPC2 images subtended only a fraction of an orbit. The

orbital variation at these longer wavelengths is likely to be less than 10% full amplitude (Anderson et al. 1997). However, the X-ray flux from this object varies considerably on timescales of weeks, and the optical luminosity may do so as well.

In the upper panel of Fig. 4.9, we overplot a $T_{\rm eff} = 24000$ K Kurucz model ([Fe/H] $= -1.0$, log $g = 5.0$) as well as a $T_{\rm BB} = 35000$ K blackbody curve. The blackbody fits the spectrum and WFPC2 points only crudely. The Kurucz model used, however, appears to fit the data extremely well. This implies that there is a Balmer decrement in Star K's SED, but we caution that the measurement of m_{439} is severely hampered by contamination and the error bar given may be too small. Until this region can be studied with a contamination-free spectrum, the existence of a Balmer decrement remains uncertain.

In the lower panel, we show the same observations, but with an accretion disk model 2 overplotted. This is a very similar model as discussed by Arons & King (1993) in their study of this system, although only two *HST* FOC datapoints were available at that time. The system parameters seem fairly certain for this LMXB: the primary is a neutron star, probably with mass about $1.4\,M_\odot$, and the secondary is likely to be something like a helium degenerate dwarf with mass about $0.07\,M_\odot$ and radius $0.03\,R_\odot$ (Arons & King 1993). We use inclination $i = 43$ estimated by Anderson et al. (1997). For the observed orbital period of 685 s, a binary separation of only $0.19\,R_\odot$ and a Roche lobe radius $R_L = 0.12\,R_\odot$ is implied.

Unfortunately, the two models considered here do not permit a good fit at $R_D \leq R_L$. For model 1, a good fit is achieved for $R_D = 1.8\,R_L = 0.22\,R_\odot$, $\dot{M} = 39.7 \times 10^{-9} M_\odot$ yr^{-1}. For model 2, a smaller disk is permitted but a good fit can only be achieved $R_D = 1.6\,R_L = 0.19\,R_\odot$, $\dot{M} = 7.75 \times 10^{-9} M_\odot$ yr^{-1} (upper curve in Fig. 4.9). The extra region beyond R_L is required to add enough cool radiation to reproduce the observed slope of the UV continuum at the high L_X. If we constrain $R_D = R_L$ the resulting curve is too steep at the best fit accretion rate $\dot{M} = 15.0 \times 10^{-9} M_\odot$ yr^{-1} (lower curve).

The implications of these results is unclear. The most likely interpretation is that our understanding of the geometry or the temperature profile of the disk is more complex than has been considered here. We have explored adding additional components to the model, including the heated secondary discussed by Arons & King (1993) and a cool edge to a thick disk, neither of which are able to add enough cool flux to flatten the model SED sufficiently. Another reasonable interpretation is a failing of the data: there may be significant contamination in the spectrum and photometry by the extremely dense environment (even by *HST* standards) around this object. If the model and observations are a reasonably accurate representation of this system, the conclusion must be that the accretion disk is not confined by the Roche lobe radius, but rather is able to fill the entire system with optically thick material. Increasing the neutron star mass to 2.4 $M_\odot$ reduces the required $\dot{M}$ parameter and increases the system size a, but R_D must also increase and a good fit still requires $R_D \approx a$.

Finally we point out that the m_{439} measurement is not fit by either curve; either the measurement is in error, the object exhibited $\sim 50\%$ variation between the F336W and F439W observations, or a substantial Balmer decrement is present in this object's spectrum. No reasonable parameters (including $R_D > 1\ R_\odot$) for this disk model allow a spectrum which simultaneously fits the UV spectrum and the m_{439} measurement. We do note the possible strong, broad Ly α absorption, which may imply a significant decrement.

4.3.4 Star S in NGC 6712

The dereddened FOS spectra and WFPC2 magnitudes are plotted in Fig. 4.10; the UV spectrum is heavily binned 12×. We note that the magnitude of the UV spectrum is 100× lower than was presented in Downes et al. (1996); we attribute this discrepancy to a binning error in that paper. The filled circles are WFPC2 detections (photometric uncertainties are smaller than the symbol sizes) and the triangle is an upper limit, since the object was not detected in the F160W exposure. These exposures were all

obtained at the same epoch during which variability was found to be only 4% at 3000 Å (Homer et al. 1996). It is immediately clear that the optical FOS spectrum and the WFPC2 magnitudes are incompatible longward of 4300 Å, not merely in amplitude but also in slope. Either the temperature of this source has changed dramatically between the observations, or the FOS spectrum is contaminated (the object is not blended with other stars in the WFPC2 frames).

We estimate the amount of contamination flux in this preservicing mission spectrum by convolving the F555W WFPC2 image with a Tiny Tim (Krist 1993) WF/PC F555W PSF, and measuring the amount of flux which falls in a simulated 0.″5 FOS aperture. When the aperture is centered perfectly on Star S, we find that there should be 50% more flux from neighboring PSFs than from the LMXB. If the aperture is moved away from the brightest neighbor by 0.″2 the contaminating and target flux are equal. As the precise position of the aperture is not known and our simulation of the PSF seen at the time by FOS is crude, we conclude from this only that there will contaminating light equal to within a factor of 2 of the light from Star S at 5000 Å.

As the WFPC2 magnitudes are uncontaminated, we fit a blackbody curve to these data points and find that $T_{BB} = 19000$ K provides a good representation of the data. We then search for a Kurucz model which when arbitrarily scaled and added to the blackbody spectrum accurately creates the FOS G650L spectrum. The selected Kurucz model of $T_{\rm eff} = 5000$ K ([Fe/H] $= -1.0$, $\log g = 3.0$) and the final combined spectrum are shown in the top panel of Fig. 4.10. The agreement is excellent, and may explain the faint detection of the G band in the FOS spectrum. In the lower panel, we repeat the exercise with a hot Kurucz model instead of the pure blackbody curve. The result is similar, and we conclude that this optical spectrum is severely contaminated and is not useful for studying the SED of Star A, and is therefore excluded for the rest of the discussion. We suggest that the blackbody curve fit to this spectrum by Downes et al. (1996) is not a relevant parameter for this system. It is of course possible that the source varied, but we expect contaminating flux equal

to or greater than is modeled here, so the simplest explanation is that the difference is completely due to contamination.

In the upper panel of Fig. 4.11, we show the same data except for the optical spectrum. We overplot the best fitting blackbody spectrum $T_{BB} = 19000$ K and Kurucz stellar atmosphere $T_{\rm eff} = 22000$ K. Both models fit the WFPC2 photometry quite well. The Kurucz model seems to fit somewhat better as the photometry suggests a Balmer decrement is present. However, the Balmer lines certainly cannot be as strong as in the model else they would have been detected in the spectrum. However, the lines are highly dependent on the surface gravity used. Neither the blackbody spectrum nor the Kurucz model fit the UV spectrum very well, and the Kurucz model is perhaps even incompatible with the m_{160} upper limit.

In the lower panel of Fig. 4.11, we show the same observations, but with the best fit for the disk model 2 overplotted. For model 1, the parameters $R_D = R_L = 0.18\,R_\odot$, $\dot{M} = 2.77 \times 10^{-9} M_\odot$ yr^{-1}, and inclination $i = 30°$ yield a good fit. For model 2 we use the same R_D and i and find $\dot{M} = 0.65 \times 10^{-9} M_\odot$ yr^{-1} provides a slightly better fit to the available observations. Slightly larger R_D values would also yield acceptable if not even slightly better fits to the data, but we limit $R_D \leq R_L$ here.

The UV spectrum is reasonably well fit by this model longward of 1500 Å, and the signal is so low shortward of 1500 Å that the discrepancy is not alarming. This model is also just barely compatible with the m_{160} upper limit. As with previous models, the WFPC2 photometry hints of a very slight Balmer decrement.

4.3.5 Star AC211 in M 15

The dereddened FOS spectra and WFPC2 magnitudes are plotted in Fig. 4.12. The larger filled circles are WFPC2 detections obtained at a single epoch and the smaller circles represent a sampling of other measurements taken at different epochs; this clearly shows the magnitude of variability of this object, which will make this analysis more difficult. Although, as with the Star S, the WFPC2 magnitudes do not match

the FOS optical spectrum, the difference appears to be merely a constant offset, not surprising for this object. Since the slope of the WFPC2 magnitudes and the optical spectrum are nearly identical, we infer that the spectrum is *not* contaminated by nearby neighbors. It is possible that the light from AC 211 is contaminated by a bright star so close that even WFPC2 cannot resolve them, but this chance seems remote unless that star is part of the system or has been recently ejected.

A blackbody fit to the optical spectrum yields an excellent fit at $T_{BB} = 11200$ K; a blackbody fit to the UV spectrum also yields an excellent fit, but at $T_{BB} = 22000$ K. The UV spectrum can also be fit well by a Kurucz model of $T_{\rm eff} = 10500$ K ([Fe/H] $= -1.0$, $\log g = 5.0$). Unfortunately, it is immediately apparent that any of the aforementioned models fit only one of the FOS spectra and match the other data poorly.

In the lower panel of Fig. 4.12, we show the same observations, but with the best accretion disk model 2 overplotted. Model 1 does not fit at all since to achieve the required luminosity requires a ridiculous $\dot{M} = 500 \times 10^{-9} M_\odot$ yr^{-1}, which in turn cannot produce the flat SED with any reasonable disk size. Model 2 can plausibly reproduce some aspects of the data: at $R_D = R_L = 1.9\,R_\odot$, $\dot{M} = 9.04 \times 10^{-9} M_\odot$ yr^{-1}, and inclination $i = 70°$ the UV spectrum is reasonably well fit, but the SED is a bit too steep in the optical. If the size of the disk is allowed to fill the entire system $R_D = a = 4.4\,R_\odot$, then model 2 parameters yield a decent fit to the optical spectrum at $\dot{M} = 8.0 \times 10^{-9} M_\odot$ yr^{-1}, and inclination $i = 70°$, but then the shape of the UV spectrum is poorly reproduced.

However, even a casual inspection of the optical and UV spectra reveals that the two do not correspond to each other in an obvious manner. The UV spectrum is steeper than the optical spectrum and longest wavelength edge is only marginally higher in flux than the short wavelength end of the optical spectrum. This implies either a nearly flat region between 2500 and 3500 Å or a sudden decrement. A flat region seems unlikely and the optical spectrum should show some sign of a Balmer

decrement if it were present. The WFPC2 magnitudes clearly strongly rule out a Balmer decrement. The most likely explanation for this then is marked variability between the optical and UV spectra, accompanied by a change in spectral slope.

In order to assess the likelihood of such variability, we first examine the variability within the spectra. These FOS spectra were read out several times per exposure, and we plot the total calibrated counts (i.e. corrected for instrumental artifacts, but not converted to flux units) for each readout vs. time since the start of the first spectrum in Fig. 4.12. Only about 5% variability is observed between the two optical spectra. The first UV spectrum, however, is observed to undergo a 11% change during the exposure. The count rate has rebounded again by the last exposure. It is certainly plausible that the UV flux of the object has dropped between the end of the optical exposures and the start of the UV exposures (an interval of 1.5 hr). All these exposures occurred between phase 0.6 and 0.8 which appears to be a reasonably flat region of the average light curve of Ilovaisky et al. (1993). However, one set of 1985 observations in Fig. 4 of that paper clearly shows a 1.0 mag drop in U between phase 0.7 and 0.8, so this behavior seems reasonable. Further, m_{336} magnitudes in Table 4.4 show a brightening by 0.8 mag in 1.5 hr (between phase 0.47 and 0.56, which is not obviously a particularly steep region in the light curve of AC 211). In any event, it is clear from the light curve of Ilovaisky et al. (1993) that this object varies erratically, and we thus suggest that it is quite possible that the discrepancy between the optical and UV light curves is merely due to intrinsic variability in the object. It is also usually the case that variability amplitude is much higher in the ultraviolet.

If we accept variability which moved the UV spectrum up by 1.0 magnitude, the disk model 2 fits crudely although is not quite cool enough in the optical. Also, the broad absorption around Ly α which may indicate a significant deviation from our blackbody assumption is not explained by the model. The construction of a model which can accurately reproduce this huge feature will be an undertaking for the future.

In Fig. 4.14 we entertain two other interpretations. In the upper panel, we com-

bine two appropriately scaled single-temperature models, a $T_{BB} = 22000$ K blackbody curve and a Kurucz model of $T_{\rm eff} = 6500$ K ([Fe/H] $= -1.0$, $\log g = 4.0$). This, again, requires the assumption of considerable variability between the UV and optical spectra, but matches the shapes of all available data well (except for the Ly α absorption). Why it would be appropriate to combine these two models is unclear. An extremely close accidental superposition is one possibility. Other options include: the secondary is extremely bright with a $T_{\rm eff} = 6500$ K spectrum, the accretion disk somehow looks like this, the system is a triple with such a star (a giant presumably) in it.

If we wish to reject the idea of variability, we can examine another option. An extremely contrived model which includes the superposition of three spectra almost works: a combination $T_{BB} = 22000$ K blackbody curve and $T_{\rm eff} = 10500$ K Kurucz model fits the UV fairly well (as each individual curve fits), and when that is combined with a suitably scaled $T_{\rm eff} = 7250$ K Kurucz model, the result fits both the UV and optical spectra quite well. The model and the optical spectrum deviate at the Balmer decrement, but the spectrum may be unreliable here (see above). However, the WFPC2 magnitudes rule out this complex picture because the single-epoch measurements show that any Balmer decrement present must be very small. In the figure, we shift up the WFPC2 magnitudes by 0.45 mag and plot as filled triangles. Our contrived model is compatible with the F439W and F555W measurements, but clearly incompatible with the F336W measurement. As the only physics which can explain the discrepancy between the UV and optical spectra without variability is the Balmer decrement, the WFPC2 magnitudes confirm that the discontinuity must be due to intrinsic variability.

4.4 Discussion

Comparing the SEDs of the five globular cluster LMXBs we have examined thus far, we find that two classes appear to be emerging. To illustrate this we plot in Fig. 4.15

the fitted accretion disk models on an absolute magnitude scale, i.e. the fits from the previous section corrected for the distance to each cluster. Each curve is labeled with the cluster containing the source. The orbital period, if known, is labeled at the right for each source. It should once again be noted that each of these sources is variable to some degree, and there maybe small color differences during times of different luminosities. Of the two models plotted in Fig. 4.9, the better fitting, $R_D = 1.6\,R_L$ model curve is shown here in Fig. 4.15. At far UV wavelengths the amount of flux continues to increase in all of these sources where other hot cluster stars begin to fall off. In fact, the brighter GC LMXBs are found to completely dominate the cluster light at $\sim$ 1400 Å as seen in Fig. 4.16.

The two most luminous (at $\sim$ 5000 Å) sources also have the flattest SEDs and the longest periods. The longer periods indicate that the systems are physically larger and therefore allow larger accretion disks which are able to process more X-rays into optical light. The outer edges of the disk are far enough from the neutron star that the temperatures can fall to $\sim$ 11000 K. The three less luminous (at $\sim$ 5000 Å) sources studied here have steeper SEDs. Two of the three are known to have extremely short periods (0.19 and 0.36 hr) implying that the accretion disks must be very small to fit within the Roche lobe radius of the primaries and are therefore still very hot ($\geq$ 15000 K) at their outer edges. As the SED of the source in NGC 1851 is very similar to Star S in NGC 6712, we predict that the NGC 1851 system will also prove to be an ultracompact system with orbital period less than 1 hr.

From applying these models to a group of reasonably uniform data on five different objects, we are able to draw some conclusions about the accuracy of the models. First we conclude that model 1, where the surface temperature of the disk is a result of accretion heating only, can describe the ultracompact systems reasonably well, but cannot describe the larger systems at all. Model 2, which also includes heating from X-ray reprocessing, can describe all of the systems well except perhaps in the case of the M 15 source. However the high-amplitude variability of this source makes the

present data difficult to interpret by any means and thus this should likely not be regarded as a failing in the model yet.

Another remarkable result of the application of model 2 is that in all cases except for the object in NGC 1851 the outer disk radius R_D has reached the limit of the Roche lobe radius R_L. These models require that the accretion disks fill the Roche lobe of the primary, and in several cases the models would be better off if the accretion disk would be even larger, filling the entire system. The predicted spectra are quite sensitive to R_D as most of the light at optical wavelengths is generated at the outer edges. Therefore it may be that model 2 simply does not accurately reflect the actual temperature profile in these systems, that the outer regions are cooler than predicted in this way. If Star A in NGC 1851 follows this pattern, the system should have an extremely short period, around 10 min

As part of model 2 we calculate L_X as a function of $\dot{M}$ in order to determine the amount of reprocessed X-rays. However, a comparison of the relative values of $\dot{M}$ predicted by the models and the observed L_X shows little correlation. This has been noted before by Vrtilek et al. (1991) where $\dot{M}$ from UV spectral fits was compared with simultaneous X-ray observations of Sco X–1. This can be explained if X-ray flux observed from a large distance depends heavily on system geometrical alignments whereas the large solid angle of the accretion disk is far less sensitive to these effects.

Table 4.1: Photometry for Star A in NGC 1851 from *HST* data

Object Name	HDA [a] rootname	UT Date	UT Start	Exposure Time (s)	Filter / Grating	mag	error (1σ)	phase
Star A	u2vo0302t	05/10/95	17:40:16	40	F555W	21.6	0.3	
Star A	u2vo0304t	05/10/95	17:45:16	160	F439W	20.48	0.2	
Star A	u2vo0305t	05/10/95	17:49:16	160	F439W	20.37	0.2	
Star A	u2vo0306t	05/10/95	17:54:17	600	F218W	19.35	0.13	
Star A	u2vo0307t	05/10/95	18:07:17	1000	F218W	18.81	0.08	
Star A	u2va0101t	10/04/96	06:23:16	900	F336W	19.73	0.10	
Star A	u2va0102t	10/04/96	06:41:16	900	F336W	19.73	0.10	
Star A	u2va0103t	10/04/96	07:00:16	300	F439W	20.46	0.10	
Star A	u2va0104t	10/04/96	07:56:16	300	F439W	20.46	0.10	
Star A	u2va0105t	10/04/96	08:04:16	300	F439W	20.46	0.10	
Star A	u2va0106t	10/04/96	08:12:16	300	F439W	20.46	0.10	
Star A	u2va0107t	10/04/96	08:21:16	900	F336W	19.73	0.10	
Star A	u2va0108t	10/04/96	09:32:16	900	F336W	19.73	0.10	
Star A	y3hg0205p	10/01/97	10:09:32	2510	G160L	–	–	
Star A	y3hg0206p	10/01/97	11:45:37	1300	G160L	–	–	

[a] Hubble Data Archive dataset name

Table 4.2: Photometry for Star K in NGC 6624 from *HST* data

Object Name	HDA [a] rootname	UT Date	UT Start	Exposure Time (s)	Filter / Grating	mag	error (1σ)	phase
Star K	u2as0105t	17/04/94	23:00:17	50	F439W	17.99	0.20	
Star K	u2as0106t	17/04/94	23:03:17	50	F439W	17.99	0.20	
Star K	u2as0107t	17/04/94	23:07:17	200	F336W	17.62	0.20	
Star K	u2as0108t	17/04/94	23:13:17	200	F336W	17.62	0.20	
Star K	y3590202t	01/05/96	16:40:52	873	G160L	–	–	
Star K	y3590203t	01/05/96	17:47:21	2207	G160L	–	–	
Star K	y3590204t	01/05/96	19:23:35	2207	G160L	–	–	
Star K	y3590205t	01/05/96	21:00:05	2207	G160L	–	–	
Star K	y3590206t	01/05/96	22:36:40	2207	G160L	–	–	

[a] Hubble Data Archive dataset name

Table 4.3: Photometry for Star S in NGC 6712 from *HST* data

Object Name	HDA [a] rootname	UT Date	UT Start	Exposure Time (s)	Filter / Grating	mag	error (1σ)	phase
Star S	y1ba0103t	03/05/93	17:38:08	2249	G650L	–	–	
Star S	y1ba0104t	03/05/93	19:12:40	2249	G650L	–	–	
Star S	y24x0103t	08/09/94	08:51:17	380	G160L	–	–	
Star S	y24x0104t	08/09/94	09:48:32	2309	G160L	–	–	
Star S	y24x0105t	08/09/94	11:24:40	2309	G160L	–	–	
Star S	y24x0106t	08/09/94	13:01:54	1099	G160L	–	–	
Star S	u2of010st	25/05/95	21:25:17	300	F300W	19.74	0.03	
Star S	u2of010yt	25/05/95	23:01:17	300	F300W	19.72	0.03	
Star S	u2of0117t	26/05/95	01:50:17	300	F300W	19.72	0.03	
Star S	u2of0201t	28/05/95	13:16:16	160	F336W	19.69	0.04	
Star S	u2of0202t	28/05/95	13:21:16	160	F439W	19.86	0.03	
Star S	u2of0203t	28/05/95	13:26:16	60	F555W	20.32	0.03	
Star S	u2of0204t	28/05/95	13:30:16	60	F675W	20.75	0.03	
Star S	u2of0205t	28/05/95	13:34:16	120	F814W	21.16	0.03	
Star S	u2of0206t	28/05/95	13:39:17	800	F160BW	> 19.0	0.3	

[a] Hubble Data Archive dataset name

Table 4.4: Photometry for AC 211 in M 15 from *HST* data

Object Name	HDA [a] rootname	UT Date	UT Start	Exposure Time (s)	Filter / Grating	mag	error (1σ)	phase
AC 211	y2hz0104t	30/04/95	17:57:35	1049	G650L	–	–	0.61
AC 211	y2hz0105t	30/04/95	18:20:42	749	G650L	–	–	0.63
AC 211	y2hz0107t	30/04/95	20:03:15	810	G160L	–	–	0.73
AC 211	y2hz0108t	30/04/95	21:11:38	990	G160L	–	–	0.80
AC 211	u2as0201t	07/04/94	00:48:17	8	F555W	16.06	0.01	0.44
AC 211	u2as0202n	07/04/94	00:50:17	8	F555W	16.02	0.01	0.44
AC 211	u2as0203t	07/04/94	00:52:17	8	F555W	16.02	0.01	0.44
AC 211	u2as0204t	07/04/94	00:54:17	8	F555W	16.04	0.01	0.44
AC 211	u2as0205t	07/04/94	00:57:17	40	F439W	15.48	0.01	0.45
AC 211	u2as0206t	07/04/94	00:59:17	40	F439W	15.48	0.01	0.45
AC 211	u2as0207t	07/04/94	01:02:17	200	F336W	15.08	0.01	0.45
AC 211	u2as0208t	07/04/94	01:08:17	200	F336W	15.04	0.01	0.46
AC 211	u2hr0101t	30/08/94	13:39:16	100	F555W	16.29	0.01	0.55
AC 211	u2jg0101t	26/10/94	11:32:17	200	F336W	16.13	0.01	0.37
AC 211	u2jg0102t	26/10/94	11:38:17	200	F336W	16.06	0.01	0.38
AC 211	u2jg0103t	26/10/94	11:44:17	600	F336W	16.04	0.01	0.38
AC 211	u2jg0104t	26/10/94	11:57:17	600	F336W	15.98	0.01	0.39
AC 211	u2jg0105t	26/10/94	12:57:17	600	F336W	16.07	0.01	0.45
AC 211	u2jg0106t	26/10/94	13:10:17	600	F336W	15.88	0.01	0.47
AC 211	u2jg0107t	26/10/94	13:26:17	200	F336W	15.55	0.01	0.48
AC 211	u2jg0108t	26/10/94	13:32:17	200	F336W	15.60	0.01	0.49
AC 211	u2jg0109t	26/10/94	14:33:17	600	F336W	15.13	0.01	0.55
AC 211	u2jg010at	26/10/94	14:46:17	600	F336W	15.08	0.01	0.56
AC 211	u2jg010bt	26/10/94	14:59:17	600	F336W	15.09	0.01	0.57

[a] Hubble Data Archive dataset name

Table 4.5: Best model parameters for LMXB spectral energy distributions

	Model 1				Model 2			
System Name	R_D/R_L	$\dot{M}$	i	Quality	R_D/R_L	$\dot{M}$	i	Quality
NGC 1851 Star A	1.0	0.55	45	good	0.7	0.25	45	good for $P = 22$ min
					0.58	1.20	80	good for $P = 63$ min
					1.0	0.26	45	good for $P = 12$ min
NGC 6441 Star U1	1.0	62.30	60	poor	1.0	2.27	60	good
NGC 6624 Star K	1.8	39.70	43	good	1.6	7.75	43	good
					1.0	15.0	43	poor
NGC 6712 Star S	1.0	2.77	30	good	1.0	0.65	30	good
M 15 Star AC211	1.0	500	70	poor	1.0	9.04	70	fair

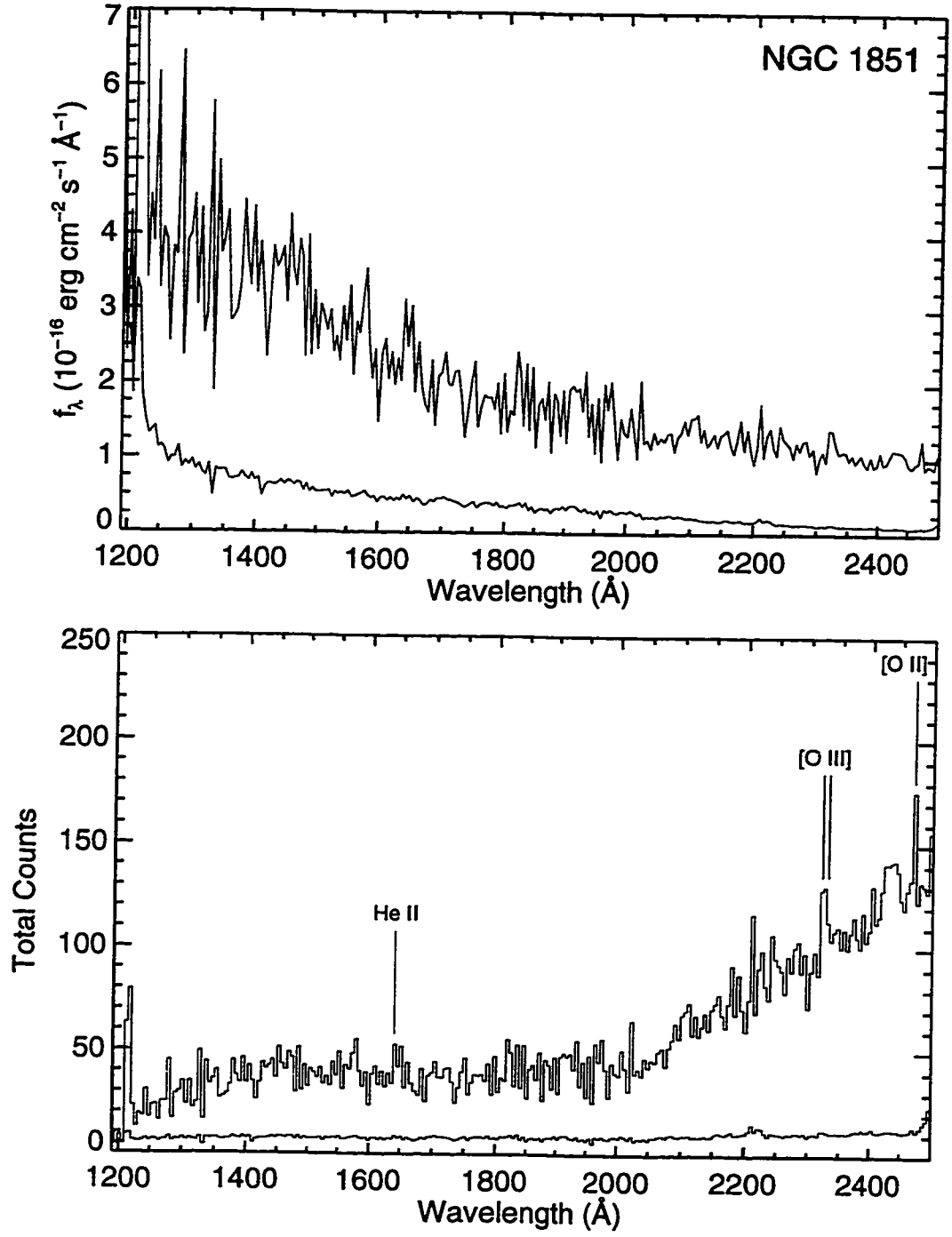

Figure 4.1: *Top Panel:* FOS G160L UV spectrum of Star A in NGC 1851. Below the spectrum is the 1σ uncertainty curve. This spectrum has been binned $3\times$ to increase S/N, but has not been corrected for reddening, which is only $E(B-V) = 0.02$ for NGC 1851. *Bottom Panel:* Same spectrum as above but in units of total counts per 5.2 Å bin. The location of He II λ1640, and two other possible features are marked; see text for a discussion of these features.

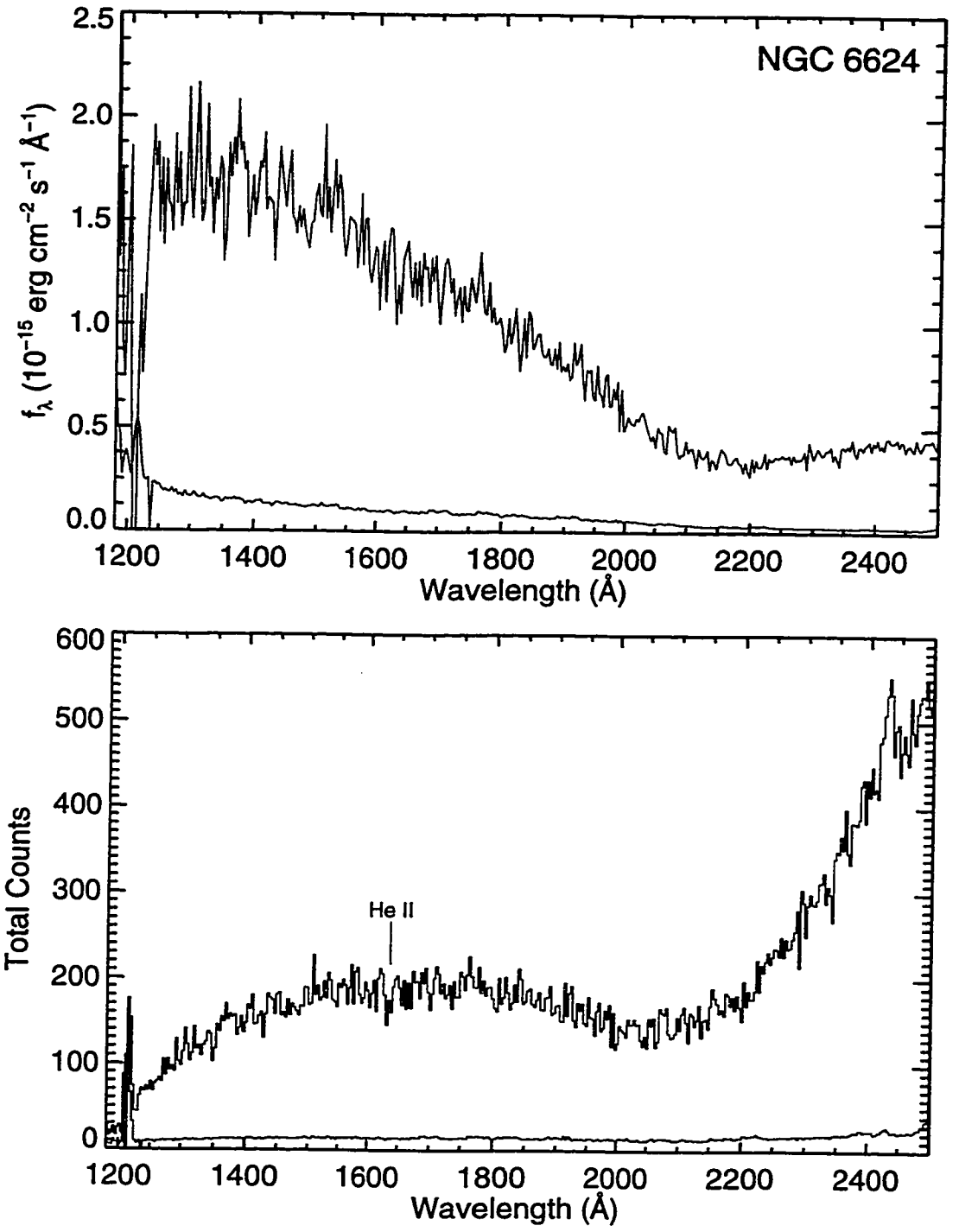

Figure 4.2: *Top Panel:* FOS G160L UV spectrum of Star K in NGC 6624. Below the spectrum is the 1σ uncertainty curve. This spectrum has been binned $2\times$ to increase S/N, but has not been corrected for reddening, which is a substantial $E(B-V) = 0.28$ for NGC 6624. *Bottom Panel:* Same spectrum as above but in units of total counts per 3.4 Å bin. The location of He II λ1640 is marked; see text for further details.

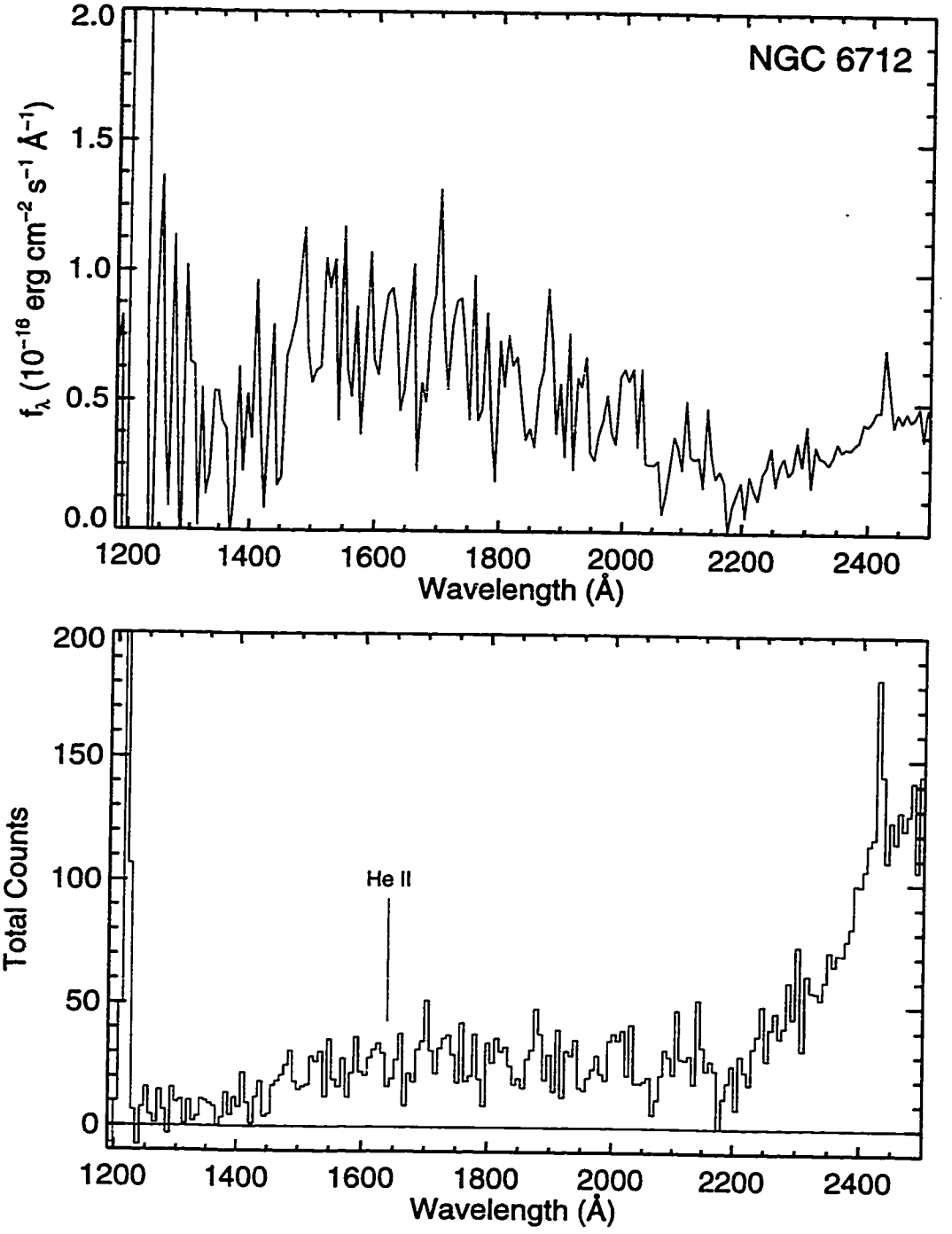

Figure 4.3: *Top Panel:* FOS G160L UV spectrum of Star S in NGC 6712. This spectrum has been binned 4× to increase S/N, but has not been corrected for reddening, which is a substantial $E(B-V) = 0.46$ for NGC 6712. *Bottom Panel:* Same spectrum as above but in units of total counts per 7 Å bin. The location of He II λ1640 is marked; see text for further details.

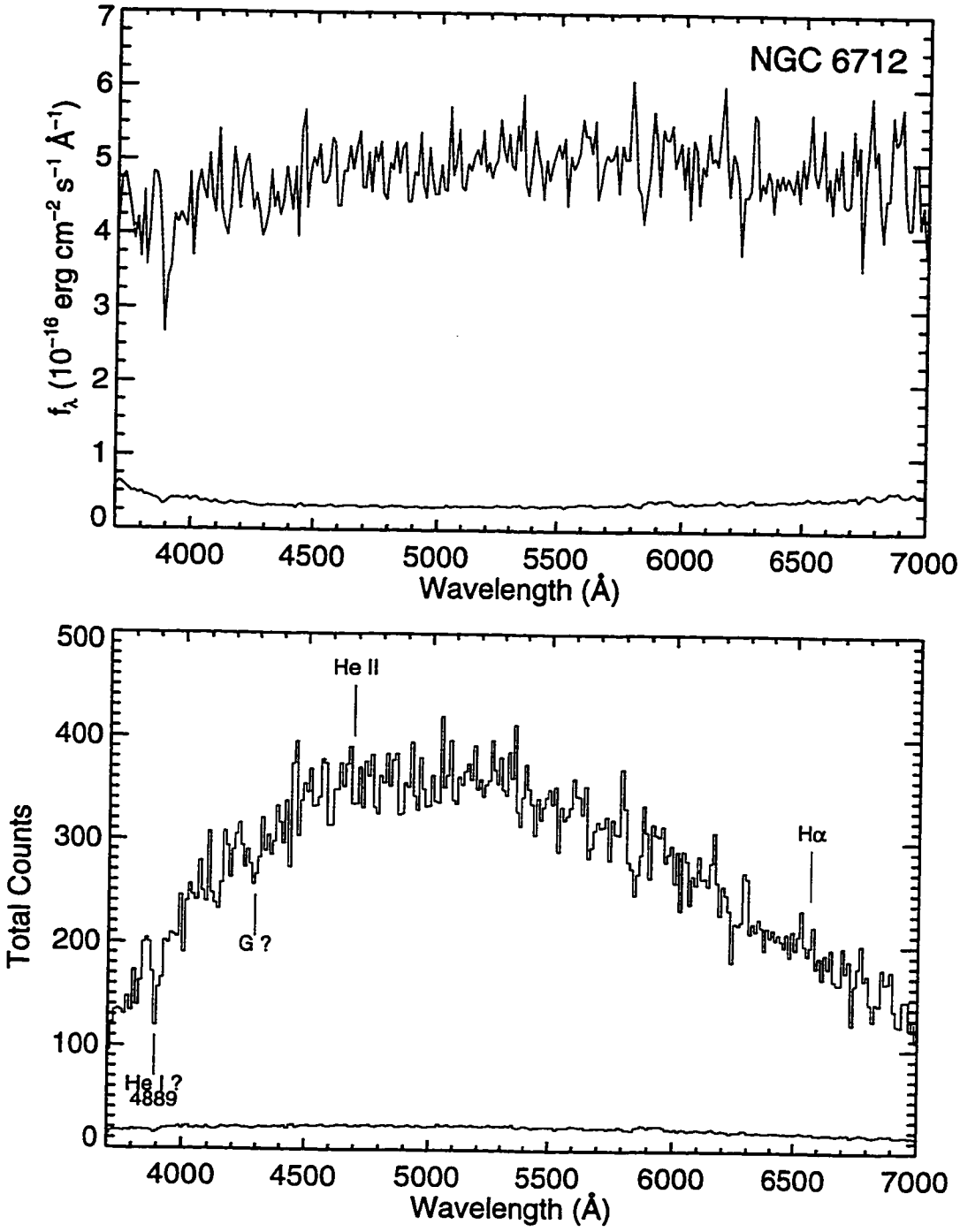

Figure 4.4: *Top Panel:* FOS G650L optical spectrum of Star S in NGC 6712. Below the spectrum is the 1σ uncertainty curve. This spectrum has been binned $2\times$ to increase S/N, but has not been corrected for $E(B-V) = 0.46$. *Bottom Panel:* Same spectrum as above but in units of total counts per 12 Å bin. The locations of He II λ4686 and Hα are marked, and we suggest two possible absorption identifications: He I λ4889 and the G band; see text for further details.

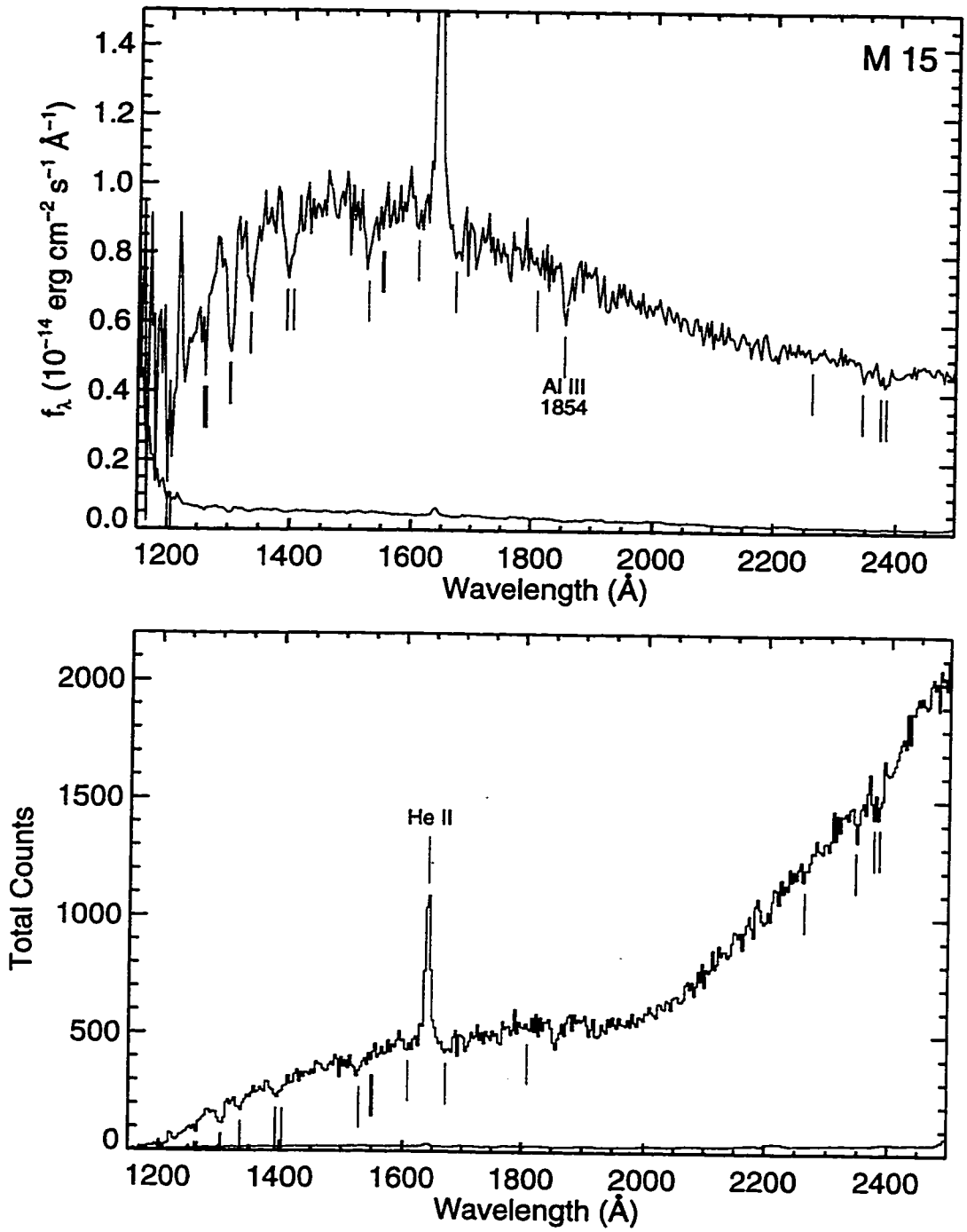

Figure 4.5: *Top Panel:* FOS G160L UV spectrum of AC 211 in M 15. This spectrum has been binned 2× to increase S/N, but has not been corrected for reddening, which is a modest $E(B-V) = 0.05$ for M 15. The locations of common interstellar absorption lines are marked in addition to the curious Al III λ1854 feature. *Bottom Panel:* Same spectrum as above but in units of total counts per 3.5 Å bin.

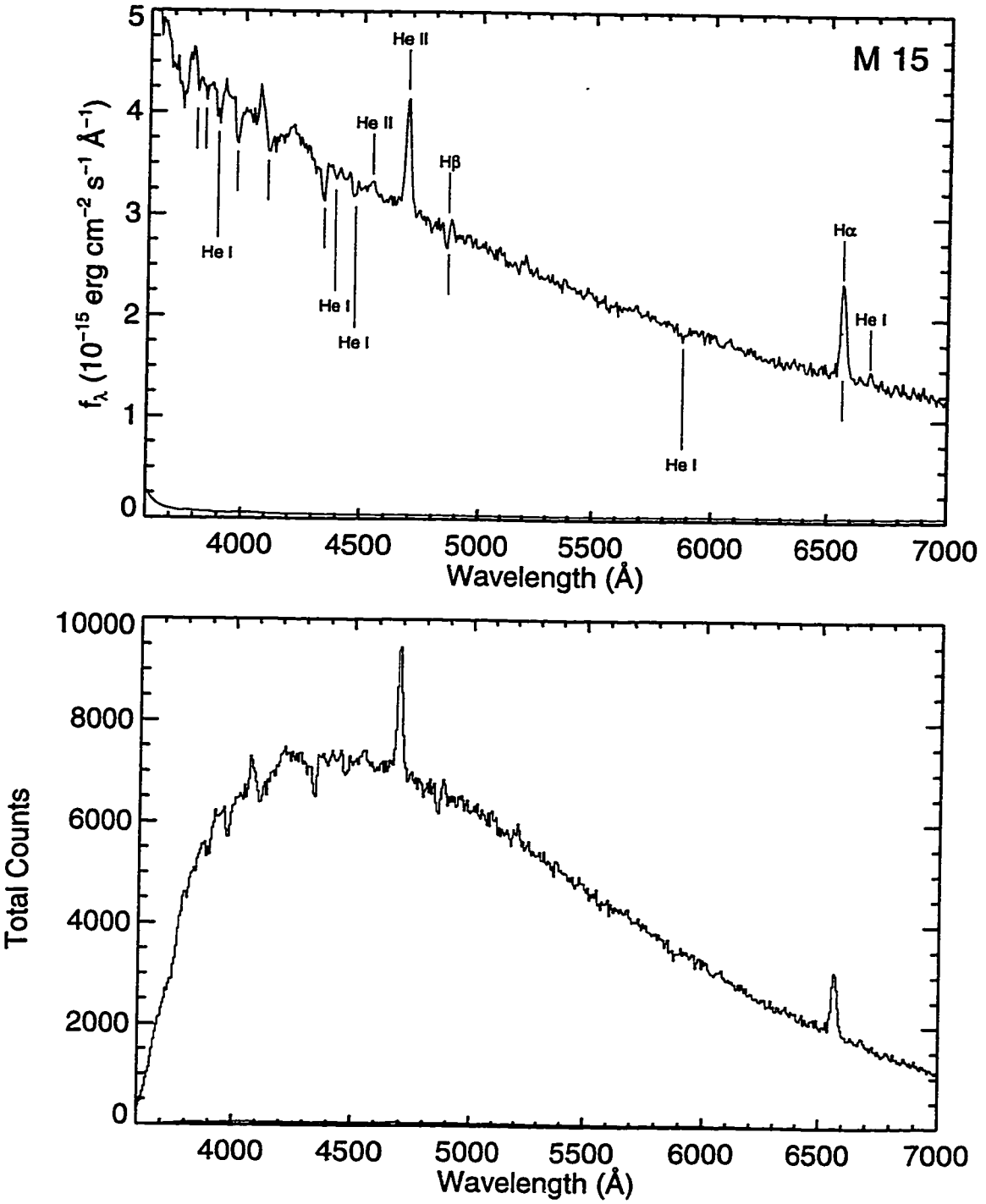

Figure 4.6: *Top Panel:* FOS G650L UV spectrum of AC 211 in M 15. Below the spectrum is the 1σ uncertainty curve. This spectrum has neither been binned nor corrected for $E(B-V) = 0.05$. Various emission and absorption lines dicussed in the text are marked. *Bottom Panel:* Same spectrum as above but in units of total counts per 6 Å bin.

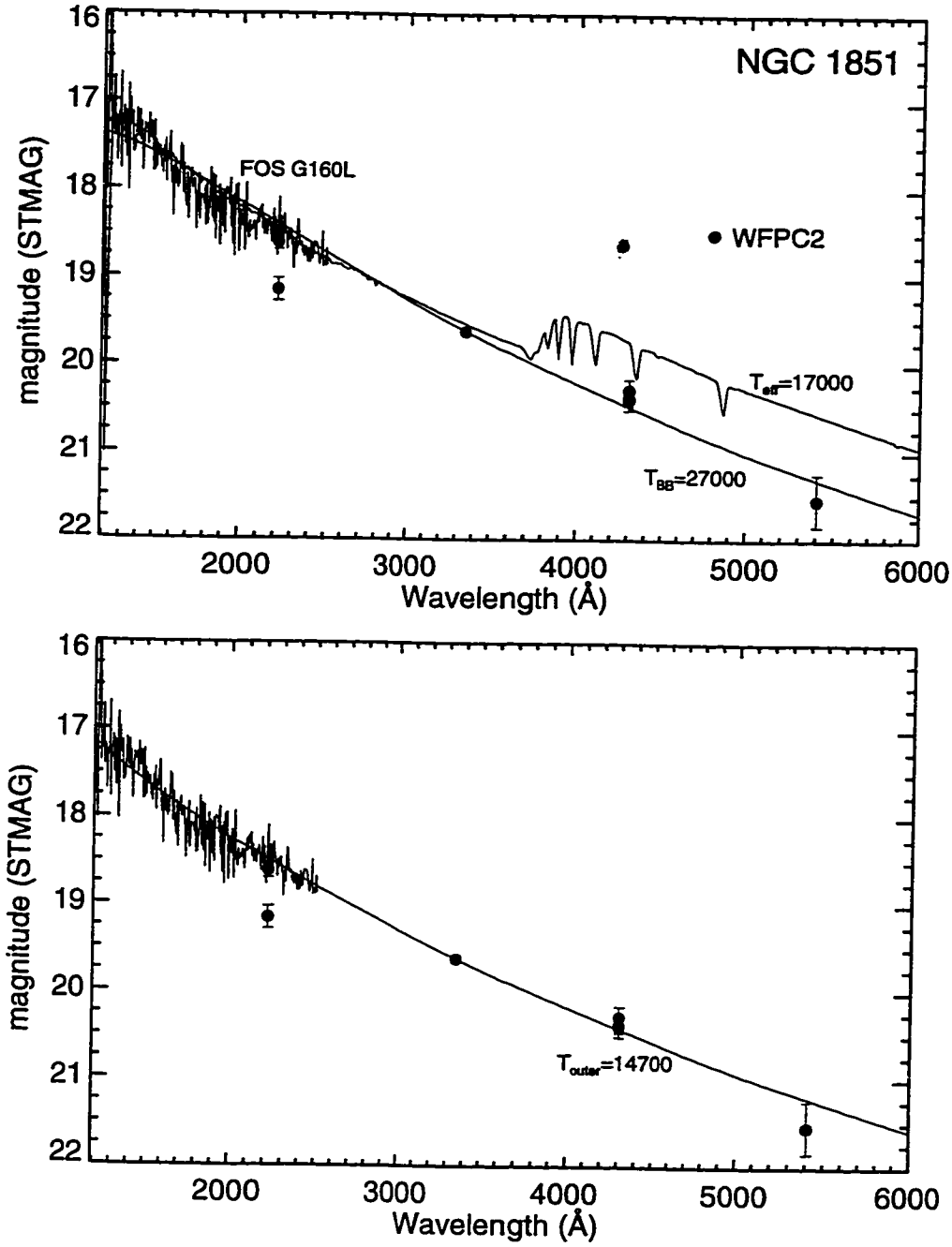

Figure 4.7: *Top Panel:* FOS G160L UV spectrum and WFPC2 broadband magnitude measurements for Star A in NGC 1851, all dereddened with E($B-V$) = 0.02. Overlaid are a $T_{\rm eff}$ = 17000 K Kurucz model and a $T_{\rm BB}$ = 27000 K blackbody spectrum. A single-temperature model provides a fair representation of the SED. *Bottom Panel:* Same observations as above, with a truncated-disk model overplotted. The model 2 parameters used, $R_D = 0.7\,R_L = 0.13\,R_\odot$, $\dot{M} = 0.25 \times 10^{-9} M_\odot$ yr^{-1}, and inclination $i = 45°$ which imply $T_{\rm outer}$ = 14700 K, indicate that this is an ultra-compact system.

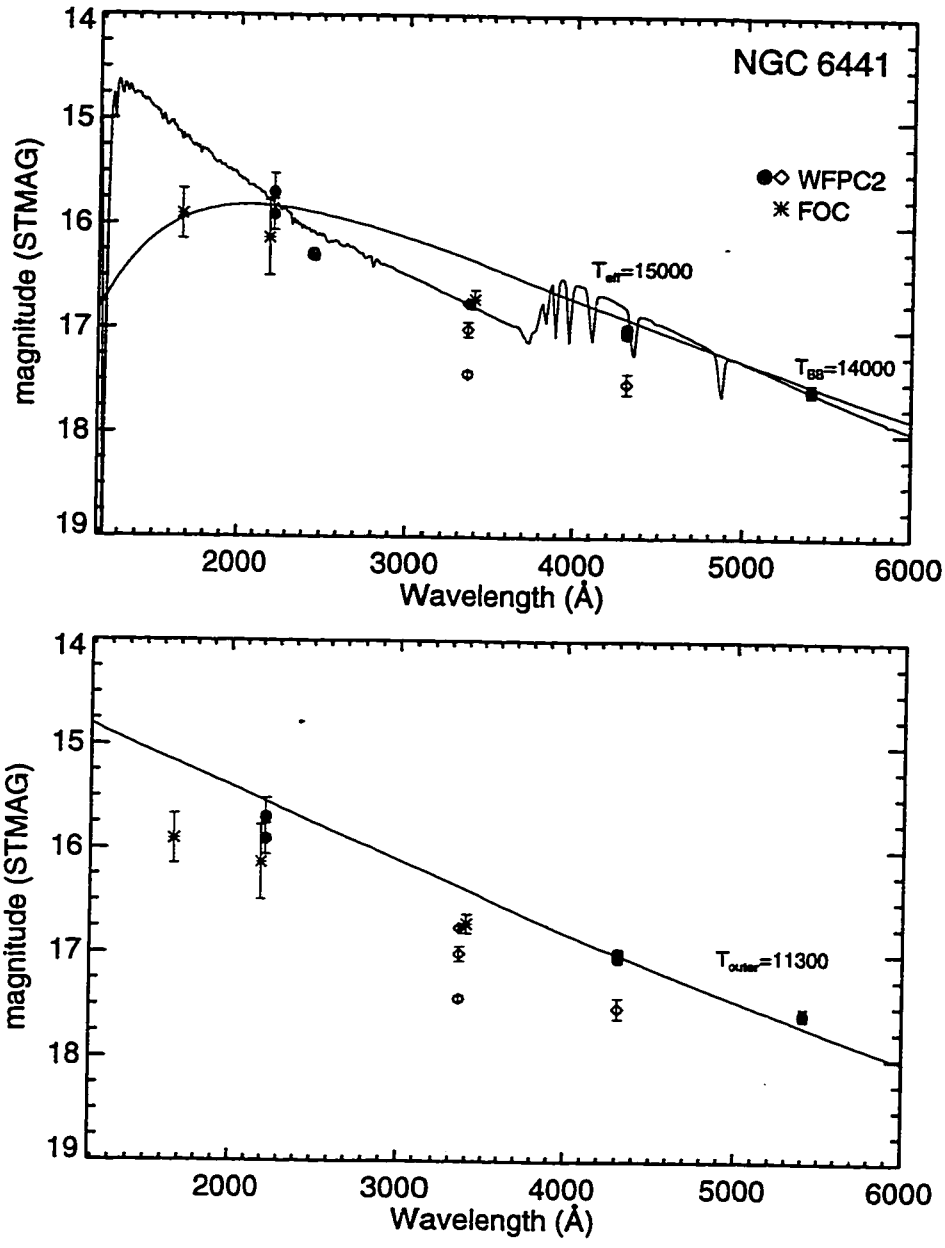

Figure 4.8: *Top Panel:* WFPC2 and FOC broadband magnitude measurements for Star U1 in NGC6441, all dereddened with $E(B-V) = 0.42$. Variability of the source is clearly indicated between *HST* visits and even during a single visit (each of the three visits is plotted with a different symbol). Overlaid are a $T_{\rm BB} = 14000$ K blackbody spectrum and a $T_{\rm eff} = 15000$ K Kurucz model which both fit the filled circle measurements acceptably. *Bottom Panel:* Same observations as above, with a truncated-disk model 2 overplotted. The model parameters for this curve are $R_D = R_L = 0.93\,R_\odot$, $\dot{M} = 2.27 \times 10^{-9} M_\odot$ yr^{-1}, and inclination $i = 60°$ which imply $T_{\rm outer} = 11300$ K.

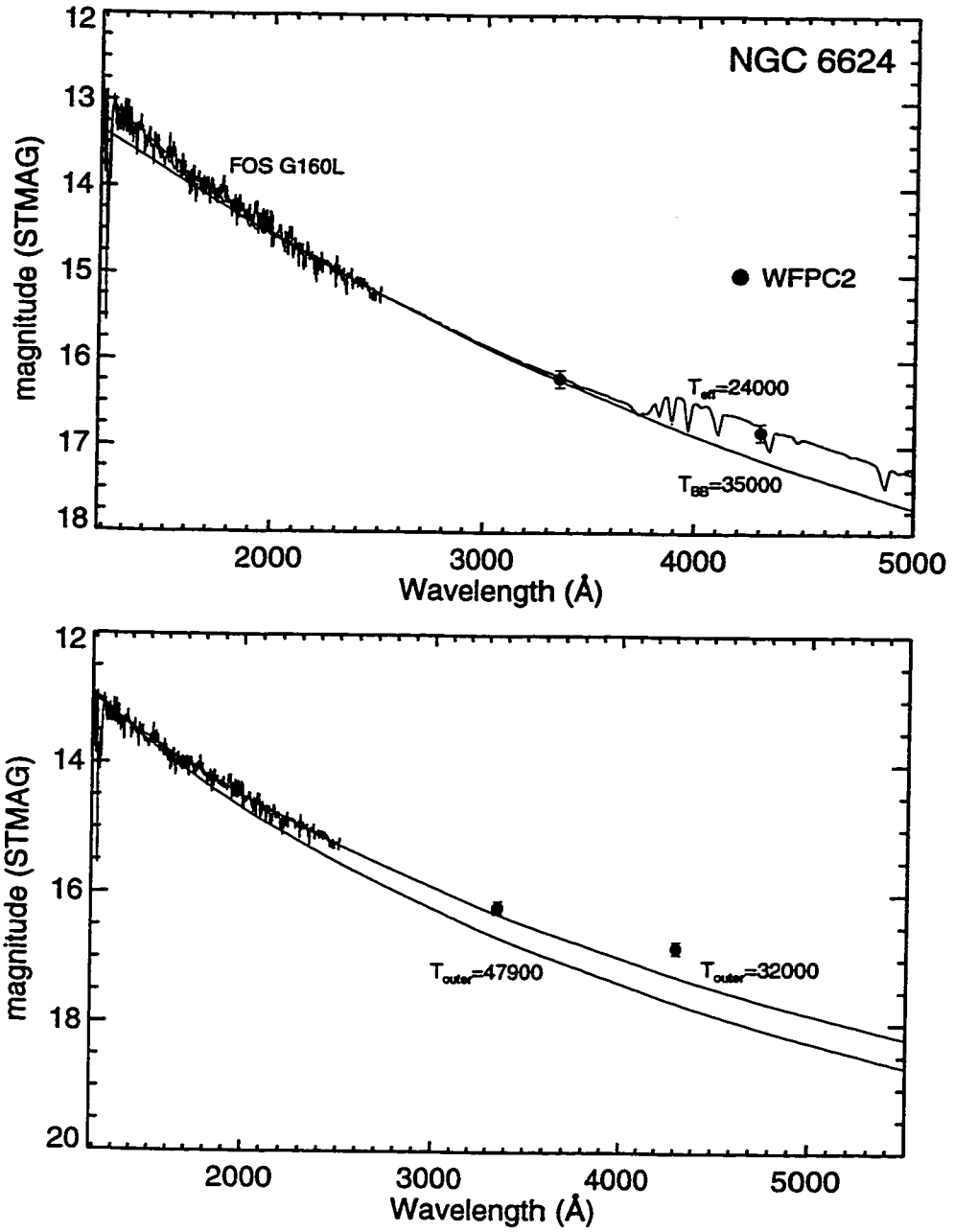

Figure 4.9: *Top Panel:* FOS G160L UV spectrum and WFPC2 broadband magnitude measurements for Star K in NGC 6624, all dereddened with $E(B-V) = 0.28$. Overlaid are a $T_{\rm eff} = 24000$ K Kurucz model and a $T_{\rm BB} = 35000$ K blackbody spectrum. The single-temperature stellar atmosphere model appears to provide an excellent representation of the SED. *Bottom Panel:* Same observations as above, with two truncated-disk models overplotted. The model 2 parameters used for the upper curve are $\dot{M} = 7.75 \times 10^{-9} M_\odot$, $i = 30°$, and $R_D = 1.6\,R_L = 0.19\,R_\odot$, which implies $T_{\rm outer} = 32000$ K. In the lower curve we limit $R_D = R_L$ for which $\dot{M} = 15.0 \times 10^{-9} M_\odot$ yr^{-1} predicts the flux at 1500 Å but yields too steep a slope at longer wavelengths.

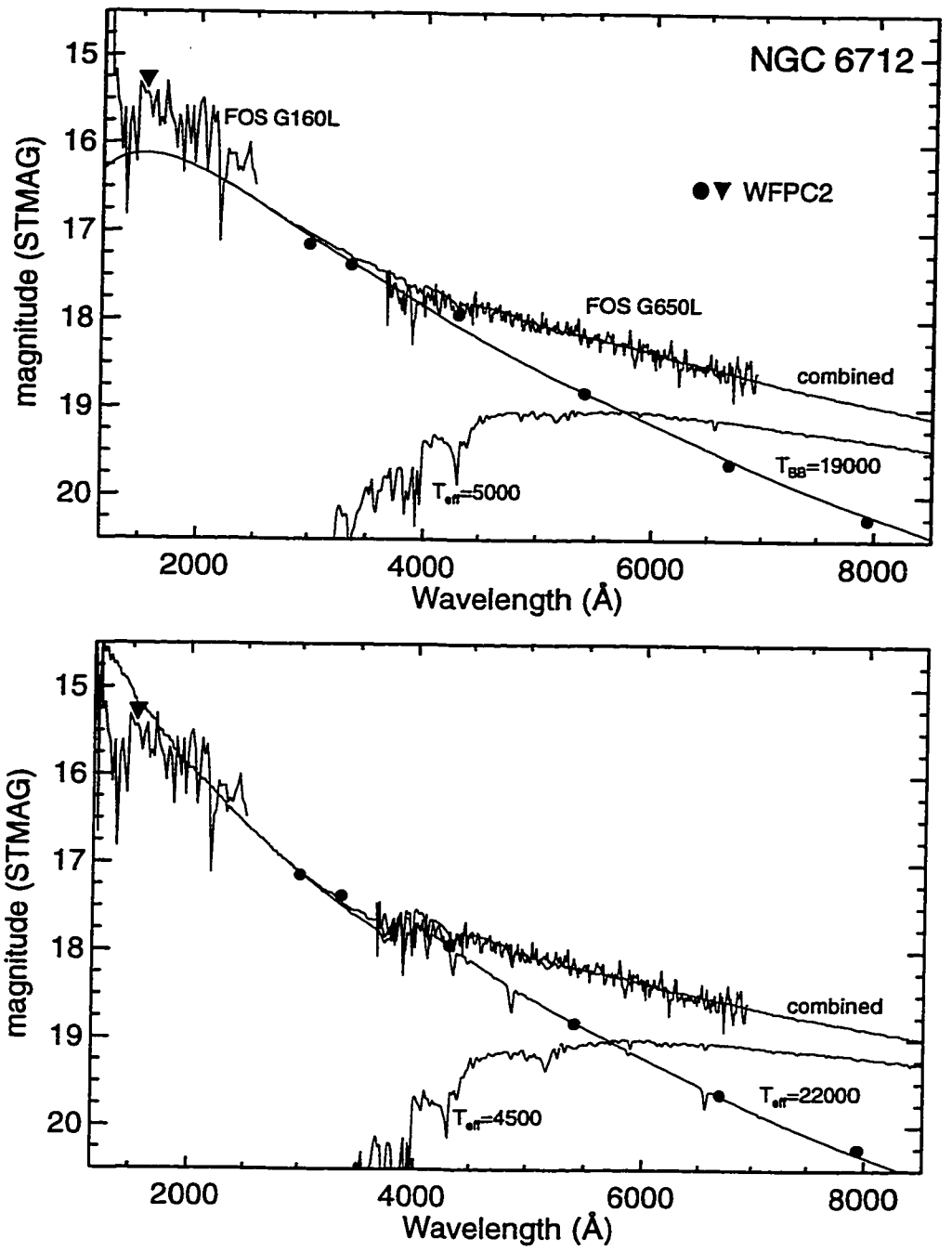

Figure 4.10: *Top Panel:* FOS spectra and WFPC2 broadband magnitude measurements for Star S in NGC6712, all dereddened with $E(B-V) = 0.46$. Overlaid are a $T_{BB} = 19000$ K blackbody spectrum which matches the photometry well, and $T_{eff} = 5000$ K Kurucz model which when combined with the blackbody spectrum describes the FOS optical spectrum well. We interpret this as an indication that the spectrum is contaminated with light from neighbor stars. *Bottom Panel:* Same as above, but with a $T_{eff} = 22000$ K Kurucz model instead of the blackbody spectrum.

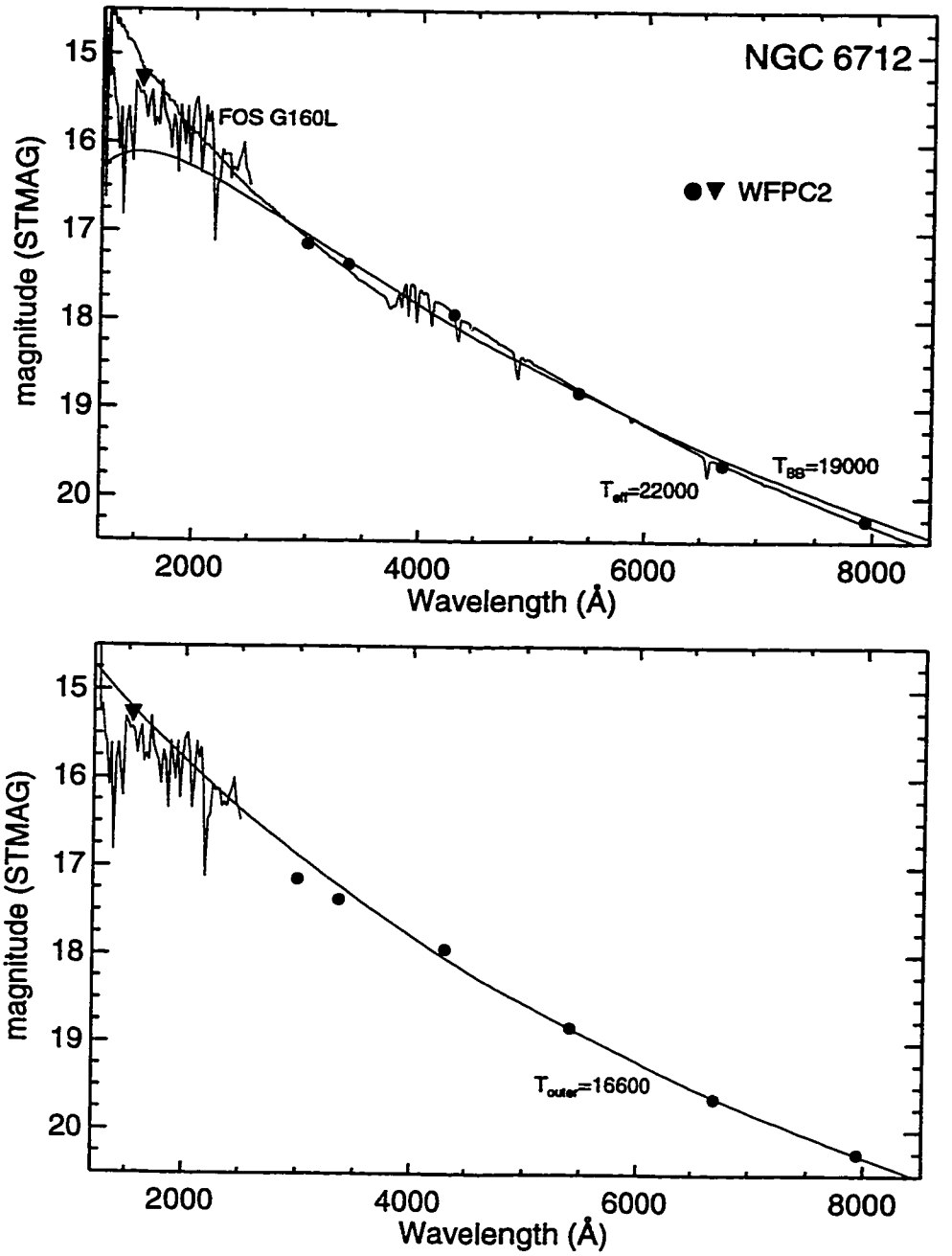

Figure 4.11: *Top Panel:* FOS G160L UV spectrum and WFPC2 broadband magnitude measurements for Star S in NGC 6712, all dereddened with $E(B-V) = 0.46$. Overlaid are a $T_{\rm eff} = 22000$ K Kurucz model and a $T_{\rm BB} = 19000$ K blackbody spectrum. The single-temperature stellar atmosphere model provides a good representation of the SED. *Bottom Panel:* Same observations as above, with a truncated-disk model overplotted. The model 2 parameters for this curve are $R_D = R_L = 0.18\,R_\odot$, $\dot{M} = 0.65 \times 10^{-9} M_\odot$ yr^{-1}, and inclination $i = 30°$ which imply $T_{\rm outer} = 16600$ K.

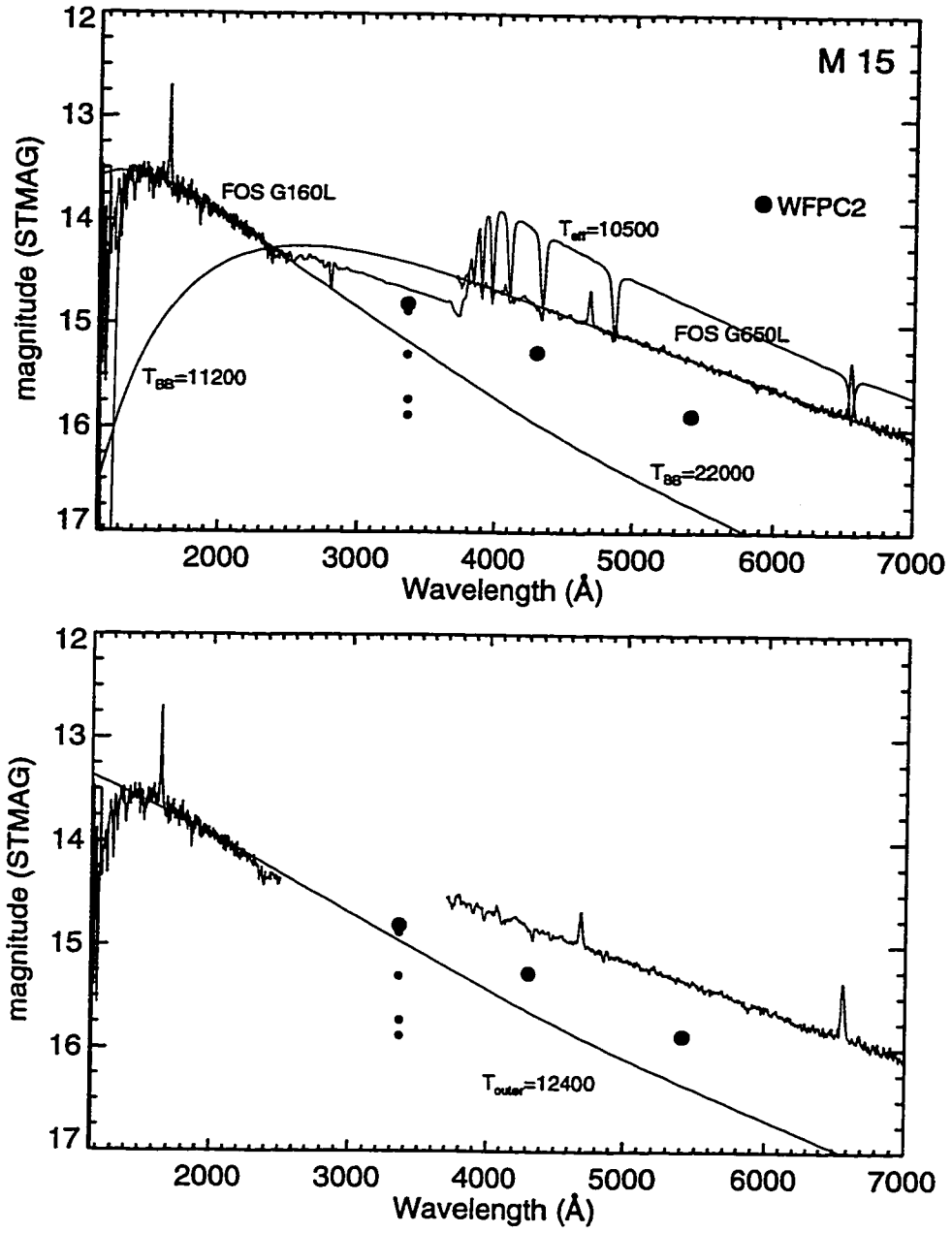

Figure 4.12: *Top Panel:* FOS spectra and WFPC2 broadband magnitude measurements for AC 211 in M 15, all dereddened with $E(B-V) = 0.05$. Overlaid are a $T_{\rm BB} = 22000$ K blackbody spectrum and a $T_{\rm eff} = 10500$ K Kurucz model which both fit the UV spectrum acceptably, and a $T_{\rm BB} = 11200$ K blackbody spectrum which fits the optical spectrum well. Clearly none of these models fit all of the data, however. *Bottom Panel:* Same observations as above, with a truncated-disk model overplotted. The model 2 parameters for this curve are $R_D = R_L = 1.9\,R_\odot$, $\dot{M} = 9.04 \times 10^{-9} M_\odot$ yr^{-1}, and inclination $i = 70°$, which imply $T_{\rm outer} = 12400$ K. This fit is clearly not entirely satisfactory.

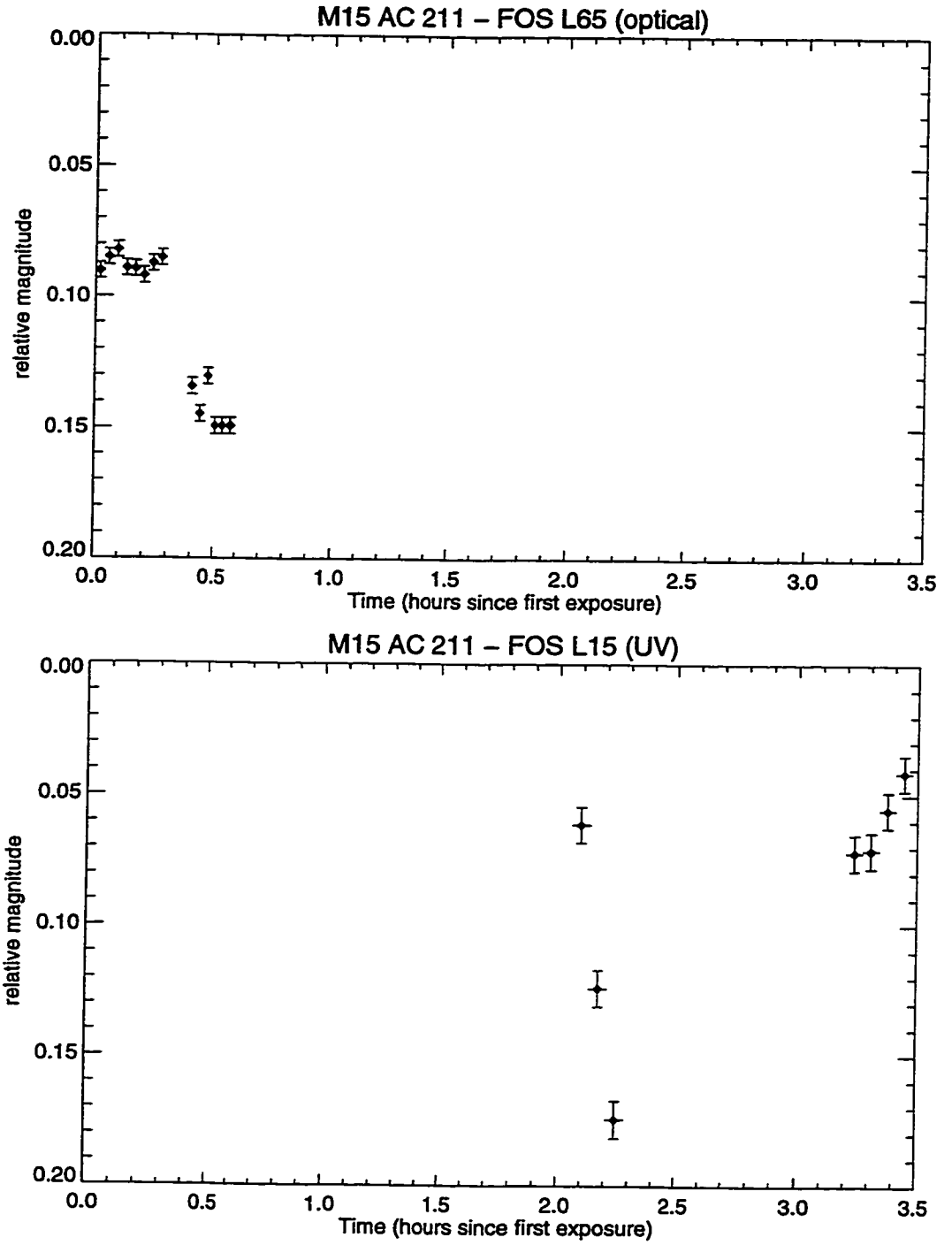

Figure 4.13: *Top Panel:* Count rates of the FOS optical spectra converted to magnitudes with an arbitrary zero point. The brightness appears to have changed only 5%. *Bottom Panel:* Count rates of the FOS UV spectra converted to magnitudes with an arbitrary zero point. The brightness appears to vary by 13% during these exposures, but far great variability between the optical and UV spectra is plausible.

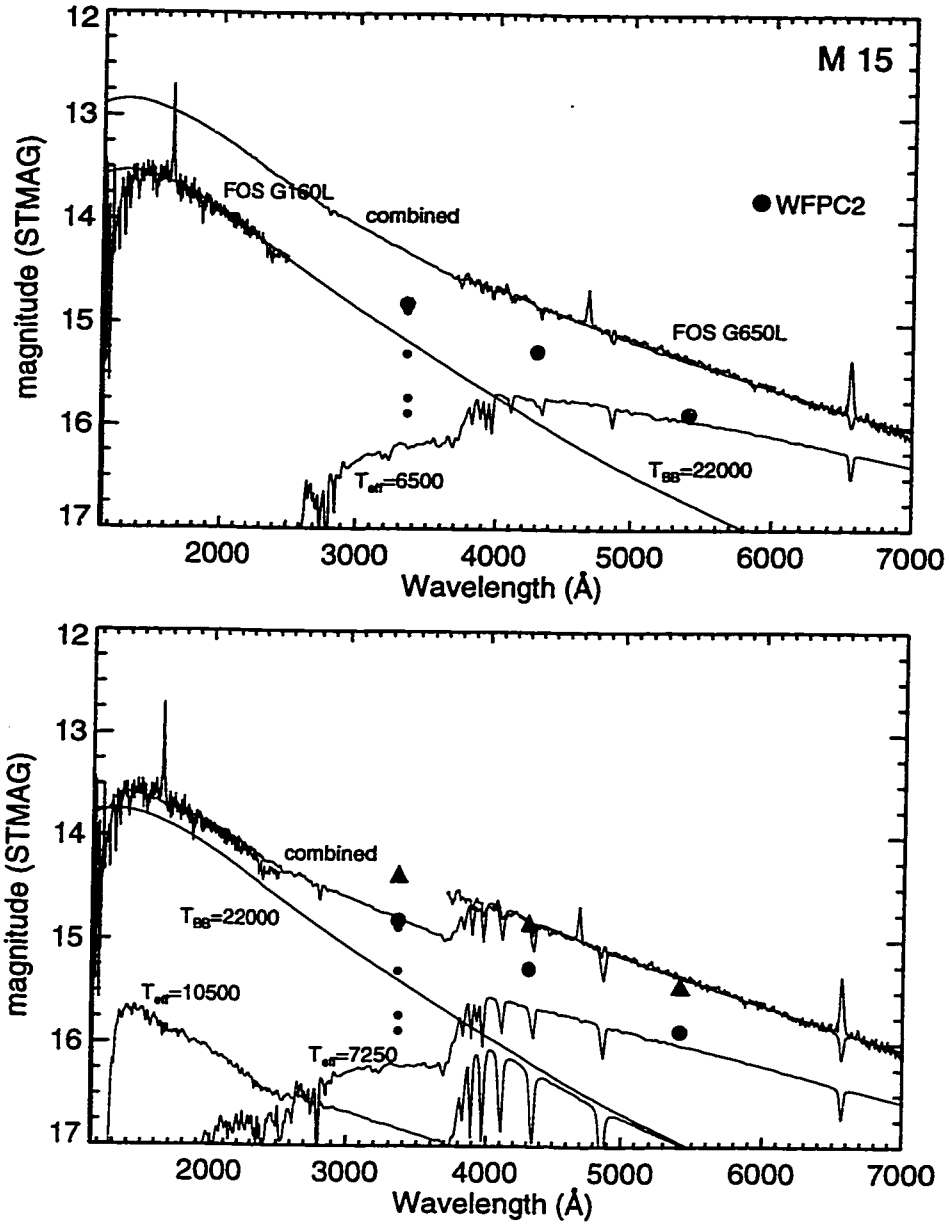

Figure 4.14: *Top Panel:* FOS spectra and WFPC2 broadband magnitude measurements for AC 211 in M 15, all dereddened with $E(B-V) = 0.05$. Overlaid are a $T_{\rm BB} = 22000$ K blackbody spectrum, a $T_{\rm eff} = 6500$ K Kurucz model, and the sum of the two. If the UV spectrum is scaled up by 0.75 mag, this model is consistent with all of the data, although it is not clear what physical picture this may be describing. *Bottom Panel:* Same observations as above, but with the sum of three suitably models overplotted: a $T_{\rm BB} = 22000$ K blackbody spectrum, a $T_{\rm eff} = 10500$ K Kurucz model, and a $T_{\rm eff} = 7250$ K Kurucz model. This contrived model can reproduce the optical and UV spectrum shapes and amplitudes, but it inconsistent with the WFPC2 photometry which rules out such a strong Balmer decrement at least at the time that those data were taken.

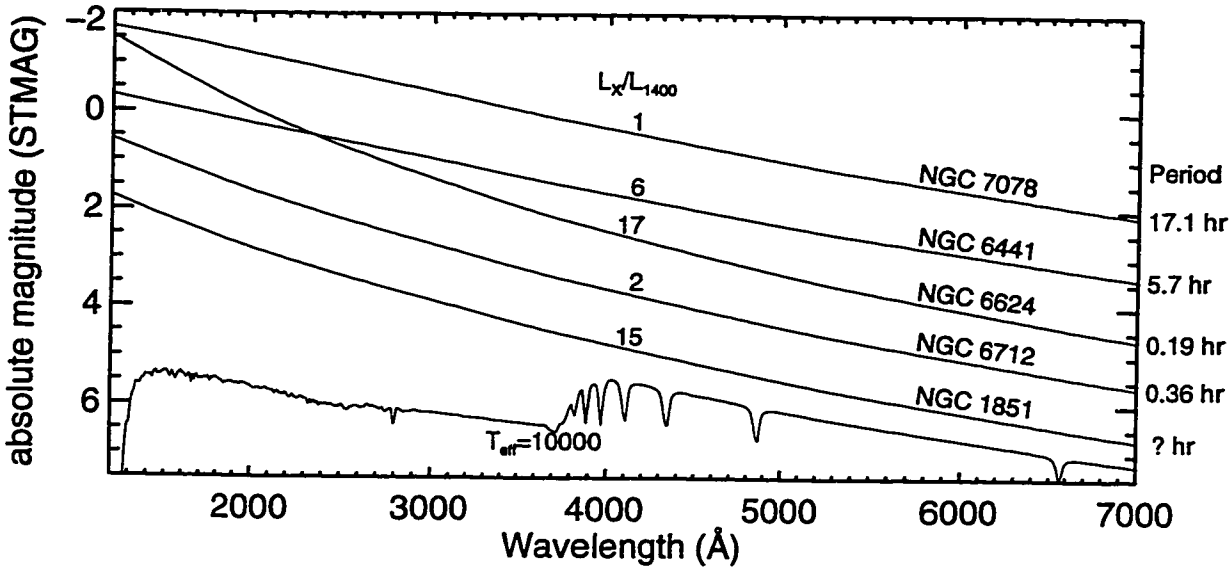

Figure 4.15: The best accretion disk models of the each of the five globular cluster sources corrected for distance and reddening to the host clusters. Each curve is labeled with the host cluster name. Orbital periods, if known, are labeled at the right of the diagram, as well as the observed ratio of 1–10 keV X-ray flux to that at 1400 Å, normalized for convenience to the value for NGC 7078 (=M 15). The short period systems have steeper SEDs shortward of 5000 Å and fainter luminosities. At the bottom a $T_{\rm eff} = 10000$ K Kurucz model is plotted for comparison.

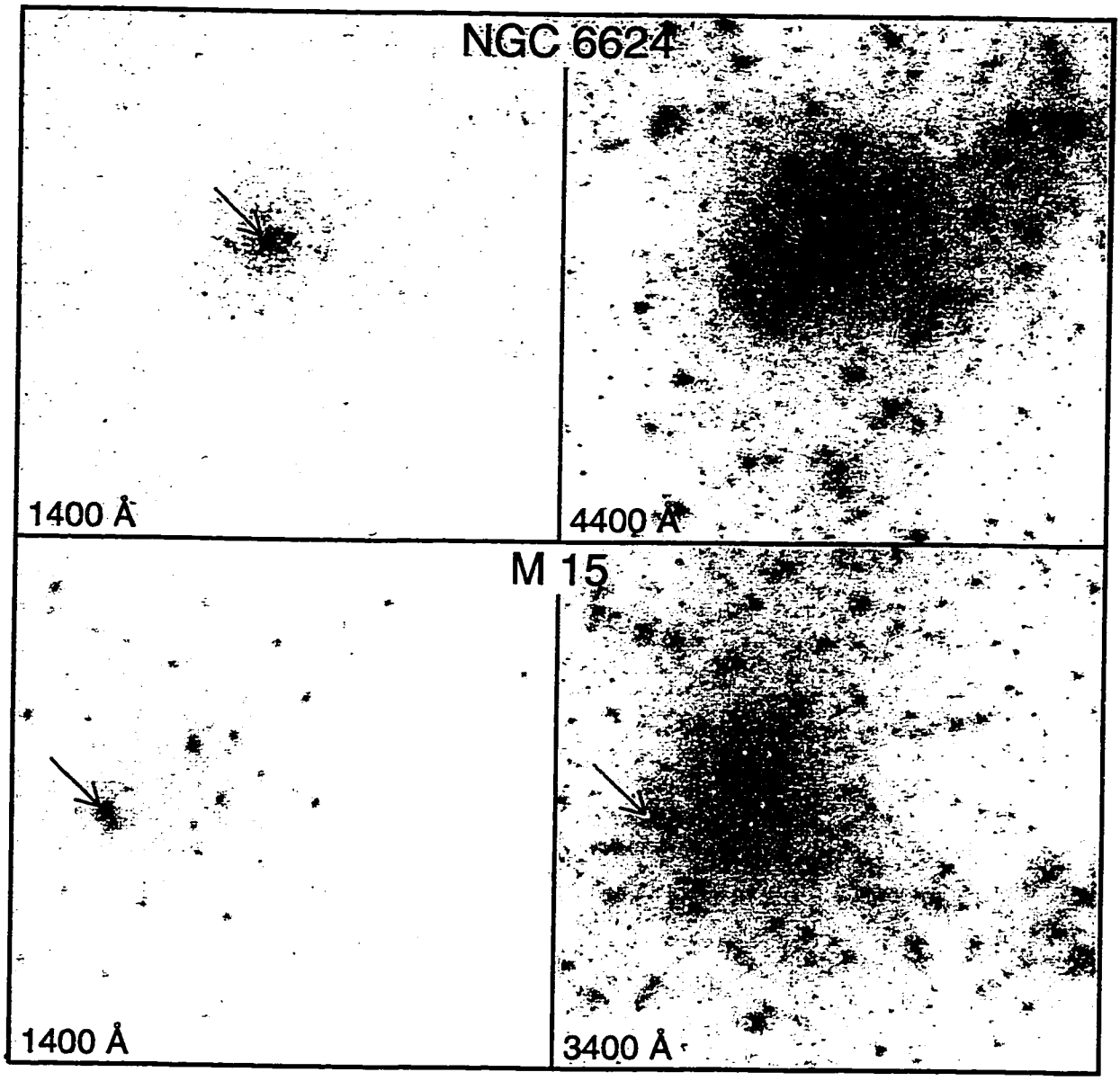

Figure 4.16: Archival HST FOC images of the cores of NGC 6624 and M 15, at 1400 Å and blue wavelengths. Note how prominently the X-ray source counterparts (*arrows*) appear at 1400 Å and how well the remainder of the cluster is suppressed. Each frame measures 10″ square. (Spherical abberation is apparent in these pre-repair mission images, and the blue M 15 data have very poor image quality due to FOC overlight.)

Chapter 5

CONCLUSION

In this work three new optical counterparts to luminous X-ray binaries in globular clusters have been suggested, thereby doubling the number of optical counterpart candidates. Two are very likely correct although require additional work to confirm the identifications, while the third remains somewhat tentative due to the positional discrepancy with the X-ray coordinates and the fact that the entire error circle is not surveyed.

In NGC 1851, our high spatial resolution WFPC2 multicolor images resolve ~200 objects in the 3″ radius *Einstein* X-ray error circle, 40 times as many as in previous ground-based work. A color-magnitude diagram of the cluster clearly reveals a markedly UV-excess object with B~21, (U−B) ~ −0.9 only 2″ from the X-ray position. Three other UV-excess objects are also present among the ~16,000 objects in the surveyed region of the cluster, leaving a ~5% probability that a UV-excess object has fallen in the X-ray error circle by chance. Some variability is seen in this candidate between two F218W images, lending some confidence to this object, but clearly a more complete study is required.

In NGC 6441, our multicolor images reveal a single, markedly UV-excess object with $m_{336} = 19.0$, $m_{439} = 19.3$, within the 3″ X-ray error circle, which itself also contains hundreds of stars. Furthermore, we observe an ultraviolet intensity variation of 30% for this object over 0.5 hr, as well as an even greater variation in m_{439} between two *HST* observations taken approximately one year apart. The combination of considerable UV-excess and significant variability strongly favors this object as the optical counterpart to the low-mass X-ray binary X 1746–370, despite the ambiguity

introduced by other, similarly UV-excess stars present in the cluster.

In NGC 6652, U and B ground-based images allow us to set a limit $M_{B_0} \gtrsim 3.5$ for the counterpart at the time of those observations, provided that the color is $(U-B)_0 \sim -1$, similar to the sources known in other clusters. Archival *Hubble Space Telescope* observations survey most but not all of the 1σ X-ray error circle, and allow us to set limits $M_{B_0} > 5.9$ and $M_{B_0} > 5.2$ in the WF/PC and WFPC2 regions, respectively. In the WF/PC images we do weakly detect a faint object with UV-excess, but it is located $11\farcs7$ from the *ROSAT* X-ray position. This considerable (2.3σ) discrepancy in position suggests that this candidate be treated with caution, but it remains the only reasonable one advanced thus far. We measure for this star $m_{439} = 20.2 \pm 0.2$, $(m_{336} - m_{439}) = -0.5 \pm 0.2$, and estimate $M_{B_0} = 5.5$, $(U-B)_0 = -0.9$, similar to other known optical counterparts. If this candidate is not the identification, our limits imply that the true counterpart, not yet identified, is probably the optically-faintest cluster source yet known, or alternatively that it did not show significant UV excess at the time of these observations.

A sufficient number of high-luminosity globular cluster X-ray source counterparts is now available that we can begin to study their properties as a class. We present a homogeneous set of *HST* photometry on these objects, and compare their optical properties with those of field low-mass X-ray binaries. The mean $(U-B)_0$ color of the cluster sources is identical to that of the field sources, and the mean M_{B_0} is similar in range, but fainter on average than bursters in the field. The ratio of optical to X-ray flux of cluster sources seems to show a significantly larger dispersion than that of the field sources. If our tentative identification in NGC 6652 is in fact the counterpart of the X-ray source, the previous inference that many globular cluster X-ray sources are optically subluminous with respect to low-mass X-ray binaries in the field is further strengthened.

The GC LMXBs seem to conform well the previously suggested optical luminosity, X-ray luminosity, orbital period relation (van Paradijs & McClintock 1994). If the

source in NGC 1851, for which no orbital period has yet been determined, follows this pattern, we predict that the period will likely be less than 0.85 hr. Similarly, if Star 49 in NGC 6652 is indeed the correct optical counterpart, this diagram suggests that its orbital period will also prove to be less than 1 hr. If these predictions come to pass, it will mean that two-thirds of GC LMXBs for which orbital periods are known have orbital periods less than 1 hr, and are therefore quite likely double degenerate ultra-compact binaries. Such a high fraction of ultra-compact systems would be remarkable and may indicate that binaries in the cores of globular clusters undergo many stellar encounters over their lifetimes, becoming more tightly bound after each interaction.

In addition to being able to compare the luminosities and colors with other LMXBs, there are now also sufficient observations to intercompare the UV/optical spectral energy distributions (SEDs) of GC LMXBs. We have presented a new FOS spectrum for Star A in NGC 1851 and reanalyzed the spectra for the systems in M 15, NGC 6624 and NGC 6712. Combining these spectra with broadband magnitude measurements from archival *HST* data gives us sufficient spectral coverage to test various simple models and further understand the nature of these systems.

We find that in many cases a simple single-temperature, arbitrarily scaled Kurucz model adequately describes the SED, but far greater insight is achieved by applying an irradiated accretion disk model. The GC LMXBs are particularly useful for this as the distance and reddening of these systems is quite well understood, unlike most field LMXBs. Summarized by Fig. 4.15, we find the sources in NGC 6441 and M 15 to be optically quite luminous with comparatively shallow SEDs. The faint sources in NGC 6712 and NGC 1851 have significantly steeper SEDs, and are most likely underluminous because their orbital separations and thus accretion disks are small. The case of NGC 6624 appears slightly different from the others with an average optical luminosity yet with the steepest SED slope. This is most likely due to its extremely high accretion rate (L_X is $\sim 10\times$ higher than any of the other GC LMXBs) and small size. From its luminosity, we infer that Star 49 in NGC 6652 will have

similar system parameters and SED to Star A in NGC 1851. In any case Star 49 will be an important object for further study, as it is quite isolated and can be resolved out into the infrared. In addition the cluster is only slightly reddened and thus UV observations will be efficient.

This attempt at modeling these LMXB systems has evoked some additional questions. Many of the broadband photometry datapoints have suggested a possible small Balmer decrement. The FOS spectra do not yield much evidence for such a decrement but the wavelength coverage in this region of the spectrum is not good. The current models use only pure blackbody emission with reasonably good success. It would very interesting to measure the Balmer decrement well for a few of these sources, to determine if detailed model atmospheres need ever be employed in these accretion disk models.

As the SED for Star A in NGC 1851 amply demonstrates, a series of well-calibrated, near simultaneous flux measurements over a broad spectral range is perhaps even more valuable than a spectrum for fitting a model, except in the ultraviolet where the spectral shape changes rapidly. Additional broadband measurements of several of these sources would improve our ability to properly fit the SEDs. Most of the UV spectra, although often fairly weak in this region, show very wide Ly α absorption. This is difficult to reconcile with the apparently very weak or non-existent Balmer decrement and needs to be examined further.

A very important missing piece in this picture is the orbital period for Star A in NGC 1851. Fortunately, there are upcoming *HST* observations which may well yield a period for this system. We are planning UV STIS MAMA imaging observations to be executed in 1999. We opted to perform UV observations because the flux from the neighboring star is thus minimized and orbital modulation due to the changing aspect of the heated side of the secondary is typically more pronounced at shorter wavelengths. It will be interesting to see if the period for this system will conform to the predictions presented herein.

Upcoming *HST* STIS spectroscopic observations of Star U1 in NGC 6441 are also being planned for observation in 1999. Although the SED appears to be quite flat based on the available photometry, the UV region is not very well constrained. The planned observations will provide moderate-quality optical spectra during an entire 5.7 hr orbit. This should allow an investigation of the SED amplitude and shape throughout the orbit of this significantly variable object. While the short period objects did not exhibit detectable emission lines, we may expect evidence of some emission lines, due to the similarity with AC 211 in M 15.

Star K in NGC 6624 would benefit from higher resolution broadband imaging from 2000 – 6000 Å. Current WFPC2 images do not have sufficient resolution to accurately measure magnitudes for this object due to the crowding by its 0.″08 distant neighbor. High resolution STIS imaging observations would likely yield good measurements out to the V band. Such measurements would allow a better assessment of any contamination in the present UV spectrum, and resolve the discrepancy in the m_{439} measurement discussed here. The problem encountered here where a model $R_D < R_L$ does not fit may simply be the result of contamination that high-resolution imaging could quantify, rather than a failing of the model.

Star S in NGC 6712 is one of the most isolated of the luminous globular cluster X-ray sources, and as such has the widest spectra coverage: 1200 – 8000 Å. Even at 8000 Å the emission from this object is not swamped by neighboring stars. That makes this object an ideal candidate for near infrared studies. It would be possible to follow the emission from this source out to the K band to see if there are significant departures from the best-fit model derived here. A confirmation in the IR of the orbital period which was derived with *HST* UV observations (Homer et al. 1996) would be beneficial, as well as the resulting comparison of UV to IR modulation amplitude. As this object is not extremely crowded, ground-based adaptive optics techniques may be adequately suited for such an investigation.

The large amplitude, short timescale variability of AC 211 in M 15 has severely

hampered our attempt to model the small amount of *HST* observations available in the archive. A much clearer understanding could be achieved by a longer campaign of spectra during an entire or a large fraction of an orbit combined with simultaneous observations from other instruments. Such a project is being carried out with *HST*, but the first set of the FOS observations in the archive from this program were not properly executed and are useless; the program will be executed again with STIS in the near future. This object is also sufficiently bright and isolated that a study extending into the infrared by ground-based telescopes might be feasible.

Aside from these five objects, there remains one globular cluster source for which a similar UV to near IR SED study should be easily achieved. The system in NGC 6652 benefits from low extinction and a relatively low crowding environment (by *HST* standards). A program which will observe this source with AXAF to derive a vastly improved $\sim 1''$ X-ray position has been accepted. A future set of WFPC2 observations of this cluster with the F336W and F439W filters will almost surely confirm the current candidate or provide a better optical counterpart for this system. Follow-on spectroscopic and broadband observations will constrain the SED of this system as has been done in this work for the other sources. High precision time series photometry similar to that performed on Star S in NGC 6712 (Homer et al. 1996), which turned up a 21.4 min periodicity, will also likely be feasible as NGC 6652 is of similar concentration and has far less extinction. The preliminary work thus far hints of another low optical luminosity system similar to Star A in NGC 1851.

Progress in furthering understanding of the remaining six luminous globular cluster X-ray sources at UV and optical wavelengths will be difficult due to the large extinction and crowded environments. UV spectra would likely require prohibitively long exposures times with current space instruments. Broadband optical magnitude measurements may still be possible for some of the these sources, providing some constraints on their SEDs, but most of them will likely require a move into the near infrared to search for counterparts. None of these extincted sources have known X-ray

periods and thus IR work may afford the only way to determine orbital periods for these systems.

One source in particular for which there is yet no optical counterpart deserves special mention. The Rapid Burster in the cluster Liller 1 is perhaps unique in the Galaxy, a source which displays both type I and type II bursts. A likely radio counterpart has recently been identified (Rutledge et al. 1998) with very accurate coordinates, which will make a search for an optical counterpart much easier than the previous X-ray coordinates would have allowed. A search is severely hampered by large extinction to the cluster, making only infrared searches feasible. The source is normally in a quiescent state but undergoes a strong quasiperiodic X-ray outburst every $\sim$ 200 days. We are undertaking a program to isolate the infrared counterpart during the expected 1998 September outburst with the ARC 3.5 m telescope (Deutsch, Anderson, & Margon 1998). Reasonably good data have been acquired and analysis is underway.

For the remaining five heavily reddened sources high-resolution infrared searches have not yet been attempted to our knowledge. These sources will be observed with AXAF in cycle 1 and the resulting $\sim 1''$ accuracy positions will vastly improve the chances of discovering and studying their infrared counterparts. Thus far X-ray and optical frames have been correlated using the *HST* Guide Star Catalog and Digitized Sky Survey which afford $\sigma\sim0\farcs5$ accuracy (Russell et al. 1990). With the new AXAF positions, a better system will be needed and the USNO A1.1 Catalog, based on the Tycho Catalog (ESA 1997), will soon be available to yield optical positions to better than $0\farcs1$. Searches for these objects will benefit greatly from having much smaller error circles and thus there will be an order of magnitude fewer objects which must be considered.

Our understanding of the luminous globular cluster X-ray sources has improved dramatically in the last five years, before which only a single source was optically

identified. We have now been able to examine and model the UV/optical SEDs for five of them, with additional progress already on the horizon. However, the potential of these sources for improving our understanding of cluster dynamics and LMXBs as a class has still not been fully realized.

BIBLIOGRAPHY

Anderson, S. F., Margon, B., Deutsch, E. W., & Downes, R. A. 1993, AJ, 106, 1049

Anderson, S. F., Margon, B., Deutsch, E. W., Downes, R. A., & Allen, R. G. 1997, ApJ, 482, L69

Arons, J., & King, I. R. 1993, ApJ, 413, L121

Aurière, M., Bonnet-Bidaud, J. M., & Koch-Miramond, L. 1994, A&A, 284, 457 (ABK)

Aurière, M., & Koch-Miramond, L. 1992, A&A, 263, 82

Aurière, M., Le Fèvre, O., & Terzan, A. 1984, A&A, 138, 415

Aurière, M., Maucherat, A., Cordoni, J.-P., Fort, B., & Picat, J. P. 1986, A&A, 158, 158

Bahcall, J. N., & Ostriker, J. P. 1975, Nature, 256, 23

Bailyn, C. D., Cool, A., Grindlay, J. E., Cohn, H., Lugger, P. M., & McClure, R. D. 1991, in ASP Conf. Ser. 13, The Formation and Evolution of Star Clusters, ed. K. Janes (San Francisco: ASP), 363

Bailyn, C. D., Grindlay, J. E., Cohn, H., & Lugger, P. M. 1988, ApJ, 331, 303

Bertelli, G., Bressan, A., Chiosi, C., Fagotto, F. & Nasi, E. 1994, A&AS, 106, 275

Bhattacharya, D. 1995, in X-Ray Binaries, ed. W. H. G. Lewin, J. van Paradijs, & E. P. J. van den Heuvel (Cambridge: Cambridge Univ.), 233

Bland-Hawthorn, J., & Jones, D. H. 1998, Publ. Astron. Soc. Austr., in press, preprint astro-ph/9707315

Callanan, P. J., Penny, A. J., & Charles, P. A. 1995, MNRAS, 273, 201

Charles, P. A., Jones, D. C., & Naylor, T. 1986, Nature, 323, 417

Chen, W., Shrader, C. R., & Livio, M. 1997, ApJ, 491, 312

Clark, G. W. 1975, ApJ, 199, L143

Clark, G. W., Markert, T. H., & Li, F. 1975, ApJ, 199, L93

Cropper, M., Harrop-Allin, M. K., Mason, K. O., Mittaz, J. P. D., Potter, S. B., Ramsay, Gavin 1998, MNRAS, 293, L57

Cudworth, K. M. 1988, AJ, 96, 105

David, L. P., Harnden, F. R., Kearns, K. E., & Zombeck, M. V. 1992, The ROSAT High Resolution Imager, US ROSAT Science Data Center, 4

Deutsch, E. W. 1998, in Proceedings of the IX Canary Islands Winter School of Astrophysics, in press

Deutsch, E. W., Anderson, S. F., & Margon, B. 1998, BAAS, 30, in press

Deutsch, E. W., Anderson, S. F., Margon, B., & Downes, R. A. 1994, BAAS, 26, 1488

Deutsch, E. W., Anderson, S. F., Margon, B., & Downes, R. A. 1996a, BAAS, 28, 1328

Deutsch, E. W., Anderson, S. F., Margon, B., & Downes, R. A. 1996b, ApJ, 472, L97

Deutsch, E. W., Anderson, S. F., Margon, B., & Downes, R. A. 1998, ApJ, 493, 775

Deutsch, E. W., Margon, B., & Anderson, S. F. 1997, BAAS, 29, 803

Deutsch, E. W., Margon, B., & Anderson, S. F. 1998a, AJ, 116, 1301

Deutsch, E. W., Margon, B., & Anderson, S. F. 1998b, BAAS, 30, 921

Deutsch, E. W., Margon, B., Wachter, S., & Anderson, S. F. 1996c, ApJ, 471, 979

Djorgovski, S. 1993, in ASP Conf. Ser. 50, Structure and Dynamics of Globular Clusters, ed. S. G. Djorgovski & G. Meylan (San Francisco: ASP), 373

Downes, R. A., Anderson, S. F., & Margon, B. 1996, PASP, 108, 688

Elson, R., Hut, P., & Inagaki, S. 1987, ARAA, 25, 565

ESA 1997, The Hipparcos and Tycho Catalogues, ESA SP-1200

Foreman, W., & Jones, C. 1976, ApJ, 207, L177

Gnedin, O. Y., & Ostriker, J. P. 1997, ApJ, 474, 223

Gotthelf, E. V., & Kulkarni, S. R. 1997, ApJ, 490, L161

Grindlay, J. 1981, in X-ray Astronomy with the Einstein Satellite, ed. R. Giacconi (Dordrecht: Reidel), 79

Grindlay, J. E. 1985, in IAU Symp. 113, Dynamics of Star Clusters, ed. J. Goodman & P. Hut (Dordrecht: Kluwer), 43

Grindlay, J. E. 1995, in ASP Conf. Ser. 72, Millisecond Pulsars: A Decade of Surprise, ed. A. S. Fruchter, M. Tavani, & D. C. Backer (San Francisco: ASP), 57

Grindlay, J., & Gursky, H. 1976, ApJ, 205, L131

Grindlay, J. E., Hertz, P., Steiner, J. E., Murray, S. S., & Lightman, A. P. 1984, ApJ, 282, L13

Guerriero, R. et al. 1998, MNRAS, submitted (preprint astro-ph/9807110)

Hertz, P., & Wood, K. S. 1985, ApJ, 290, 171

Holtzman, J. A., Burrows, C. J., Casertano, S., Hester, J. J., Trauger, J. T., Watson, A. M., & Worthey, G. 1995a, PASP, 107, 1065

Holtzman, J. A., et al. 1995b, PASP, 107, 156

Homer, L., & Charles, P. A. 1998, New Astronomy, in press (preprint astro-ph/9808323)

Homer, L., Charles, P. A., Naylor, T., van Paradijs, J., Aurière, M., & Koch-Miramond, L. 1996, MNRAS, 282, L37

Hut, P., McMillan, S. L. W., Goodman, J., Mateo, M., Phinney, E. S., Pryor, C., Richer, H. B., Verbunt, F., & Weinberg, M. 1992, PASP, 104, 981

Ilovaisky, S. A., Aurière, M., Chevalier, C., Koch-Miramond, L., Cordoni, J.-P., & Angebault, L. P. 1987, A&A, 179, L1

Ilovaisky, S. A., Aurière, M., Koch-Miramond, L., Chevalier, C., Cordoni, J.-P., & Crowe, R. A. 1993, A&A, 270, 139

in 't Zand, J., Heise, J., Bazzano, A., Ubertini, P., Smith, M. J. S., & Torroni, V. 1998a, IAUC 6997

in 't Zand, J. J. M., Verbunt, F., Heise, J., Muller, J. M., Bazzano, A., Cocchi, M., Natalucci, L., & Ubertini, P. 1998b, A&A, 329, L37

Jacoby, G. H., & Fullton, L. 1994, BAAS, 26, 1384

Jacoby, G. H., Morse, J., Fullton, L., Kwitter, K., & Henry, R. B. C. 1996, BAAS,

29, 1353

Jacoby, G. H., Morse, J., Fullton, L. K., Kwitter, K. B., & Henry, R. B. C. 1997, AJ, 114, 2611

Johnston, H. M., Verbunt, F., & Hasinger, G. 1995, A&A, 298, L21

Johnston, H. M., Verbunt, F., & Hasinger, G. 1996, A&A, 309, 116

Katz, J. I. 1975, Nature, 253, 698

King, A. 1995, in X-Ray Binaries, ed. W. H. G. Lewin, J. van Paradijs, & E. P. J. van den Heuvel (Cambridge: Cambridge Univ.), 419

King, I. R. et al. 1993, ApJ, 413, L117

Krist, J. 1993, in *Astronomical Data Analysis Software and Systems II*, ASP Conference Series 52, ed. R. J. Hanisch, R. J. V. Bissenden, & J. Barnes, p. 530

Kommers, J. M., Fox, D. W., Lewin, W. H. G., Rutledge, R. E., van Paradijs, J., Kouveliotou, C. 1997, ApJ, 482, L53

Kurucz, R. L. 1992, in IAU Symposium No. 149, The Stellar Population of Galaxies, ed. B. Barbuy & A. Renzini (Dordrecht: Kluwer), 225

Landsman, W. B. 1993, in ASP Conf. Ser. 52, Astronomical Data Analysis Software and Systems II, ed. R. J. Hanisch, R. J. V. Bissenden, & J. Barnes (San Francisco: ASP), 256

Lasker, B. M., Sturch, C. R., McLean, B. J., Russell, J. L., Jenkner, H., & Shara, M. M. 1990, AJ, 99, 2019

Lawrence, A., et al. 1983, ApJ, 267, 301

Lewin, W. H. G. 1977, Annals N. Y. Acad. Sci, 302, 210

Lewin, W. H. G., & Joss, P. C. 1983, in Accretion Driven Stellar X-ray Sources, ed. W. H. G. Lewin, & E. P. J. van den Heuvel (Cambridge: University Press), 41

Lewin, W. H. G., van Paradijs, J., & Taam, R. 1995, in X-ray Binaries, ed. W. H. G. Lewin, J. van Paradijs, & E. P. J. van den Heuvel (Cambridge: University Press), 175

Li, F., & Clark, G. 1977, IAUC 3095

Lindler, D. J., & Bohlin, R. C. 1994, FOS Instrument Science Report, CAL/FOS-125, STScI

Margon, B., Anderson, S. F., Downes, R. A., & Bohlin, R. C. 1992, in Science with the *Hubble Space Telescope*, ed. P. Benvenuti & E. Schreier (Garching: ESO), 421

Margon, B., & Bolte, M. 1987, ApJ, 321, L61

Makishima, K., et al. 1981, ApJ, 247, L23

McMillan, S. L. W., Pryor, C., & Phinney, E. S. 1998, in Highlights of Astronomy Vol. 11 (JD15 at the 23rd General Assembly of the IAU, Kyoto 1997) (preprint astro-ph/9710262)

Mukai, K., & Smale, A. 1998, BAAS, 30, 922

Naylor, T., & Charles, P. A. 1989, MNRAS 236, 1P

Naylor, T., Charles, P. A., Drew, J. E., & Hassall, B. J. M. 1988, MNRAS 233, 285

Naylor, T., Charles, P. A., Hassall, B. J. M., Raymond, J. C., & Nassiopoulos, G. 1992, MNRAS, 255, 1

Nieto, J.-L., et al. 1990, A&A, 239, 155

Ortolani, S., Bica, E., & Barbuy, B. 1994, A&A, 286, 444

Ostriker, J. P. 1997, paper delivered to Ostriker Festschrift, Princeton NJ, May 1997

Parmar, A. N., Stella, L., Giommi, P. 1989, A&A, 222, 96

Peterson, C. J. 1993, in ASP Conf. Ser. 50, Structure and Dynamics of Globular Clusters, ed. S. G. Djorgovski & G. Meylan (San Francisco: ASP), 337

Predehl, P., Hasinger, G., & Verbunt, F. 1991, A&A, 246, L21

Rappaport, S., Dewey, D., Levine, A., & Macri, L. 1994, ApJ, 423, 633

Rich, R. M., et al. 1997, ApJ, 484, L25

Rich, R. M., Minniti, D., & Liebert, J. 1993, ApJ, 406, 489

Russell, J. L., Lasker, B. M., McLean, B. J., Sturch, C. R., & Jenkner H. 1990, AJ, 99, 2059

Rutledge, R., Moore, C., Fox, D., Lewin, W., & van Paradijs, J. 1998, IAUC, 6813

Saha, A., Sandage, A., Labhardt, L., Tammann, G. A., Macchetto, F. D., Panagia,

N. 1996, ApJ, 466, 55

Sansom, A. E., Dotani, T., Asai, K. & Lehto, H. J. 1993, MNRAS, 262, 429

Savage, B. D. & Mathis, J. S. 1979, ARAA, 17, 73

Schechter, P., Mateo, M., & Saha, A. 1993, PASP, 105, 1342

Shakura, N. I., & Sunyaev, R. A. 1973, A&A, 24, 337

Silk, J., & Arons, J. 1975, ApJ, 200, L131

Stella, L., Priedhorsky, W., & White, N. E. 1987, ApJ, 312, L17

Sztajno, M., Fujimoto, M. Y., van Paradijs, J., Vacca, W. D., Lewin, W. H. G., Penninx, W., & Trümper, J. 1987, MNRAS, 226, 39

Trager, S. C., Djorgovski, S. & King, I. R. 1993, in ASP Conf. Ser. 50, Structure and Dynamics of Globular Clusters, ed. S. G. Djorgovski & G. Meylan (San Francisco: ASP), 347

van Paradijs, J. 1983, in Accretion Driven X-ray Sources, ed. W. Lewin & E. van den Heuvel (Cambridge: Cambridge Univ.), 189

van Paradijs, J. 1995, in X-Ray Binaries, ed. W. H. G. Lewin, J. van Paradijs, & E. P. J. van den Heuvel (Cambridge: Cambridge Univ.), 536

van Paradijs, J., & McClintock, J. E. 1994, A&A, 290 133 (vPM94)

van Paradijs, J., & McClintock, J. E. 1995, in X-Ray Binaries, ed. W. H. G. Lewin, J. van Paradijs, & E. P. J. van den Heuvel (Cambridge: Cambridge Univ.), 58 (vPM)

Verbunt, F. 1998, in ASP Conf. Ser. _, Astrophysical Disks, ed. J. Sellwood & J. J. Goodman (San Francisco: ASP), in press (preprint astro-ph/9809028)

Verbunt, F., & Hut, P. 1987, in IAU Symp. 125, The Origin and Evolution of Neutron Stars, ed. D. J. Helfand & J. H. Huang (Dordrecht: Kluwer), 187

Verbunt, F., Bunk, W., Hasinger, G., & Johnston, H. M. 1995, A&A, 300, 732

Vrtilek, S. D., Penninx, W., Raymond, J. C., Verbunt, F., Hertz, P., Wood, K., Lewin, W. H. G., & Mitsuda, K. 1991, ApJ, 376, 278

Vrtilek, S. D., Raymond, J. C., Garcia, M. R., Verbunt, F., Hasinger, G., & Kürster,

M. 1990, A&A, 235, 162

Voges, W. 1998, private communication

Warwick, R. S., Norton, A. J., Turner, M. J. L., Watson, M. G., Willingale, R. 1988, MNRAS, 232, 551

White, N. E., Nagase, F., & Parmar, A. N. 1995, in X-Ray Binaries, ed. W. H. G. Lewin, J. van Paradijs, & E. P. J. van den Heuvel (Cambridge: Cambridge Univ.), 1

VITA

Eric William Deutsch

Address:

Department of Astronomy
University of Washington
Box 351580
Seattle, WA 98195-1580

email: deutsch@astro.washington.edu
Phone: (206) 616-2788, 543-2888
FAX: (206) 685-0403
WWW: http://www.astro.washington.edu/deutsch/

Education:

Ph. D., Astronomy, University of Washington, 1998 (expected).
M. S., Astronomy, University of Washington, 1994.
B. A., Physics, The Johns Hopkins University, 1992.

Positions:

Research Assistant, University of Washington, 1992–present.
Teaching Assistant, University of Washington, 1994–1995.
Research Assistant, Space Telescope Science Institute, 1989–1992.

Refereed Publications:

1. "The Meinunger '*Nicht Rote*' Objects", Margon, B., & Deutsch, E. W. 1999, PASP, in press

2. "A Search for the Optical Counterpart of the Luminous X-ray Source in NGC 6652", Deutsch, E. W., Margon, B., & Anderson, S. F. 1998, AJ, 116, 1301

3. "The Optical Afterglow of GRB 971214: R and J Photometry", Diercks, A., Deutsch, E. W., Castander, F. J., Corson, C, Gilmore, G., Lamb, D. Q., Tanvir, N., Turner, E. L., & Wyse, R. 1998, ApJ, 503, L105

4. "Optical and near-infrared follow-up observations of GRB 980329", Palazzi et al. 1998, A&A, 336, L95

5. "A Technique for Narrowband Time Series Photometry: the X-ray Star V2116 Oph", Deutsch, E. W., Margon, B., & Bland-Hawthorn, J. 1998, PASP, 110, 912

6. "Complex Velocity Fields in the Shell of T Pyxidis", Margon, B., & Deutsch, E. W. 1998, ApJ, 498, L61

7. "The Probable Optical Counterpart of the Luminous X-ray Source in NGC 6441", Deutsch, E. W., Anderson, S. F., Margon, B., & Downes, R. A. 1998, ApJ, 493, 775

8. "CC Bootis: QSO, Not Variable Halo Giant", Margon, B., & Deutsch, E. W. 1997, PASP, 109, 673

9. "Time-Resolved Ultraviolet Observations of the Globular Cluster X-ray Source in NGC 6624: The Shortest Known Period Binary System", Anderson, S. F., Margon, B., Deutsch, E. W., Downes, R. A., & Allen, R. G. 1997, ApJ, 482, L69

10. "An Ultraviolet-Excess Optical Candidate for the Luminous Globular Cluster X-ray Source in NGC 1851", Deutsch, E. W., Anderson, S. F., Margon, B., & Downes, R. A. 1996, ApJ, 472, L97

11. "HST Imaging of Bright Galactic X-ray Binaries in Crowded Fields", Deutsch, E. W., Margon, B., Wachter, S., & Anderson, S. F. 1996, ApJ, 471, 979

12. "Positions and Proper Motions of Dwarf Carbon Stars", Deutsch, E. W. 1994, PASP, 106, 1134

13. "The Structure of the Inner Eastern Spiral Arm of M83", Deutsch, E. W., & Allen, R. J. 1993, AJ, 106, 1812

14. "Ultraviolet Imaging Telescope: Globular Clusters in M31", Bohlin, R. C., Deutsch, E. W., McQuade, K. A., Hill, J. K., Landsman, W. B., O'Connell, R. W., Roberts, M. S., Smith, A. M., & Stecher, T. P. 1993, ApJ, 417, 127

15. "Ultraviolet-excess Selection of the Counterpart to a Globular Cluster X-ray Burster: HST Images of the Core of NGC 6712", Anderson, S. F., Margon, B., Deutsch, E. W., & Downes, R. A. 1993, AJ, 106, 1049

Papers Delivered to Scientific Meetings:

1. "Infrared Imaging of the Cluster Liller 1 During the Active Phase of the Rapid Burster", Deutsch, E. W., Anderson, S. F., & Margon, B. 1998, BAAS, 30, in press

2. "UV/Optical Spectral Energy Distributions of Luminous X-ray Binaries in Globular Clusters", Deutsch, E. W., Margon, B., & Anderson, S. F. 1998, BAAS, 30, 921

3. "Narrowband Time Series Photometry of the X-ray Star V2116 Oph with TTF", Deutsch, E. W., Margon, B.,& Bland-Hawthorn, J. 1997, BAAS, 29, 1389

4. "The Optical Counterparts of Globular Cluster Low-mass X-ray Binaries", Deutsch, E. W. 1998, Proceedings of the IX Canary Islands Winter School of Astrophysics, in press

5. "A Search for the Optical Counterpart of the Luminous X-ray Source in NGC 6652", Deutsch, E. W., Margon, B., & Anderson, S. F. 1997, BAAS, 29, 803

6. "A Candidate for the Optical Counterpart of the Luminous X-ray Source in NGC 6441", Deutsch, E. W., Anderson, S. F., Margon, B., & Downes, R. A. 1996, BAAS, 28, 1328

7. "First Detection of an 11 Minute UV Modulation from the Counterpart for the Luminous Globular X-ray Source in NGC 6624" Anderson, S. F., Margon, B., Deutsch, E. W., Downes, R. A., & Allen, R. G. 1996, BAAS, 28, 1327

8. "On the Nature of the LMC Supersoft X-ray Source CAL 87", Wachter, S., Deutsch, E. W., Margon, B., & Anderson, S. F. 1996, BAAS, 28, 923

9. "HST WFPC Imaging of Candidate Optical Counterparts for a Globular Cluster X-ray Source in NGC 1851", Deutsch, E. W., Anderson, S. F., Margon, B., & Downes, R.A. 1995, BAAS, 26, 1488

10. "Very Deep ROSAT PSPC Observations of Three Globular Clusters", Margon, B., Deutsch, E., Silber, A., Lewin, W. H. G., van Paradijs, J., & van der Klis, M. 1994, BAAS, 26, 872

11. "Very Deep ROSAT PSPC Observation of Three Globular Clusters: Success in the Core, Failure in the Outskirts", Margon, B., Deutsch, E., Silber, A., Lewin, W. H. G., van Paradijs, J., & van der Klis, M. 1994, in New Horizon of X-ray Astronomy, ed. F. Makino & T. Ohashi (Tokyo: Universal Academy Press), 395

12. "The Structure of the Inner Eastern Spiral Arm of M83", Deutsch, E. W., & Allen, R. J. 1993, BAAS, 25, 797

13. "Ultraviolet Imaging Telescope: Globular Clusters in M31", Bohlin, R. C., Deutsch, E. W., McQuade, K. A., Hill, J. K., Landsman, W. B., O'Connell, R. W., Roberts, M. S., Smith, A. M., & Stecher, T. P. 1993, BAAS, 25, 884

IMAGE EVALUATION TEST TARGET (QA-3)

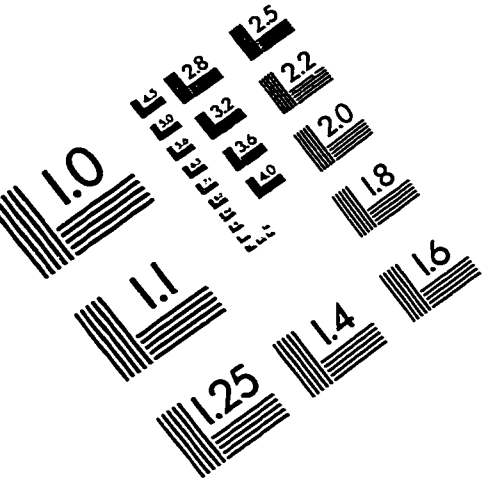

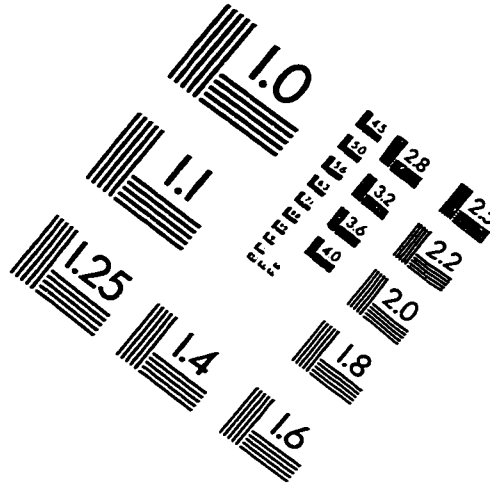

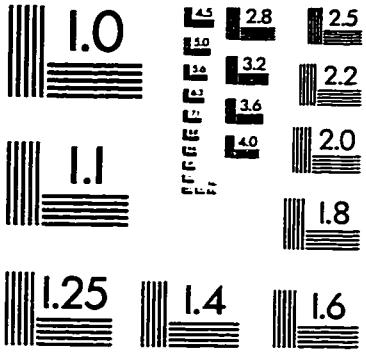

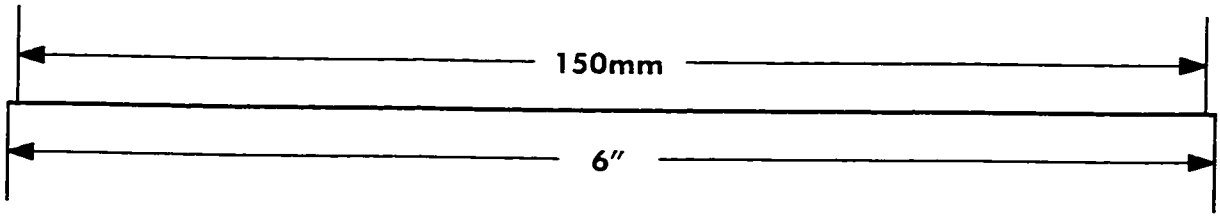

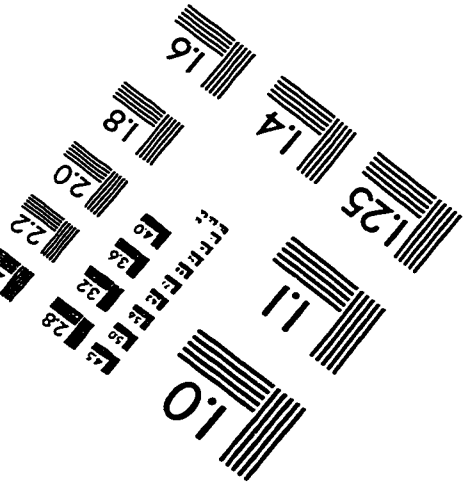

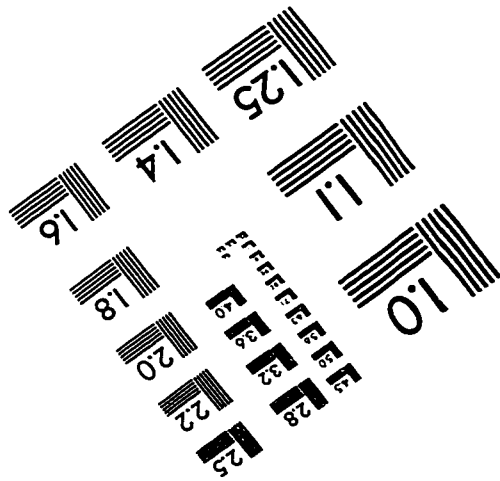

APPLIED IMAGE, Inc
1653 East Main Street
Rochester, NY 14609 USA
Phone: 716/482-0300
Fax: 716/288-5989